Promising Catalytic Systems for CO2 Hydrogenation into CH4: A Review of Recent Studies

Authors:

M. Carmen Bacariza, Daniela Spataru, Leila Karam, José M. Lopes, Carlos Henriques

Abstract:

The increasing utilization of renewable sources for electricity production turns CO2 methanation into a key process in the future energy context, as this reaction allows storing the temporary renewable electricity surplus in the natural gas network (Power-to-Gas). This kind of chemical reaction requires the use of a catalyst and thus it has gained the attention of many researchers thriving to achieve active, selective and stable materials in a remarkable number of studies. The existing papers published in literature in the past few years about CO2 methanation tackled the catalysts composition and their related performances and mechanisms, which served as a basis for researchers to further extend their in-depth investigations in the reported systems. In summary, the focus was mainly in the enhancement of the synthesized materials that involved the active metal phase (i.e., boosting its dispersion), the different types of solid supports, and the frequent addition of a second metal oxide (usually behaving as a promoter). The current manuscript aims in recapping a huge number of trials and is divided based on the support nature: SiO2, Al2O3, CeO2, ZrO2, MgO, hydrotalcites, carbons and zeolites, and proposes the main properties to be kept for obtaining highly efficient carbon dioxide methanation catalysts.

Promising Catalytic Systems for CO$_2$ Hydrogenation into CH$_4$: A Review of Recent Studies

M. Carmen Bacariza [1,2,*] **, Daniela Spataru** [1,2] **, Leila Karam** [3,4] **, José M. Lopes** [5] **and Carlos Henriques** [5]

[1]   c5Lab—Sustainable Construction Materials Association, Edifício Central Park, Rua Central Park 6, 2795-242 Linda-a-Velha, Portugal; dspataru@c5lab.pt

[2]   Centro de Química Estrutural, Instituto Superior Técnico, Universidade de Lisboa, Av Rovisco Pais, 1049-001 Lisboa, Portugal

[3]   Sorbonne Université, Campus Pierre et Marie Curie, Laboratoire de Réactivité de Surface, UMR CNRS 7197, 4 Place Jussieu, F-75005 Paris, France; laylakaram_22@hotmail.com

[4]   Department of Chemical Engineering, Faculty of Engineering, University of Balamand, P.O. Box 33 Amioun El Koura, Lebanon

[5]   Centro de Química Estrutural and Departamento de Engenharia Química, Instituto Superior Técnico, Universidade de Lisboa, Av Rovisco Pais, 1049-001 Lisboa, Portugal; jmlopes@tecnico.ulisboa.pt (J.M.L.); carlos.henriques@tecnico.ulisboa.pt (C.H.)

*   Correspondence: maria.rey@tecnico.ulisboa.pt

Abstract: The increasing utilization of renewable sources for electricity production turns CO$_2$ methanation into a key process in the future energy context, as this reaction allows storing the temporary renewable electricity surplus in the natural gas network (Power-to-Gas). This kind of chemical reaction requires the use of a catalyst and thus it has gained the attention of many researchers thriving to achieve active, selective and stable materials in a remarkable number of studies. The existing papers published in literature in the past few years about CO$_2$ methanation tackled the catalysts composition and their related performances and mechanisms, which served as a basis for researchers to further extend their in-depth investigations in the reported systems. In summary, the focus was mainly in the enhancement of the synthesized materials that involved the active metal phase (i.e., boosting its dispersion), the different types of solid supports, and the frequent addition of a second metal oxide (usually behaving as a promoter). The current manuscript aims in recapping a huge number of trials and is divided based on the support nature: SiO$_2$, Al$_2$O$_3$, CeO$_2$, ZrO$_2$, MgO, hydrotalcites, carbons and zeolites, and proposes the main properties to be kept for obtaining highly efficient carbon dioxide methanation catalysts.

Keywords: CO$_2$ conversion; CO$_2$ methanation; Sabatier reaction; Power-to-Gas; heterogeneous catalysts; active metals; supports; reaction mechanism

1. Introduction

The promotion of electricity production using renewable sources is in the origin of a general interest for electric energy storage systems able to deal with their well-known intermittency [1–3]. Among all, the use of the temporary overproduction of renewable electricity for the synthesis of fuels (energy vectors) has attracted attention [1,3–6]. CO$_2$ methanation is foreseen to play a key role in the future energy context [4,5], especially because CH$_4$ is the main component of natural gas, which allows its injection in the existing and well-established network (Power-to-Gas) [7].

In addition, important efforts must be carried out in order to constrain CO$_2$ emissions in the next years [8–10], being the development of suitable technologies for its capture and conversion to

value-added products mandatory for reducing the contribution of sectors such as cement industries, responsible for 7–8% of global CO_2 emissions [11,12]. Even if CO_2 could be transformed into chemicals and fuels, its usage as feedstock is limited to a few industrial processes (synthesis of urea and derivatives, salicylic acid and carbonates) [13–15] due to its thermodynamic stability and, as a result, the high energy substances or electro-reductive processes typically needed for its transformation into other chemicals [16]. CO_2 conversion into CH_4 (Figure 1) represents a suitable alternative if implemented in cement industries, as they could use natural gas for combustion processes, reducing energy demands and CO_2 emissions simultaneously.
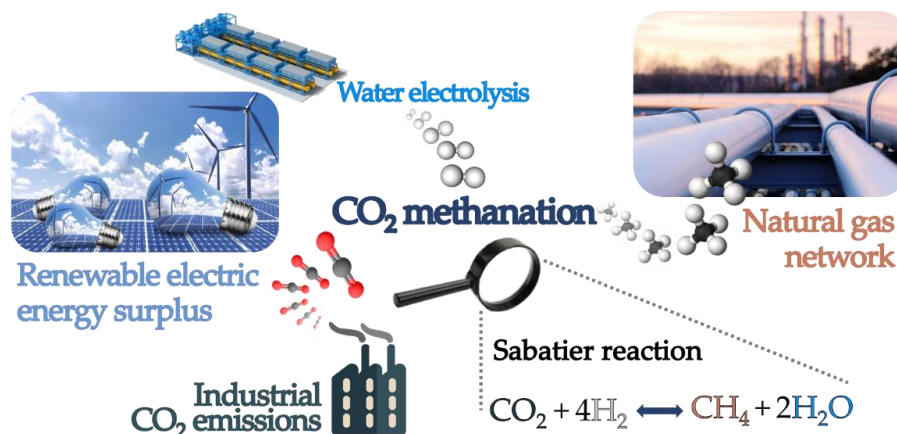

Figure 1. CO_2 methanation in the Power-to-Gas context.

Besides green hydrogen production and CO_2 capture, CO_2 methanation efficiency depends on the used catalysts. Therefore, finding active, selective and stable materials is considered as the core of the process [17]. Taking into account the significant number of publications dealing with this topic, the present work elaborates a review and compares recent studies regarding heterogeneous supported catalysts for conventional thermal CO_2 hydrogenation to CH_4. The results will be presented and organized based on the support's nature. This work aims to complement excellent reviews published in the area of carbon dioxide methanation in the last few years [17–29]. The main findings reported will be summarized and the best performances (T: reaction temperature, X_{CO2}: CO_2 conversion, S_{CH4}: selectivity to CH_4) will be presented along with the main preparation (active metal(s) loading—wt%, given in italic in all the tables—and incorporation method) and operation (T_{red}: reduction temperature, H_2/CO_2 ratio, Q_T/W: flowrate per mass of catalyst) conditions applied. Additionally, and taking into account that CO_2 methanation mechanism is strongly influenced by the catalyst's composition, the main findings regarding mechanistic approaches will be also included.

Despite the fact that only a few studies have dealt with the use of unsupported catalysts for CO_2 methanation, their results must be taken into account. Indeed, Choe et al. [30] and Ren et al. [31] carried out theoretical mechanistic studies using Ni(111). Both proposed that CO_2 methanation proceeds with CO as intermediate, suggesting a mechanism based on several elementary steps consisting in two different processes: carbon formation (from CO_2 dissociation into CO and O, and the subsequent CO dissociation into C and O) and C hydrogenation to CH_4, being concluded that CO dissociation was the rate-determining step of the process. Zhao et al. [32] also developed self-supported cobalt nanoparticles composed of $Co_x(CoO)_{1-x}$ with different ratios of x = Co/(Co + CoO) via reduction of precursor Co_3O_4. The $Co_{0.2}(CoO)_{0.8}$ sample exhibited the highest catalytic performances and was active even at low temperatures (160–180 °C), which was attributed to the increased amount and moderate binding of adsorbed CO_2 on CoO sites. However, these results were obtained with a significantly high contact time.

Going back to the main purpose of this review, the following paragraphs will be divided based on the support nature applied in the CO_2 methanation reaction, as shown in Figure 2. Inside each

section, a brief elaboration of the type of metal used, the method of the support preparation, the way of the metal active phase deposition and the type of promoter used will be presented equally. Needless to say, a deep analysis of the efficiency of the prepared materials will be explained in order to help researchers in finding the best route for achieving a robust catalyst capable of reaching high catalytic conversions and high rates at even low temperatures.
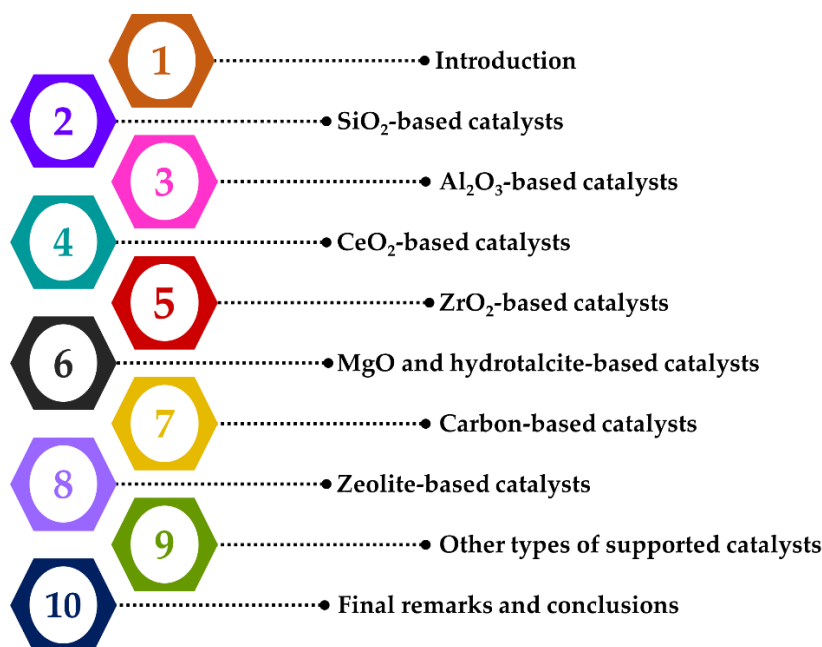

Figure 2. Structure of the present review article in terms of chapters and corresponding topics.

2. SiO$_2$-Based Catalysts

Regarding the use of supported catalysts, the firstly analyzed material is SiO$_2$. The main catalytic systems found in the literature and the type of metal dispersed over the silica surface can be viewed in Table 1. with the most remarkable findings summarized below.

Table 1. SiO$_2$-based materials reported in literature for CO$_2$ methanation reaction.

Catalyst	Preparation Method	T_{red} (°C)	H$_2$:CO$_2$	Q_T/W (mL g^{-1} h^{-1})	Best Catalytic Performances			Ref.
					T (°C)	X_{CO2} (%)	S_{CH4} (%)	
*10*Ni/SiO$_2$	Impregnation	500	4:1	120,000	350	10	90	[33]
*40*Ni/SiO$_2$	Impregnation	500	4:1	10,000	370	62	90	[34]
*40*Ni/SiO$_2$	Ammonia-evaporation	500	4:1	10,000	370	80	95	[34]
*10*Ni-MgO/SiO$_2$	Co-impregnation	450	4:1	24,000	400	72	98	[35]
*6.2*Pd-MgO/SiO$_2$	Reverse microemulsion	450	4:1	7320	450	59	95	[36,37]
*80*Ni-Co/SiO$_2$	Co-precipitation	350	4:1	30,000	350	49	98	[38]
*1*Rh/CeO$_2$/SiO$_2$	Impregnation	500	3:1	n.a.	230	10	n.a.	[39]
*6*Ni-La-Mo/SiO$_2$	Impregnation	700	4:1	15,000	300	75	100	[40]

2.1. Monometallic SiO$_2$-Supported Catalysts

Wu et al. [33] studied SiO$_2$-supported catalysts with 0.5 and 10 wt% Ni incorporated by impregnation. They reported that the verified differences in the Ni^0 particles size between the samples with different Ni loadings led to a strong effect on the kinetic parameters of CO$_2$ hydrogenation, the formation pathways of CO and CH$_4$ and the reaction selectivity. Higher Ni loading enhanced the CH$_4$ selectivity while, with 0.5 wt% of Ni, the formation of CO was more relevant. In addition, Ye et al. [34]

synthesized two Ni/SiO$_2$ catalysts using different preparation methods: ammonia evaporation and impregnation. While ammonia evaporation led to the formation of nickel phyllosilicate, impregnation promoted the incorporation of Ni as NiO. The higher performances revealed by the sample prepared by ammonia evaporation were attributed to the NiPS phase, playing a relevant role in the reaction due to its lamellar nature, responsible for an increased specific surface area, a higher number of surface acids groups and the anchoring of well-dispersed Ni nanoparticles in the channels, establishing stronger metal-support interactions.

2.2. Bi- and Trimetallic SiO$_2$-Supported Catalysts

Guo et al. [35] prepared Ni–Mg/SiO$_2$ catalysts (10 wt% Ni and 1, 2 or 4 wt% Mg) in order to evaluate the effects of Mg loading and the impregnation strategy (co-impregnation or sequential) in the performances. Authors reported that the incorporation of 1 wt% of Mg as MgO was responsible for an enhancement of Ni species dispersion by suppressing sintering phenomenon on Ni particles. Additionally, MgO favored CO$_2$ adsorption and activation. Complementary, co-impregnation led to the highest activity and stability, which was attributed to the synergistic effects established between Ni and Mg species. Park et al. [37] studied Pd/SiO$_2$, Mg/SiO$_2$, Pd–Mg/SiO$_2$, Pd–Fe/SiO$_2$, Pd–Ni/SiO$_2$, Ni/SiO$_2$ and Pd–Li/SiO$_2$ catalysts prepared by reverse microemulsion. Authors prepared other two samples (Pd/SiO$_2$ and Mg/Pd/SiO$_2$) using the impregnation method for comparison purposes. They obtained the highest performances with 6.2%Pd–3.6%Mg/SiO$_2$ sample (synthesized by reverse microemulsion), consisting of Pd aggregates within an amorphous Mg–Si oxide matrix. They also verified that replacing Mg by Fe or Ni led to the same activity while the selectivity to CH$_4$ was considerably lower, especially in the Pd–Fe/SiO$_2$ sample. Furthermore, Ali et al. [38] studied Ni–Co/SiO$_2$ catalysts prepared by co-precipitation of the Ni and Co precursor salts and the Si source (TEOS) with 80 wt% Ni and 20 wt% Co. Authors evaluated the effect of the calcination temperature (300, 350, 400, 450 and 500 °C) in the metallic species and textural properties, with the best results being obtained with 400 °C and attributed to the lower size of the Ni and Co particles in this sample.

Branco et al. [41] studied the effects of adding lanthanides (La, Ce, Pr, Sm, Dy and Yb) to the formulation of Ni-supported SiO$_2$ catalysts. Authors prepared silica by electrospinning and added the metals by impregnation method. Lanthanides were responsible for an important improvement of the catalytic performances, which was attributed to the enhancement of nickel reducibility and dispersion as well as to the increase of the basicity. Among all, Pr was identified as the most outstanding promoter. Trovarelli et al. [39] prepared SiO$_2$-supported catalysts containing 1 wt% Rh and 1.6 to 28.4 wt% CeO$_2$ (Rh/CeO$_2$, Rh/SiO$_2$, Ce/SiO$_2$, Rh–Ce/SiO$_2$). They concluded that smaller CeO$_2$ crystallites are formed when supporting CeO$_2$ on SiO$_2$. In addition, Rh was found as responsible for a further re-dispersion of CeO$_2$ crystallites. The high activity and selectivity revealed by Rh/CeO$_2$/SiO$_2$ samples was attributed to the presence of surface vacancies at the interface between Rh and CeO$_2$, enhancing CO$_2$ activation. Li et al. [40] studied the performances of LaNi$_{1-x}$Mo$_x$O$_3$ oxides with perovskite-type structure (6.0 wt% Ni and 1.0, 1.5 and 2.0 wt% of Mo) supported over SiO$_2$. For comparison purposes, they also prepared three additional catalysts: LaNiO$_3$/SiO$_2$, LaMoO$_3$/SiO$_2$ and unsupported LaNiO$_3$. As a result, the presence of Mo in the sample contributed to higher catalytic performances and stability. Indeed, the positive effect of this metal was further enhanced when intensifying its loading since it revealed much higher resistance to Ni nanoparticles sintering. Finally, Vogt et al. [42] evaluated the effect of KOH (derived from H$_2$ production process) in the activity of Ni-based SiO$_2$ catalysts. Authors applied in situ (setup combining H$_2$O electrolysis and CO$_2$ methanation steps) and ex situ (KOH impregnation over Ni/SiO$_2$ catalysts) strategies and verified that, while the first increases the obtained catalytic performances, the second leads to catalysts deactivation. They attributed the negative effect of impregnating KOH over the catalysts to the establishment of stronger interactions with CO, thus limiting CO$_2$ methanation. On the contrary, KOH aerosols (in situ) could, according to the authors, increase the hydrogenation rate of CH$_x$ species and/or even facilitate water formation/desorption.

2.3. Mesoporous Silica-Based Catalysts

In the last years, mesoporous-based samples and especially silicas such as KIT–6, SBA–15, MCM–41 or KCC–1 have gained a great attention due to their positive feature of managing in confining nickel particles preventing sintering. The main reported findings on such type of supports are discussed below and summarized in Table 2.

Table 2. Mesoporous SiO_2-based materials reported in literature for CO_2 methanation reaction.

Catalyst	Preparation Method	SA [a] (m² g⁻¹)	T_{red} (°C)	$H_2:CO_2$	Q_T/W (mL g⁻¹ h⁻¹)	Best Catalytic Performances			Ref.
						T (°C)	X_{CO2} (%)	S_{CH4} (%)	
5Rh/MSN	Impregnation	933 (3.6)	500	4:1	50,000	350	99	100	[43]
10Ni/MSN	Impregnation	662 (3.5)	500	4:1	50,000	350	85	100	[44]
50Ni/MSN	Impregnation	134 (2.3)	450	4:1	15,000	375	96	100	[45]
20Co/KIT–6	Impregnation	369 (6.4)	400	4.6:1	22,000	280	49	100	[46,47]
25Co–KIT–6	Impregnation	323 (~8)	400	4:1	60,000	360	53	95	[48,49]
Fe–KIT–6	HS [b]	435 (6.5)	350	4:1	50,000	500	16	3	[50]
20Ni–V₂O₅/KIT–6	Impregnation	n.a.	550	4:1	96,000	350	87	100	[51]
15Ni-SBA–15	One-pot HS [b]	574 (4.5)	500	4:1	10,000	420	76	96	[52]
10Ni/SBA–15	Grafting	551 (6.3)	550	4:1	20,000	450	80	92	[53]
15Ni/SBA–15	Impregnation	235 (8.7)	470	4:1	86,200	400	65	93	[54]
CeO₂/15Ni/SBA–15	Impregnation	320 (8.3)	470	4:1	86,200	350	70	97	[54]
74Ni–Pd/SBA–15	Impregnation	535 (6.4)	600	4:1	6000	430	96	97	[55]
3Ni–MCM–41	One-pot HS [b]	1480 (2.9)	700	4:1	5760	400	17	96	[56]
15Ni/MCM–41	Impregnation	847 (1.9)	470	4:1	86,200	400	70	93	[54]
CeO₂/15Ni/MCM–41	Impregnation	589 (2.0)	470	4:1	86,200	400	75	95	[54]
20Ni–CeO₂/MCM–41	Deposition-precipitation	302 (4.6)	470	4:1	3000	380	86	100	[57]
Ni–Y₂O₃/MgO–MCM–41	DS method [c]	445 (3.4)	600	4:1	9000	400	65	85	[58]
KCC–1	Microemulsion	773 (4.6)	550	4:1	50,000	450	49	84	[59]
5Co/KCC–1	Impregnation	318 (4.9)	500	4:1	4500	400	72	n.a.	[60]
5Ni/KCC–1	Impregnation	537 (4.7)	500	4:1	4500	400	93	>95	[60]
20Ni/KCC–1	Impregnation	216 (3.4)	500	4:1	12,000	375	82	98	[61]
10Ni/FDU–12	Impregnation	506 (8.6)	600	4:1	60,000	425	79	97	[62]
10Ni–CeO₂/FDU—12	Impregnation	500 (8.7)	600	4:1	60,000	400	81	97	[62]

[a] Surface area determined by Brunauer–Emmett–Teller (BET) method. Values in brackets in this column correspond to pore diameters (nm); [b] Hydrothermal synthesis; [c] Direct synthesis method.

- Mesoporous silica nanoparticle (MSN)-based catalysts

Mesoporous silica nanoparticles (MSNs) present unique characteristics such as an ordered and nanosize porous structure with well-defined and tunable pore sizes (1.5–10 nm) and high textural properties (e.g., pore volume, surface area) [63]. Aziz et al. [43] studied metal-promoted mesostructured silica nanoparticles (MSN, prepared by sol-gel method) using 5 wt% of Rh, Ru, Ni, Fe, Ir, Cu, Zn, V, Cr, Mn, Al or Zr incorporated by impregnation. Authors found that Rh/MSN catalyst was the most active while Ir/MSN presented the poorest activity. Additionally, no catalytic activity was revealed by the Zn/MSN, V/MSN, Cr/MSN, Mn/MSN, Al/MSN and Zr/MSN in the studied temperature range. The same authors [63] prepared 5 wt% Ni-based catalysts supported on MSN, MCM–41, HY zeolite, SiO_2 and Al_2O_3. The activity was found to follow the order: Ni/MSN > Ni/MCM–41 > Ni/HY > Ni/SiO₂ > Ni/Al₂O₃. The better results of the MSN supported catalyst were assigned to the presence of both intra- and inter-particle porosity, which led to a higher concentration of basic sites in this sample. Researchers who worked on these materials also verified the relevance of the basicity in the catalytic performances and highlighted the fact that CO_2 methanation activity increased with the concentration of basic sites. Again, same authors [44] studied the influence of Ni loading and the presence of steam in the reactor feed flow. Regarding the metal content, the catalytic results of the prepared materials followed the order: 10%Ni/MSN ≈ 5%Ni/MSN > 3%Ni/MSN > 1%Ni/MSN. However, higher Ni loadings decreased catalysts crystallinity, surface area and basic sites. Consequently, the order of the obtained performances was due to a balance between basic sites and available metallic Ni sites. Additionally, authors emphasized that the presence of steam in the feed stream induced a negative effect on the activity (30% of activity loss after 5 h) and attributed this behavior to the formation of

CO_2 through the water gas shift (WGS) reaction between intermediate CO molecules and the excess of water, to the acceleration of Ni sintering and to the collapse of the support. Recently, Nguyen et al. [45] reported a highly active 50 wt% Ni-MSN catalyst. MSN support was prepared by sol-gel method while Ni was incorporated by impregnation using urea together with nickel nitrate, which was responsible for an enhancement in the reducibility and dispersion of Ni species and favored CO_2 adsorption capacity. They also optimized the calcination time (2, 3 or 4 h) and verified the best results when using the intermediate value (3 h). They finally included 1% of CO in the reaction flow, increasing the overall yield by its effective conversion to CH_4.

- KIT–6-based catalysts

KIT–6 mesoporous silica presents a 3–D channel network with thick pore walls, hydrothermal stability, high surface area and large pore volume [64,65]. Its interconnected 3–D structure promotes the location of active species inside the porous system, favoring metallic dispersion and diffusional processes and hindering pores blockage [64,65]. Zhou et al. [46,47] prepared mesoporous Co/KIT–6 and Co/meso–SiO_2 catalysts with the same Co content (wt% not specified) via hydrogen reduction. Co was better dispersed on KIT–6 than on SiO_2, explaining the higher activity revealed by Co/KIT–6 sample. In addition, the highly ordered and mesoporous structure of the Co/KIT–6 catalyst improved the selectivity to CH_4. Liu et al. [48] studied the effect of Co content on the performances of Co/KIT–6 catalysts, concluding that the best Co loading was 25 wt%. However, for the 15 to 20 wt% Co loading based samples there was a limitation in the number of active sites. In addition, 30 wt% Co catalyst presented larger and less dispersed Co particles with lower specific surface area and a disordered pore structure that hindered the diffusion and migration of CO_2 and H_2 molecules towards Co active sites. The same authors [49] investigated the influence of the reduction temperature in Co/KIT–6 catalysts activity towards CO_2 methanation. They obtained the best results by reducing the sample at 400 °C, due to the larger specific surface area formed, the higher number of Co species reduced and the increased CO_2 adsorption and activation capacity. Additionally, Merkache et al. [50] prepared Fe–KIT–6 materials with Si/Fe molar ratios of 10, 30 and 60. The best performances were reported for the sample with higher Fe content (n_{Si}/n_{Fe} = 10) and were attributed to the higher concentration of metallic active sites on the KIT–6 structure. Cao et al. [51] reported recently Ni–V/KIT–6 catalysts, with metal loadings varying from 5 to 40 wt% Ni and 0.1 to 2 wt% V. They obtained the best results when using 20 wt% Ni and 0.5 wt% V, achieving a high metal dispersion. The surface basicity of the materials was further boosted by a synergistic effect between Ni and V (present as V_2O_5 in the catalysts).

- SBA–15-based catalysts

SBA–15 presents dual porosity composed by mesoporous and intrawall micropores or secondary mesoporous channels. It presents large surface areas, thick pore walls (3–6 nm), uniformly distributed cylindrical channels (5–10 nm) and high hydrothermal stability [66]. Liu et al. [52] prepared Ni-based SBA–15 catalysts by one-pot hydrothermal method with a 3–D network structure and 15 wt% of Ni. For comparison purposes, they also prepared an impregnated sample containing 15 wt% Ni over SBA–15 support. Ni/SBA–15$_{One-pot}$ catalyst presented higher surface area, larger pore volume, better dispersion, higher catalytic activity and anti-sintering properties for Ni^0 particles. In addition, Lu et al. [53] prepared Ni/SBA–15 catalysts by grafting method. A chemical bond was formed between silicon and Ni atoms via an oxygen atom (–O–Ni–O–Si–O–), by using Ni ammonia complex ions with NH_3/Ni molar ratios of 2 to 4 (equivalent to 4 to 10 wt% Ni). No bulk nickel oxides were depicted in the Ni-grafted SBA–15 sample and the CO_2 conversion and methane selectivity were higher than those obtained for equivalent Ni/SBA–15 catalysts prepared by impregnation. Authors also indicated that the increase of the Ni content enhanced the activity and selectivity. Bacariza et al. [54] prepared Ni and Ce/Ni impregnated SBA–15 catalysts with 15 wt% Ni and 15 wt% Ce and with SBA–15 prepared by a conventional and a microwaves-assisted hydrothermal treatment. Despite the synthesis method of the support, relevant performances were detected, with the microwave-method sample presenting

slightly higher conversions, especially between 250 and 350 °C. Additionally, an enhancement of the performances was observed by adding Ce, being this attributed to the role of CeO_2 species as active sites for CO_2 activation. Finally, Li et al. [55] investigated bimetallic Ni–Pd/SBA–15 alloy catalyst for selective hydrogenation of CO_2 to methane by changing the atomic ratio of Ni/Pd ($Ni_{0.25}Pd_{0.75}$, $Ni_{0.50}Pd_{0.50}$ and $Ni_{0.75}Pd_{0.25}$). Regarding the metal content, the order of catalytic activity was the following: $Ni_{0.75}Pd_{0.25}$/SBA–15 > $Ni_{0.50}Pd_{0.5}$/SBA–15 > $Ni_{0.25}Pd_{0.75}$/SBA–15 > Ni/SBA–15 > Pd/SBA–15. The excellent catalytic activity of $Ni_{0.75}Pd_{0.25}$/SBA–15 was related to the synergistic effect between Ni and Pd species. In this way, the charge transfer from Pd to Ni atoms provided a negative charged surface, which promoted the activation of CO_2 and the dissociation of intermediates into CH_4, crucial for improving the catalytic performance.

- MCM–41-based catalysts

MCM–41 presents a purely mesoporous 2–D hexagonal structure formed by unidirectional and non-interconnecting cylindrical pores (2–10 nm of diameter) [67,68]. Du et al. [56] reported 1 to 3 wt% Ni containing MCM–41 samples with Ni ions incorporated into the MCM–41 structure. Well-dispersed Ni^0 species were formed in the samples, especially after reduction at high temperature (700 °C), leading to superior performances. Additionally, Bacariza et al. [54] prepared Ni and Ce/Ni-based MCM–41 catalysts with 15 wt% Ni and 15 wt% Ce. These samples presented greater activity than equivalent SBA–15 catalytic systems. MCM–41 was found as capable of promoting the metal-support interactions, favoring the CO_2 and H_2 activation. Additionally, the lower affinity of MCM-41 to water served as another advantage in encountering the water produced as a product in the reaction (according to the literature [44,69,70]). Finally, and as mentioned previously for other type of mesoporous silica supports, the incorporation of Ce to the Ni/MCM–41 sample triggered a boost in its performance during the methanation reaction. To better emphasize on this point, Wang et al. [57] also prepared Ni/MCM–41 promoted with CeO_2, containing different CeO_2 loadings (0, 10, 20, 30 wt%). The addition of CeO_2 improved the dispersion of Ni on the support, providing a larger specific metallic surface area and a higher reducibility. Besides, the interaction between Ni active sites, CeO_2 and the support facilitated the activation of adsorbed CO_2 species at low temperatures. Thus, within a certain composition range, the incorporation of CeO_2 was able to improve the catalytic performances, with 20 wt% CeO_2 leading to the best catalytic activity and stability. Recently, Taherian et al. [58] reported the beneficial effects of incorporating Y and Mg to Ni-based MCM–41 catalysts synthesized by direct synthesis method. The incorporation of these two metals to the MCM–41 mesoporous system decreased the average Ni^0 size by improving Ni species reducibility and creating new active sites for CO_2 activation.

- KCC–1-based catalysts

KCC–1 is formed by a fibrous surface morphology arranged in a 3–D structure forming nanospheres. Its fibrous structure facilitates the accessibility to the available surface area and improves the hydrothermal and mechanical stability [71]. Hamid et al. [59] prepared a KCC–1 material by microemulsion and used it as catalyst for CO_2 methanation in absence of active metals sites. They compared the synthesized sample to MCM–41 and SiO_2 materials. As a result, KCC–1, which presented higher basicity and oxygen vacancies than MCM–41 and SiO_2, led to the best performances. It was proposed that both CO_2 and H_2 were activated and dissociated in the KCC–1 support oxygen vacancies, where the CO_2 interaction with the material is related to the basicity. The same authors [60] reported promising results when loading KCC–1 mesoporous support with 5 wt% of Ni, Co or Zn, with superior behavior found for Ni/KCC–1. Recently, Lv et al. [61] evaluated the effects of impregnating increasing Ni loadings (5 to 25 wt%) over a fibrous KCC–1 nanospheres synthesized by microemulsion hydrothermal method. 20 wt% Ni sample exhibited better results than those found for equivalent Ni/SiO_2 and Ni/MCM–41 catalysts. The formation of dendrimer mesoporous channels not only improved the metallic dispersion due to the confinement effect but also hindered the occurrence of sintering processes. Furthermore, the appearance of intermediate carbonate species was faster when using Ni/KCC–1 instead of Ni/SiO_2 or Ni/MCM–41.

- FDU–12-based catalysts

FDU–12 is a 3–D ordered mesoporous silica with a face-centered cubic structure. It presents a window of ~9 nm and pore cages with sizes ranging from 12 to 42 nm. Its structure presents advantages when comparing to SBA-15 or MCM-41, such as higher resistance towards pores blockage due to its cage-like network [62]. Recently, Liu and Dong [62] reported, for the first time, Ni-based FDU–12 catalysts for CO_2 methanation. Authors prepared a series of 10 wt% Ni-containing FDU–12 and evaluated the influence of the impregnation solvent (water or ethylene glycol) and the effects of doping the catalysts with trehalose and Ce (3 wt%). A remarkable reduction of the average Ni^0 particle size was observed when using ethylene glycol (5.9 nm) instead of water (10 nm). These values were further improved (from 5.9 to 2.6–3.3 nm) by incorporating increasing amounts of trehalose in the impregnation solution, while Ce did not influence this parameter. The enhancement of the metallic dispersion was responsible for an improvement of the catalytic performances, being a CH_4 yield >75% obtained at 425 °C for the 10Ni/FDU–12 catalyst prepared using ethylene glycol and a fraction of trehalose. Complementarily, the already reported positive effect of Ce in the reaction was proved, being the activity boosted at lower reaction temperatures (<350 °C). Finally, authors also verified a reduction of the activation energy with the optimization of the impregnation solvent and Ce incorporation (from 116.23 to 77.49 kJ mol^{-1}).

- Comparative analysis

Taking into account the various experimental conditions used in the works reported in the literature, a proper comparison among the different types of mesoporous silica supports is difficult to establish. In this way, in an attempt to compare monometallic catalysts prepared by impregnation method, CH_4 formation rates as a function of the mass of catalyst (mol CH_4 s^{-1} g$_{cat}$$^{-1}$) and metal (mol CH_4 s^{-1} g$_{metal}$$^{-1}$) were determined, far from thermodynamic equilibrium, for a series of Ni and Co-supported SiO_2 [34] (reference), MSN [45], KIT–6 [46], SBA–15 [54], MCM–41 [54], KCC–1 [61] and FDU–12 [62] (Figure 3). As seen, the use of Ni instead of Co leads generally to better performances, which insists on the suitability of Ni as CO_2 methanation active metal. Additionally, SBA–15, MCM–41 and FDU–12 are the materials leading to the most outstanding results, both per g$_{catalyst}$ and g$_{metal}$. The catalytic performances obtained for the different mesoporous silicas will be likely influenced by several factors such as the metallic dispersion, the activation induced by the support (resulting from the metallic-support interactions), the location of the metal, the ability to activate carbon dioxide (adsorption sites, pores acting as CO_2 reservoir) or even the hydrophobicity. Even with well-designed, systematic and specific studies reported in the literature, no definitive conclusions regarding the superior performances revealed by SBA-15, MCM-41 or FDU-12 catalysts can be drawn (e.g., it is not possible to quantify certainly the contribution of each individual factor to the activity).
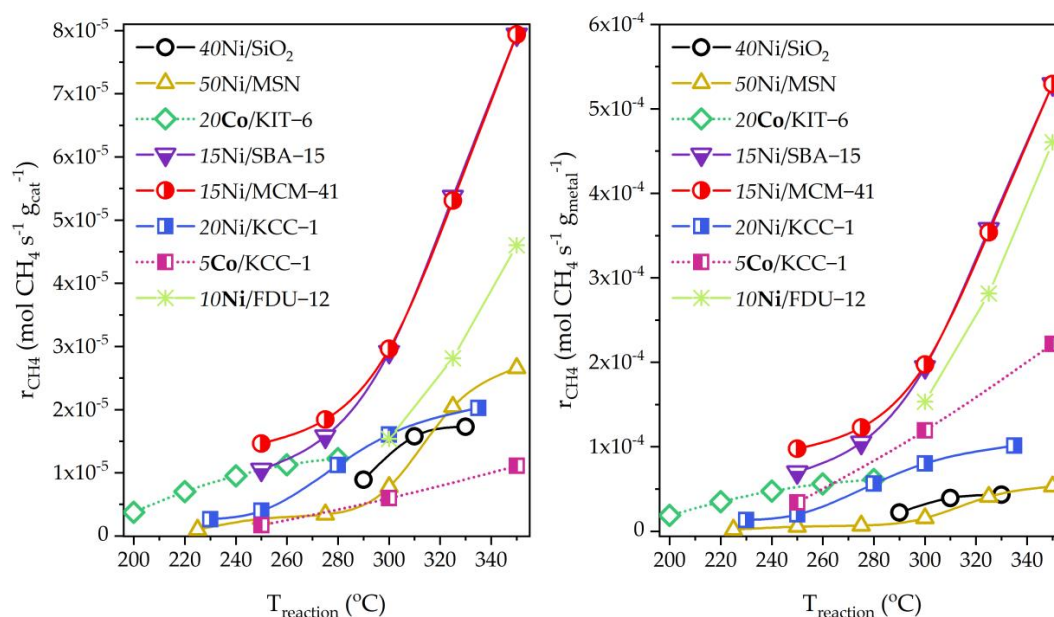
Figure 3. CH_4 production rates per mass of catalyst (left) or metal (right) determined, far from thermodynamic equilibrium, for a series of Ni and Co-supported silica materials prepared by impregnation method as a function of the reaction temperatures. Italic numbers correspond to the wt% of metal in the catalysts.

2.4. Mechanistic Aspects

Wu et al. [33] reported that Ni loading affects the selectivity to methane and the mechanism pathways over Ni/SiO_2 catalysts (Figure 4–Left). Indeed, they prepared two 0.5 and 10 wt% Ni/SiO_2 samples and proposed that formate species in a monodentate configuration are involved in CO_2 hydrogenation on both cases. On one hand, the consecutive pathway, which was favored on small Ni particles (0.5%Ni/SiO_2 catalyst, Ni^0 average size < 1 nm), was attributed to low H_2 coverage on the Ni surface, leading to dissociation of formate intermediates resulting in CO formation and high CO selectivity. On the other hand, the reaction on large Ni particles (10%Ni/SiO_2 catalyst, Ni^0 average size of 9 nm, stronger H_2 adsorption and enhanced H_2 coverage), was proposed to be controlled by mixed consecutive and parallel routes, promoting formate species hydrogenation to CO or CH_4 as part of a parallel reaction pathway. The sites corresponding to kink, corner or step positions on the Ni/SiO_2 surface were proposed as the primary active sites for CO_2 hydrogenation. In addition, Park et al. [36,37] proposed a bifunctional mechanism for $Pd–MgO/SiO_2$ catalysts (Figure 4–Right). They considered CO_2 adsorption over MgO as a surface carbonate that is sequentially hydrogenated to form methane. Consequently, in this mechanism an active metal (Pd in this case) is required for the dissociation of H_2 and the supply of H atoms to the CO_2 derived species activated on Mg sites.

Regarding mesoporous silica-based catalysts, Aziz et al. [43] considered CO as a reaction intermediate in CO_2 methanation over Ni/MSN catalysts. Indeed, they proposed the dissociation of CO_2 into CO and O on the Ni surface and the progressive hydrogenation of CO into methane. Due et al. [56] also suggested that CO_2 methanation passes through CO as intermediate over Ni/MCM-41 catalysts. Finally, Hamid et al. [59] suggested a mechanism for CO_2 methanation over KCC-1 (Figure 5), where CO_2 was activated on oxygen vacancies forming adsorbed carbonyl species. They demonstrated that linear carbonyl species were the precursors for CH_4 formation. Additionally, they implied that hydrogen was activated and dissociated in E' centres (defined as dangling bonds, $\equiv Si^*$, formed on the SiO_x material for x < 2) acting as active sites and giving rise to atomic H species.
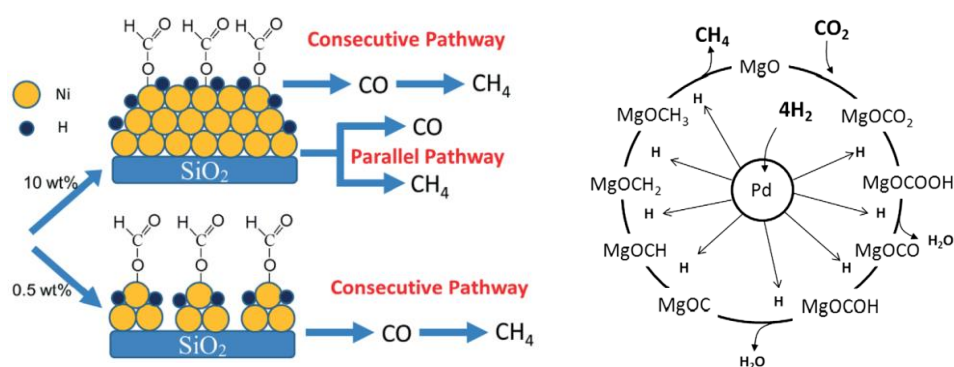
Figure 4. Mechanisms proposed for Ni/SiO$_2$ (left—reproduced with permission from Wu et al., Catalysis Science and Technology; published by Royal Society of Chemistry, 2015) [33] and Pd-MgO/SiO$_2$ (right—reproduced with permission from Park and McFarland, *Journal of Catalysis*; published by Elsevier, 2009) [37] catalysts, respectively.
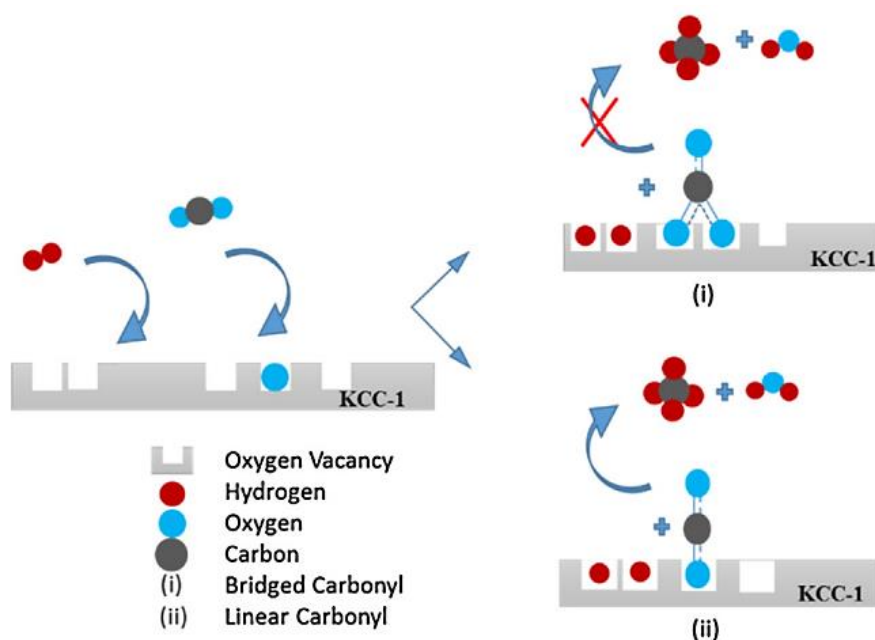

Figure 5. Mechanism proposed for KCC-1 catalysts [59]. Reproduced with permission from Hamid et al., *Applied Catalysis A*: General; published by Elsevier, 2017.

3. Al$_2$O$_3$-Based Catalysts

Alumina-based catalysts are, without doubt, the most commonly used in carbon dioxide methanation reaction. In summary, the main reported catalytic systems are disclosed below in Table 3, while the corresponding conclusions of the published works will be deeply discussed in the upcoming paragraphs.

Table 3. Al$_2$O$_3$-based materials reported in literature for CO$_2$ methanation reaction.

Catalyst	Preparation Method	T_{red} (°C)	H$_2$:CO$_2$	Q_T/W (mL g^{-1} h^{-1})	Best Catalytic Performances			Ref.
					T (°C)	X_{CO2} (%)	S_{CH4} (%)	
55Ni/Al$_2$O$_3$	Impregnation	n.a.	5:1	n.a.	500	71	86	[72,73]
12Ni/Al$_2$O$_3$	Impregnation	500	5:1	30,000	425	80	100	[74]
3Ru/Al$_2$O$_3$	Impregnation	n.a.	5:1	n.a.	350	95	96	[75]
4Ru/Al$_2$O$_3$	Impregnation	300	5:1	30,000	375	85	100	[74]

Table 3. *Cont.*

Catalyst	Preparation Method	T_{red} (°C)	H_2:CO_2	Q_T/W (mL g^{-1} h^{-1})	Best Catalytic Performances			Ref.
					T (°C)	X_{CO2} (%)	S_{CH4} (%)	
*30*Ni–Fe–Al$_2$O$_3$	Co-precipitation	700	4:1	9600	220	58	99	[76]
*13*Ni–Fe–γ–Al$_2$O$_3$	Co-precipitation	500	4:1	353,000	450	66	92	[77]
*36*Ni–Fe–Al$_2$O$_3$	Co-precipitation	500	4:1	150,000	325	98	99	[78]
*36*Ni–Mn–Al$_2$O$_3$	Co-precipitation	500	4:1	150,000	300	92	99	[79]
*8*Ni–Co–Al$_2$O$_3$	EISA one-pot	800	4:1	15,000	400	80	98	[80]
*10*Ni–Co/γ–Al$_2$O$_3$	Impregnation	400	4:1	130	325	90	100	[81]
*20*Ni/CeO$_2$/γ–Al$_2$O$_3$	Impregnation	450	3.5:1	9000	350	80	100	[82]
*15*Ni–CeO$_2$/Al$_2$O$_3$	Co-impregnation	500	4:1	15,000	350	85	100	[83]
CeO$_2$/*42*Ni–Al$_2$O$_3$	Hydrothermal	500	4:1	n.a.	250	90	99	[84]
*2*Ru/CeO$_2$/Al$_2$O$_3$	Impregnation	500	4:1	72	350	90	100	[85]
*12*Ni–Pr/γ–Al$_2$O$_3$	Impregnation	750	4:1	6000	300	98	100	[86]
*15*Ni–Mg–Al$_2$O$_3$	EISA one-pot	800	4:1	86,100	400	70	96	[87]
*15*Ni–CeO$_2$–ZrO$_2$/γ–Al$_2$O$_3$	Impregnation	600	4:1	3000	300	90	100	[88]
*5*Ru/Mn/CeO$_2$/Al$_2$O$_3$	Impregnation	n.a.	4:1	636	200	98	91	[89]
*5*Ru/Mn/Ni/Al$_2$O$_3$	Impregnation	n.a.	4:1	500	400	100	72	[90]
(CaO/*11*NiTiO$_3$)/γ–Al$_2$O$_3$	Impregnation	700	4:1	n.a.	400	53	n.a.	[91]
*12*Ni/(ZrO$_2$–Al$_2$O$_3$)	Impregnation	450	3.5:1	8100	360	70	70	[92]
*10*Ni/(Al$_2$O$_3$–ZrO$_2$)	Epoxide-driven sol-gel	500	4:1	6000	340	77	100	[93]
*5*Ru/(TiO$_2$–Al$_2$O$_3$)	Impregnation	400	4:1	60,000	375	82	100	[94]
*15*Ni/(CaO–Al$_2$O$_3$)	Impregnation	500	4:1	n.a.	450	66	92	[95]
*10*Ni–Ru–(CaO–Al$_2$O$_3$)	EISA one-pot	600	4:1	30,000	380	84	100	[96]
*20*Ni/(γ–Al$_2$O$_3$–ZrO$_2$–TiO$_2$–CeO$_2$)	Impregnation	500	4:1	20,000	300	82	98	[97]
*20*Ni/(γ–Al$_2$O$_3$–ZrO$_2$–TiO$_2$–CeO$_2$)	Impregnation	500	4:1	60,000	350	90	n.a.	[98]

3.1. Monometallic Al$_2$O$_3$-Supported Catalysts

Garbarino et al. [73] studied Ni/Al$_2$O$_3$ catalysts prepared by impregnation and with 16, 39 and 125 wt% of Ni by wt% of support. Authors performed catalytic tests without a pre-reduction treatment and obtained very low activities, confirming that Ni^0 species are indeed required for obtaining significant CO$_2$ conversion degrees. They demonstrated also that the higher the Ni content, the larger the particles but also the greater the number of active sites. Consequently, these two parameters affecting in opposite ways the performances contributed to the following activity results order: 125%Ni/Al$_2$O$_3$ > 16%Ni/Al$_2$O$_3$ > 39%Ni/Al$_2$O$_3$. The same authors [72] synthesized Ni nanoparticles (NPs) with <8 nm of size and compared their performances with the ones obtained for 125%Ni/Al$_2$O$_3$ catalyst from their previous work. Better outcome was obtained for 125%Ni/Al$_2$O$_3$ (with Ni particles of ~36 nm), while Ni NPs resulted in poorly active metallic sites. They came up with a hypothesis that the support could play a role in the activation of CO$_2$ while Ni nanoparticles could be mainly responsible for the H$_2$ dissociation, which explains the better results obtained for the supported Ni catalyst. Lately, they also reported a study comparing two 3 wt% Ru and 20 wt% Ni based Al$_2$O$_3$ catalysts [75] revealing that, despite the higher metal content of the Ni sample, Ru/Al$_2$O$_3$ led to higher performances due to the favored dispersion of Ru species. Quindimil et al. [74] investigated the influence of the metal nature (Ni, Ru) and loading (4 to 20 wt% for Ni and 1 to 5 wt% for Ru) on CO$_2$ methanation catalysts supported on Al$_2$O$_3$. Authors clearly observed that, in both cases, higher metal loading enhanced the catalytic performances, which could be due to the increase of active metal sites available for H$_2$ dissociation. However, for Ni/Al$_2$O$_3$ series, metallic dispersion decreased with metal loading due to the formation of larger particles, while the dispersion of Ru/Al$_2$O$_3$ was not significantly influenced. Moreover, it was suggested that the reducibility of the catalysts plays a key factor in the catalytic performances. Indeed, the complete reduction of ruthenium species was achieved at 250 °C, whereas for nickel-based catalysts a temperature of 900 °C was required, reducing the available Ni^0 sites for H$_2$ dissociation. Besides, at low temperature (T < 300 °C), turnover frequency (TOF) values for Ru/Al$_2$O$_3$ were considerably higher than those found for Ni/Al$_2$O$_3$, which indicates that Ru is more effective than Ni in H$_2$ dissociation. Taking this into account and considering the saturation effect on CO$_2$ conversion with metal loading, the best performances were obtained by 12%Ni/Al$_2$O$_3$ and 4%Ru/Al$_2$O$_3$

formulations, with Ru catalyst leading to higher conversion and CH_4 selectivity. As a final remark, no works studying the influence of chloride and/or chlorine doping over Ru/Al_2O_3 catalysts were found in the literature so far. This strategy could be interesting for Sabatier reaction, as promising results were reported for CO methanation [99–101].

3.2. Bimetallic Al_2O_3-Supported Catalysts

Hwang et al. [76] studied 20%Ni–5%Fe–Al_2O_3 catalysts prepared by co-precipitation using different precipitation agents (($NH_4)_2CO_3$, Na_2CO_3, NH_4OH or NaOH). They verified that Ni^0 dispersion was enhanced by using ammonium carbonate, favoring both the CO_2 conversion and the CH_4 selectivity. Serrer et al. [77] also studied the effect of Fe in Ni–Fe–γ–Al_2O_3 catalysts synthesized via homogeneous precipitation with urea, a method optimized in previous publications from the same authors [102,103]. During catalyst activation, authors observed a synergistic effect between nickel (13 wt%) and iron (4 wt%) that led to higher fractions of reduced nickel compared to the monometallic 17 wt% Ni/γ–Al_2O_3 reference. Ni remained in its reduced metal state under CO_2 methanation conditions. On the contrary, the oxidation of Fe^0 was immediately observed. This indicated that Fe exhibits a highly dynamic behavior through a $Fe^0 \rightleftharpoons Fe^{2+} \rightleftharpoons Fe^{3+}$ redox cycle, likely located at the interface between the FeO_x clusters and the surface of the metal particles, which promoted CO_2 dissociation during the reaction. Burger et al. [79] reported also highly active and thermally stable Mn- and Fe-promoted $NiAlO_x$ catalysts prepared by co-precipitation and tested under CO_2 methanation conditions using a pressure of 8 bar. They concluded that while Mn improves the CO_2 adsorption capacity (especially in terms of medium basic sites) without significantly modifying the available nickel surface area, Fe promotes thermal stability through the formation of a Ni–Fe alloy and slightly increases the CO_2 uptake. These authors [104] also reported an improvement of $NiFeAlO_x$ catalysts deactivation resistance at elevated temperature and pressure in thermodynamic equilibrium. This phenomenon was attributed to the partial segregation of (γFe, Ni) nanoparticles formed during the activation step giving rise to Fe^{2+}, offering an alternative reaction pathway through CO_2 activation on disordered Fe_yO. They also studied the effects of incorporating Fe by surface redox reaction (SRR) method on Ni-based alumina catalysts [78]. They prepared a 11 wt% Ni/Al_2O_3 catalyst by deposition-precipitation and a 48 wt% $NiAlO_x$ material by co-precipitation method. In the case of Ni/Al_2O_3-derived catalysts, higher Fe loadings (0.5 to 1.8 wt%) induced better performances (tests done at 8 bar), which was attributed to the enhancement of the electronic properties due to the formation of Ni–Fe alloys. In addition, increasing Fe loadings (3.6 to 8.6 wt%) increased the apparent thermal stability of $NiAlO_x$-derived catalysts, which was ascribed to the partial segregation of the alloyed Ni–Fe particles, in accordance with their previous studies.

Xu et al. [80] investigated a series of Co–Ni doped ordered mesoporous Al_2O_3 (OMA) oxides with different Co/(Co+Ni) molar ratios fabricated by the one-pot evaporation-induced self-assembly (EISA) method. This synthesis method produced homogeneous incorporation of metals among the Al_2O_3 framework achieving as well a high Co and Ni dispersion. Bimetallic samples exhibited higher catalytic performances than those obtained for the monometallic Ni and Co OMA catalysts, especially at lower temperatures. This trend was related to the synergetic effect between Co and Ni (Figure 6), since Co presents high activity towards CH_4 formation at low temperature, owing to remarkable CO_2 activation capacity and allowing the decrease of the apparent activation energy. In addition, they observed that only an appropriate Co/(Co + Ni) molar percentage (20%) could maximally enhance the catalytic performances. Besides, catalysts showed an outstanding thermal stability and anti-sintering properties. Alrafei et al. [81] also optimized Ni (5 to 25 wt%) and Ni–Co catalysts supported on γ–Al_2O_3. Authors prepared the alumina support in the form of extrudates and incorporated Ni and Co by impregnation (co-impregnation for bimetallic samples). They observed, in accordance with other studies already discussed, that Ni loading strongly influenced the catalytic activity, with values above 15 wt% leading to no remarkable differences. In terms of Co effect, they observed that this metal presented only

a positive impact in the performances when Ni loading was 10 wt%. They attributed this to an enhancement of nickel species reducibility and dispersion.

Figure 6. Synergistic effect proposed for *x*Co–*y*Ni–Al$_2$O$_3$ catalysts [80]. Reproduced with permission from Xu et al., *International Journal of Hydrogen Energy*; published by Elsevier, 2018.

Several studies have dealt with the beneficial incorporation of lanthanides and metal oxides to CO$_2$ methanation catalysts due to their appropriate electronic or acidic/basic properties, among all [105,106]. Indeed, Rahmani et al. [82] reported Ni-based catalysts supported on mesoporous γ–Al$_2$O$_3$ promoted with Ce, Mn, Zr and La oxides and prepared by impregnation, all samples containing 20 wt% Ni and 2 wt% of promoter. As authors identified Ce as the promoter with the most effective results, they studied the effect of Ce loading (2, 4 and 6 wt%) being observed that, despite the small differences between samples, 2 wt% Ce seems to be the most suitable content. Cerium positive effect was explained, as seen in SiO$_2$ based materials section, by the presence of oxygen vacancies in the cerium containing samples, enhancing CO$_2$ activation. In the Mn, Zr and La samples, the presence of the promoters had only an effect in the coverage of Ni sites, reducing the accessibility and causing blockage, so that no enhancement of the performances was found. Liu et al. [83] also reported the effect of adding CeO$_2$ to 15%Ni/Al$_2$O$_3$ catalysts. The catalytic performances were strongly dependent on the CeO$_2$ content, being the sample with 2 wt% Ce the one leading to the best results, as also found by Rahmani et al. [82]. The positive effect of Ce was attributed to the improved reducibility of Ni species (e.g., weakening of Ni–Al$_2$O$_3$ interactions) and enhanced activation of CO$_2$ on Ce sites. Guo et al. [84] developed an innovative catalyst by synthesizing Ni–Al$_2$O$_3$ LDHs (layered double support) and using CeO$_2$ as promoter. Authors obtained the best performances when using ~50 wt% CeO$_2$ due to the small and highly dispersed Ni^0 particles formed and due to the existence of oxygen vacancies that directly increased the active sites and promoted CO$_2$ adsorption. Tada et al. [85] verified also the effect of CeO$_2$ loading on the performances of Ru/CeO$_2$/Al$_2$O$_3$ catalysts. They observed that the performances followed the trend: Ru/30%CeO$_2$/Al$_2$O$_3$ > Ru/60%CeO$_2$/Al$_2$O$_3$ > Ru/CeO$_2$ > Ru/Al$_2$O$_3$. With a lower CeO$_2$ content (30 wt%), a larger surface area was achieved due to the smallest average size of CeO$_2$ crystallites in this sample when comparing to the rest of the tested catalysts. Additionally, authors suggested, according to the results of performed mechanistic studies, that samples without CeO$_2$ presented further difficulties in the dissociation and decomposition of intermediate formate species. Along with the previously discussed studies, Ahmad et al. [86] tested the effect of La, Ce, Pr, Eu and Gd as promoters of Ni/γ–Al$_2$O$_3$ catalysts with 5 wt% of the promoter and 12 wt% of Ni added by impregnation. In this case, Pr was pointed out as the best promoter, even if all lanthanides led to an increase of Ni dispersion without remarkable effects on the textural properties when comparing to the 12%Ni/γ–Al$_2$O$_3$ catalyst. Finally, Karam et al. [87] reported Ni–Mg–Al$_2$O$_3$ catalysts prepared by EISA one-pot and optimized the materials in terms of Mg and Ni loadings. The best performances were achieved with 7 wt% Mg and 15 wt% Ni, being higher than those revealed for other Al$_2$O$_3$ samples in the literature. This outcome was due to the important improvement of the metallic dispersion and surface basicity.

3.3. Trimetallic Al$_2$O$_3$-Supported Catalysts and Composites

Wang-Xin et al. [88] prepared highly dispersed Ni–Ce–Zr/γ–Al$_2$O$_3$ catalysts by citric acid assisted impregnation. The addition of citric acid in the preparation procedure promoted the dispersion of the Ni–Ce–Zr oxide species over the γ-Al$_2$O$_3$ surface and improved metal-support interactions.

Consequently, Ni–Ce–Zr/γ–Al$_2$O$_3$ catalysts were highly active and the higher the citric acid content used in the synthesis method the better the results. Toemen et al. [89] studied Ru/Mn/Ce/Al$_2$O$_3$ catalysts prepared by sequential impregnation with the aim of optimizing the Ce loading as well as the calcination temperature. Firstly, calcination at 1000 °C was found as the optimum temperature when comparing with the results obtained for the samples calcined at 400, 600 and 800 °C due to the modification of the phases formed during this thermal treatment. Additionally, Ce loadings of 55 to 85 wt% were tested, being the best results obtained for the 65 wt% Ce containing sample, which was attributed to higher dispersion and the favorable morphology of this catalyst.

Zamani et al. [107] carried out a deep study regarding the use of M*/Mn/Cu–Al$_2$O$_3$ (M* = Pd, Rh and Ru) catalysts prepared by impregnation. After comparing three catalysts containing the same Pd, Rh and Ru content over Mn/Cu–Al$_2$O$_3$, the best material was the one containing Ru. Consequently, as a second step, the Ru loading (1.6 to 18.4 wt%) and the calcination temperature (831 to 1168 °C) were optimized by using Design-Expert® software, where 10.9 wt% Ru and a calcination temperature of 1035 °C were described as the best conditions. Bakar et al. [90] studied Ru and Pd supported Mn/NiO/Al$_2$O$_3$ catalysts and reported Ru as a more favorable noble metal for this reaction. They also optimized the Ru/Mn/Ni ratio and the calcination temperature with better performances obtained when the parameters were 5:35:60 and 1000 °C, respectively. Authors defined this optimum catalyst as spherical nanoparticles with aggregated and agglomerated mixtures of metal species on the surface. It must be highlighted that the authors did not report any kind of pre-reduction treatment. However, they considered that unreduced NiO species could be active sites for CO$_2$ methanation. To further confirm their hypothesis, they synthesized a NiO based Al$_2$O$_3$ catalyst and reported ~15 % of CO$_2$ conversion without carrying out a pre-reduction treatment. They asserted the potential role of NiO as an active site for the reaction since, even after the tests, no reduced nickel species were observed in the samples. Franken et al. [108] prepared CoAl$_{2-x}$Mn$_x$O$_4$ (x = 0, 0.1, 0.5, 1) solid solutions by co-precipitation with the aim of understanding the effects of Mn on catalysts properties and performances. CoMn$_{0.5}$Al$_{1.5}$O$_4$ led to the best performances while the introduction of Mn into the spinel support was responsible for a reduction in the basicity and an improvement of the hydrogen spillover from Co active sites to the support surface. These modifications led to a reaction mechanism with formate species as intermediates (no CO) accompanied by a remarkable decrease of the activation energy.

Do et al. [91] studied the effect of Ca incorporation (0, 1.0, 3.0, 5.0, 7.0 and 10.0 %mol) to perovskite NiTiO$_3$ (containing ~11 wt% Ni) loaded by impregnation on γ–Al$_2$O$_3$. Ca incorporation favored the nickel dispersion, boosted the CO$_2$ adsorption capacity and improved the textural properties, which resulted not only in a remarkable increase of the performances but also in a significant stability under reaction conditions for 10 days.

Several authors also reported the suitability of Al$_2$O$_3$-based composites and mixed oxides as supports for CO$_2$ methanation catalysts. Indeed, Cai et al. [92] studied 12%Ni/(ZrO$_2$–Al$_2$O$_3$) catalysts checking not only the promoter effect of ZrO$_2$ but also the effects of the ZrO$_2$–Al$_2$O$_3$ composite preparation method (co-precipitation, impregnation of Zr over commercial γ–Al$_2$O$_3$ or drying and impregnation followed by precipitation). In all cases, Ni was incorporated by impregnation. Regarding the preparation method of ZrO$_2$–Al$_2$O$_3$, impregnation followed by precipitation led to the best catalytic performances with high stability due to the enhanced Ni species reducibility and dispersion over this support. Additionally, this sample also presented the highest basicity, which was considered by the authors as a key parameter, also favoring the methanation performances. Regarding the effect of the ZrO$_2$ loading (0, 3, 9 and 15 wt%), 3 wt% ZrO$_2$ enhanced both the activity and the stability. Lin et al. [93] also studied mesoporous Al$_2$O$_3$–ZrO$_2$ modified Ni catalysts prepared via a single-step epoxide-driven sol-gel method and varying the Al/Zr ratio and Ni loading. They observed that the incorporation of ZrO$_2$ into the Ni/Al$_2$O$_3$ structure decreased the interaction between Ni species and Al$_2$O$_3$, promoting nickel reducibility and dispersion. Thus, increasing ZrO$_2$ loading favored the formation of active metallic Ni sites and surface oxygen vacancies, which represent two key factors for improving the catalytic activity at low temperatures. However, increasing both Zr and Ni loading was found as

beneficial only for a certain range, with the catalyst containing 20% wt% Ni and an Al/Zr ratio of 1.0 presenting the best results.

Furthermore, Yang et al. [95] prepared $CaO–Al_2O_3$ composites by co-precipitation and incorporating Ni by impregnation. The best reported sample contained 15 wt% of Ni and a $CaO:Al_2O_3$ ratio of 20:80. Authors concluded that CaO was responsible for restraining the growth of NiO nanoparticles, improving its dispersion and creating a moderate interaction between NiO and Al_2O_3. Liu et al. [96] also reported ordered mesoporous Ni-Ru-doped $CaO–Al_2O_3$ composites synthesized by one-pot evaporation-induced self-assembly method with 10, 1 and 2 wt% of NiO, RuO_2 and CaO, respectively. This material was compared to reference samples such as $Ni–Al_2O_3$, $Ni-Ru–Al_2O_3$ and $Ru–Al_2O_3$. Monometallic Ru or Ni catalysts presented considerably similar CO_2 conversions due to the close average size values of the metal species in both catalysts (~10 nm). However, the selectivity to methane was quite poor in the Ni sample. The better results obtained for the Ni-Ru bimetallic sample were attributed by the authors to the synergistic effect between Ni and Ru and to the favored H_2 activation developed by Ru species. Finally, the addition of CaO enhanced the CO_2 adsorption capacity providing Ni–Ru–Ca sample a finer performance.

Xu et al. [94] studied $Ru/TiO_2–Al_2O_3$ catalysts prepared by impregnation. When comparing the performances of two 5 wt% Ru catalysts supported on Al_2O_3 and $TiO_2–Al_2O_3$, the second catalytic system exhibited a much higher activity. This was due to the more dispersed particles found in the Ti-containing sample as a result of establishing a strong interaction between Ru and TiO_2. The effect of TiO_2 content (5, 10 and 15 wt%) and the calcination temperature after $TiO_2–Al_2O_3$ synthesis were also evaluated. While TiO_2 loading did not influence the results, CO_2 conversions increased with higher calcination temperatures (from 600 to 950 °C) and decreased for 1100 °C, being 950 °C the optimum.

Abate et al. [97] prepared $\gamma–Al_2O_3–ZrO_2–TiO_2–CeO_2$ composites as supports for Ni catalysts. The best results were obtained for the sample presenting the composite composition of $\gamma-Al_2O_3:ZrO_2:TiO_2:CeO_2 = 55:15:15:15$, prepared by impregnation-precipitation method using commercial $\gamma-Al_2O_3$ powder as a host, and 20 wt% Ni. The incorporation of Ni to the composites instead of $\gamma–Al_2O_3$ provoked enhanced Ni^0 dispersion and reducibility, due to the modification of the metal-support interactions. Mebrahtu et al. [98] also studied Ni catalysts supported on ternary and quaternary alumina–zirconia–titania–ceria mixed oxides. Results showed that, for ternary oxide supported Ni, the catalytic activity depends on textural properties improvement while, for quaternary oxide supported Ni, it depends mainly on reducibility and metallic dispersion. Moreover, TiO_2 and ZrO_2 incorporation was found to modify mainly textural properties while CeO_2 addition promoted Ni dispersion and reducibility. Besides, 15 wt% of CeO_2 strengthened the catalyst stability, decreasing the deactivation rate of about one order of magnitude for the best ternary system $(20\%Ni/90\%\gamma–Al_2O_3–5\%ZrO_2–5\%TiO_2)$.

Finally, some authors focused on finding new methods to prepare Ni/Al_2O_3 catalysts. This is the case of Daroughegi et al. [109], who used ultrasound-assisted co-precipitation; Xu et al. [110], who used cold plasma; Song et al. [111], who used microwaves; Schubert et al. [112], who used double flame spray pyrolysis; Aljishi et al. [113] and Xu et al. [114], who used evaporation induced self-assembly technique (EISA) or Shang et al. [115], who used partial hydrolysis of aqueous solutions containing $Al(NO_3)_3$ and $Ni(NO_3)_2$ with $(NH_4)_2CO_3$, without templates or organic surfactants. Additionally, Le et al. [116] studied the effect of the type of Al_2O_3 crystalline phase in the performances of Ni/Al_2O_3 catalysts.

3.4. Mechanistic Aspects

Beuls et al. [117] proposed some insights for $Rh/\gamma–Al_2O_3$ catalysts mechanism at 50–150 °C and 2 atm. They suggested that CO_2 is adsorbed over the material by dissociation, forming $CO_{(ads)}$ and $O_{(ads)}$ and inducing Rh species oxidation. Indeed, Rh species oxidation state played a crucial role in the distribution of the adsorbed species on the catalysts, with Rh–dicarbonyls being identified as those leading to the formation of CH_4. In short, authors consider CO as the true reaction intermediate in their catalytic system. Garbarino et al. [73] suggested that CO_2 methanation over Ni/Al_2O_3 catalysts occurs

at the expense of CO intermediate on the corners of Ni nanoparticles interacting with alumina, likely due to the formation of formate or other oxygenate species and their further hydrogenation into CH_4. Zhang et al. [118] studied the mechanistic implications of different Ni loadings on Ni/ɤ–Al_2O_3 catalysts by diffuse reflectance infrared Fourier transform spectroscopy (DRIFTS) studies. They observed that, while low Ni contents favor the occurrence of reverse water gas shift (RWGS) reaction promoting CO formation, increasing loadings hinder the formation of stable and non-reactive carbonate species and promote formates conversion to CH_4, boosting the activity towards CO_2 methanation rather than RWGS. Finally, Cárdenas-Arenas et al. [119] proposed that CO_2 methanation proceeds over Ni/Al_2O_3 through the adsorption and consecutive chemisorption of CO_2 over hydroxyl groups created due to the H_2 reduction of the NiO–Al_2O_3 interface (Figure 7). They reported that chemisorbed CO_2 hampered carbon dioxide molecules chemisorption/dissociation and led, alternatively, to the formation of water and formates species. Even if formate species could be successively hydrogenated to methane, part of them gave rise to CO, decreasing CH_4 selectivity.
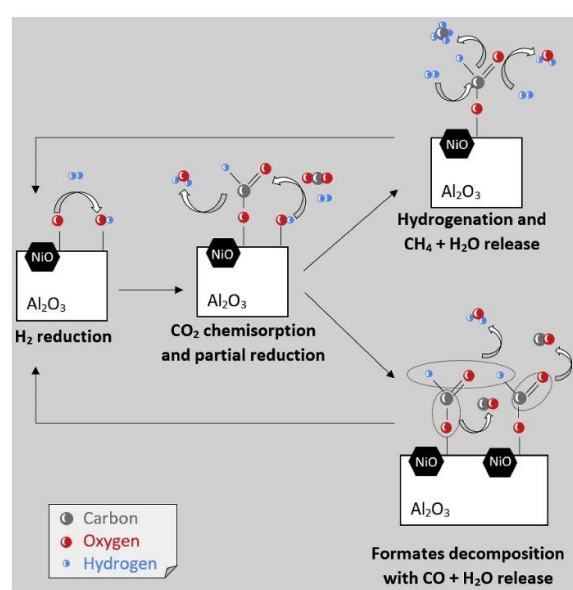

Figure 7. Mechanism proposed for Ni/Al_2O_3 catalysts [119]. Reproduced with permission from Cárdenas-Arenas et al., *Applied Catalysis B*: Environmental; published by Elsevier, 2020.

4. CeO₂-Based Catalysts

Even if cerium oxide has been typically used as a promoter for CO_2 methanation catalysts, several authors also reported interesting results when using it as support. Indeed, the most notable results can be seen in Table 4. and their main findings are discussed in the following sections.

Table 4. CeO₂-based materials reported in literature for CO_2 methanation reaction.

Catalyst	Preparation Method	T_{red} (°C)	H_2:CO_2	Q_T/W (mL g^{-1} h^{-1})	Best Catalytic Performances			Ref.
					T (°C)	X_{CO2} (%)	S_{CH4} (%)	
*10*Ni/CeO$_2$	Impregnation	600	4:1	n.a.	300	90	100	[85,120]
*32*Ni-CeO$_2$	Soft-template	400	4:1	72,000	300	87	100	[121]
*10*Ni/CeO$_2$	Impregnation	500	4:1	n.a.	300	92	100	[122]
*8.5*Ni/CeO2	Impregnation	500	4:1	30,000	375	80	100	[123]
Ce$_{0.95}$Ru$_{0.05}$O$_2$	Combustion	500	4:1	n.a.	450	55	99	[124]
*50*Ni/Ce$_x$Gd$_{1-x}$O2	Solution-combustion	800	4:1	n.a.	450	72	n.a.	[125]
*5*Ni-Ce$_{0.72}$Zr$_{0.28}$O$_2$	Sol-gel	400	4:1	22,000	400	85	99	[126,127]
*10*Ni-Ce$_x$Zr$_{1-x}$O$_2$	Ammonia evaporation	450	4:1	22,000	275	55	100	[128]
*13*Ni-NaO/CeO$_2$	Impregnation	500	50:1	60,000	250	97	96	[129]
*16*Ni-Co/CeO$_2$-ZrO$_2$	Impregnation	450	4:1	12,000	350	70	98	[130]

4.1. Monometallic CeO$_2$-Supported Catalysts

Tada et al. [85,120] studied 10 wt% Ni-based catalysts supported on CeO$_2$, γ–Al$_2$O$_3$, TiO$_2$ and MgO and identified CeO$_2$ as the best choice. The surface coverage by CO$_2$-derived species on CeO$_2$ surface as well as the partial reduction of CeO$_2$ surface was reported to be responsible for the great performances of the 10%Ni/CeO$_2$ catalyst. Atzori et al. [121] also studied NiO–CeO$_2$ mixed oxides highly active for CO$_2$ methanation and prepared by soft-template and impregnation methods. Soft-template produced Ni^0 particles of ~7 nm while impregnation contributed to the formation of larger particles (>30 nm) after the pre-reduction treatment. Despite the synthesis method and the differences in the Ni^0 size, both samples presented high catalytic performances. Consequently, authors suggested that H$_2$ activation on Ni^0 is not the critical step for a high catalytic activity at such conditions, pointing out on the important role of ceria support in the reaction pathway. The proposed explanation was that only the highly uncoordinated Ni atoms at the metal-support interface, whose number strongly depends on the average particle size, remain available to hydrogenate CO$_2$ activated on the nearby ceria sites. Ratchahat et al. [122] also prepared structured Ni/CeO$_2$ catalysts with different configurations: plain, segmented, stacked and multi-stacked. When compared to the plain configuration, the stacked and segmented ones provided an enhancement of convective heat and mass transfer due to the random flow-channels and the addition of a gap distance in the case of the stacked, which contributed to the improvement of the methanation performances at low temperature and increased the contact time. Moreover, the multi-stacked catalyst was tested under industrial-like conditions (high feed rate and pure feed gas component), being the moderate hot spot observed responsible for a re-boosting of the conversion. Furthermore, this catalyst presented high stability (<0.6% CO$_2$ conversion loss after 76 h under reaction conditions), being its shape and surface morphology maintained. Cárdenas-Arenas et al. [123] also reported Ni/CeO$_2$ catalysts prepared by different Ni-incorporation method in order to modify the Ni-Ce interaction. Authors synthesized three dimensionally ordered macroporous (3DOM) structures by co-impregnation, successive impregnation of Ni and Ce precursors or Ni impregnation after CeO$_2$ 3DOM synthesis. Besides, materials with uncontrolled structures were also prepared by co-precipitation and Ni impregnation. Authors identified two types of active sites: NiO–CeO$_2$ interface and reduced Ni^0 particles efficient for CO$_2$ and H$_2$ dissociation, respectively. The optimal sites proportion required to obtain the maximum conversion was 25% Ni^0 for H$_2$ dissociation and 75% NiO–CeO$_2$ for CO$_2$ dissociation, achieved by the Ni-uncontrolled structured catalyst prepared by impregnation. Moreover, pulse experiments with isotopic CO$_2$ confirmed that this catalyst was more effective in hydrogenating the surface carbon species.

Sharma et al. [124] studied Ni, Co, Pd and Ru doped CeO$_2$ catalysts prepared by combustion method. Ce$_x$Ru$_{1-x}$O$_2$ presented the best catalytic performances while Ni, Co and Pd induced low CH$_4$ selectivity, with Ni and Co catalyzing both methanation and RWGS reaction and Pd producing only CO. Furthermore, Vita et al. [125] studied Ni/GDC (gadolinium-doped ceria) catalysts both in powder and monolith forms. For the powder systems, the activity increased with Ni loading, which was explained by the more favourable metal-support interaction, the increased number of moderate-basic sites and the presence of surface oxygen vacancies. Powdered catalysts presented also lower CH$_4$ productivity than a high loaded monolith (0.5 g cm^{-3}), due to the high surface-to-volume ratio, good interphase mass transfer and low pressure drops of the monolithic system.

Ocampo et al. [126,127] prepared Ce$_x$Zr$_{1-x}$O$_2$ (CZ) mixed oxides as supports for 5–15 wt% Ni-based catalysts by sol gel method. CZ fluorite structure was maintained after Ni incorporation but the replacement of some Zr^{4+} by Ni^{2+} cations led to a reduction in the lattice parameter of the structure, especially in the 10 and 15 wt% Ni samples. Even if all samples presented great performances and stability, 10% Ni–CZ catalyst reported the best results due to the high oxygen storage capacity of CZ and its ability to effectively disperse Ni particles. Additionally, the incorporation of nickel cations into the CZ structure and the higher dispersion of NiO at its surface were found responsible for improving the redox properties of the materials, able to hinder sintering processes. A similar strategy was followed by Ashok et al. [128], who prepared a series of nickel catalysts supported on Ce$_x$Zr$_{1-x}$O$_2$ (CZ)

by ammonia evaporation, impregnation and deposition-precipitation methods. Among all, the Ni/CZ catalyst prepared via ammonium evaporation method led to the best performances and stability. These positive results were explained by the fact that this catalyst was activated at low temperatures, and the incorporation of some Ni cations in the ceria structure led to the creation of oxygen vacancies and to better reducibility of Ni species in this sample.

4.2. Bi- and Trimetallic CeO₂-Supported Catalysts

Le et al. [129] studied Ni–Na/SiO₂ and Ni–Na/CeO₂ catalysts prepared by impregnation in order to compare the effect of the support nature and evaluate Na loading effects. In both cases, increasing Na contents led to lower performances which is ascribed to a reduction in the textural properties and in the CO_2 adsorption capacity while higher performances were obtained by CeO₂-supported materials. In addition, Sun et al. [131] developed a novel ICCU (integrated carbon capture and utilization) process for carbon capture and methane production, using dual function materials composed by a mechanical mixture of MgO and Ru/CeO₂ catalysts with increasing Ru loadings. This ICCU process allows the simultaneous regeneration of the sorbent and the conversion of the captured CO_2 to CH_4 in a single reactor at intermediate temperature (300 °C). Authors found that MgO+10Ru/CeO₂ showed the best performance in the 1st cycle of ICCU due to a higher number of oxygen vacancies. However, after 10 cycles, MgO+5Ru/CeO₂ exhibited the highest catalytic activity because of the more favorable metal-support interactions established in this sample. Finally, Pastor-Pérez et al. [130] prepared Ni–Co/CeO₂–ZrO₂ and Ni–Mn/CeO₂–ZrO₂ catalysts (~15 wt% Ni and 3.5 wt% Co/Mn) and evaluated the impact of methane incorporation in the feed. Authors verified a negative effect of Mn on the activity, which attributed to a stronger than desired CO_2 adsorption over these sites, limiting the subsequent hydrogenation of the reactant towards methane. On the contrary, Co favored the performances through the improvement of the catalyst's electronic properties and the inhibition of Ni sintering. They also verified that incorporating methane in the feed led to a slight enhancement of the catalytic performances, which they ascribed to low temperature reforming reactions taking place simultaneously with methanation.

4.3. Mechanistic Aspects

In terms of mechanisms, Konishcheva et al. [132] proposed that CO_2 methanation proceeds over Ni/CeO₂ catalysts through the activation of CO_2 on CeO₂ surface and the stepwise hydrogenation to methane through hydrocarbonate and formate intermediates by the hydrogen spilled over from Ni. Authors considered the route where CO acts as a reaction intermediate negligible. Cárdenas-Arenas et al. [119] also reported the presence of two independent active sites for CO_2 methanation over Ni/CeO₂ (Figure 8): NiO–CeO₂ interface for CO_2 activation and Ni^0 particles for H_2 dissociation. Even if they identified water desorption as the slowest step of the mechanism, the co-existence of two types of actives sites and the high oxygen mobility of Ni/CeO₂ catalysts hindered water inhibitory effect.
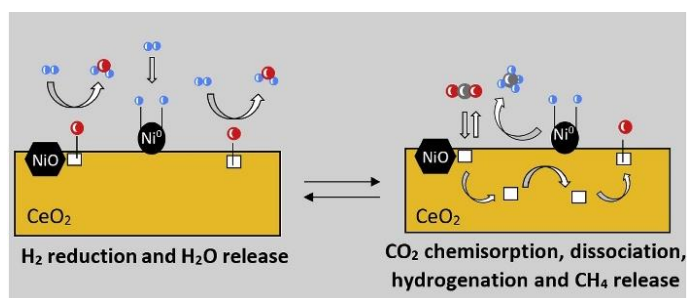

Figure 8. Mechanism proposed for Ni/CeO₂ catalysts [119]. Reproduced with permission from Cárdenas-Arenas et al., *Applied Catalysis B*: Environmental; published by Elsevier, 2020.

Aldana et al. [126] studied Ni–$Ce_xZr_{1-x}O_2$ catalysts and proposed a bifunctional mechanism without CO as intermediate species (Figure 9a). Actually, they observed that H_2 molecules were activated and dissociated into H on Ni^0 sites while CO_2 was adsorbed on the Ce–Zr support oxygen vacancies forming monodentate carbonates. These monodentate carbonates were then sequentially hydrogenated producing formates, formaldehydes, methoxy species and, finally, methane. Additionally, authors proposed a pathway for CO formation and verified its inhibitory role in the reaction (Figure 9b).
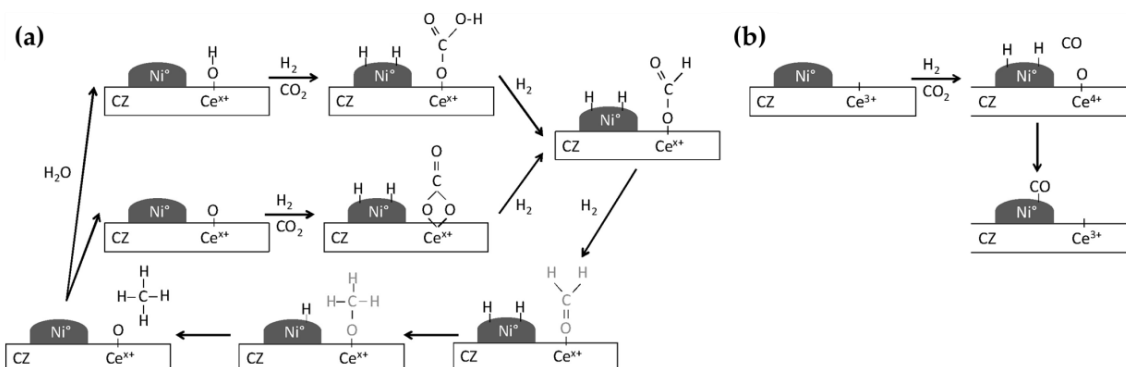

Figure 9. Mechanism proposed for (**a**) CO_2 methanation and (**b**) CO formation over Ni-$Ce_xZr_{1-x}O_2$ catalysts [126]. Reproduced with permission from Aldana et al., *Catalysis Today*; published by Elsevier, 2013.

5. ZrO_2-Based Catalysts

In terms of ZrO_2 supported catalysts, the main results found in the literature can be seen in Table 5 while the main conclusions of the published works will be discussed below.

Table 5. ZrO_2-based materials reported in literature for CO_2 methanation reaction.

Catalyst	Preparation Method	T_{red} (°C)	H_2:CO_2	Q_T/W (mL g^{-1} h^{-1})	Best Catalytic Performances			Ref.
					T (°C)	X_{CO2} (%)	S_{CH4} (%)	
10Ni/ZrO_2	Impregnation	n.a.	125:1	140,000	450	100	n.a.	[133]
15Ni/ZrO_2	Impregnation	500	4:1	n.a.	350	80	99	[134]
10Ni/ZrO_2	Impregnation [a]	500	4:1	10,000	350	80	97	[135]
15Ni/ZrO_2	Combustion	500	4:1	48,000	400	85	100	[136]
10Co/ZrO_2	Impregnation	400	4:1	3600	400	93	100	[137]
2Co/ZrO_2	Impregnation	400	4:1	72,000	400	85	99	[138]
3Ru/ZrO_2	Selective deposition method	300	4:1	n.a.	300	82	100	[139]
50Ni/Sm-ZrO_2	Mechanical mixture	300	4:1	3000	350	95	100	[140]
Ni/Y–ZrO_2	Co-impregnation	400	4:1	6300 [b]	400	38 [c]		[141]
10Ni/Y–ZrO_2	Impregnation with EDTA	500	4:1	60,000	375	60	96	[142]
75Ni/Y–ZrO_2	Extrusion	600	4:1	n.a.	300[d]	92	98	[143]
30Ni–Fe/ZrO_2	Co-impregnation	400	4:1	4980	270	100	95	[144]
30Ni–Co/ZrO_2	Co-impregnation	400	4:1	4980	270	100	95	[144]
30Ni–Cu/ZrO_2	Co-impregnation	400	4:1	4980	330	88	88	[144]
15Ni–Fe/ZrO_2	Co-impregnation	500	4:1	n.a.	400	78	96	[145]
Co–Cu/ZrO_2	Co-precipitation	300	3:1	14,400	300	68	83	[146]
6Ni–MgO/ZrO_2	Impregnation with citric acid	450	4:1	15,000	300	95	100	[147]
Ni–CaO/ZrO_2	Co-impregnation	400	4:1	6742 [b]	350	85	100	[148]

[a] Plasma decomposition instead of thermal calcination; [b] In these works Y–Al_2O_3, typical support for CO_2 methanation catalysts with ability to activate CO_2, was loaded in the reactor together with the corresponding Ni-based ZrO_2 catalyst. Consequently, the mass of Y–Al_2O_3 was also considered in the Q_T/W calculations; [c] CH_4 yield; [d] Temperature of the furnace.

5.1. Monometallic ZrO_2-Supported Catalysts

Da Silva et al. [133] studied Ni/ZrO_2 catalysts and compared them to Ni/SiO_2 samples, both prepared by impregnation and containing 10 wt% Ni. The sample supported on zirconia was more active, which authors explained by the considerably weaker interaction of CO_2 with the SiO_2

sample and the higher Ni dispersion found in the ZrO_2 catalyst. In addition, Lu et al. [134] prepared mesoporous zirconia-modified clays as supports for Ni catalysts by one-pot method (hydrothermal treatment of the mixture of the clay suspension and the $ZrO(NO_3)_2$ solution). The bimodal pore structure of the zirconia-modified clays was reported as beneficial for the dispersion of Ni. As concluded by previous authors, ZrO_2 favored the dispersion of the Ni species, preventing sintering during the reaction and reducing carbon deposition. The catalyst with 20 wt% of zirconia led to the best performances while the most stable sample was the 15%Ni/ZrO_2. Jia et al. [135] studied also 9 wt% Ni-supported ZrO_2 catalysts and reported the beneficial effect of carrying out the decomposition of the precursor salts after impregnation (calcination) using dielectric barrier discharge (DBD) plasma instead of a conventional thermal treatment at 500 °C (from 30 to 70% of CO_2 conversion at 300 °C when performing thermal and DBD plasma calcination, respectively). The positive effect of plasma was related to the remarkable enhancement of the metallic dispersion when using this non-conventional treatment. Additionally, Zhao et al. [136] prepared 10, 15 and 25 wt% Ni/ZrO_2 catalysts by combustion method using several combustion mediums such as urea, glycerol, glycol, ethanol and n-propanol. The highest performances were reported for the sample synthesized using urea, being the results attributed to the favored reducibility of the Ni species, the better dispersion and the greater CO_2 adsorption capacity.

Furthermore, Li et al. [137] reported Co-based catalysts supported on ZrO_2, Al_2O_3, SiO_2, SiC, TiO_2 and activated carbon (AC), all containing 10 wt% of Co. Their catalytic tests were performed at 30 atm of pressure, contrary to what was done in the majority of works reported for CO_2 methanation. ZrO_2 was the best performing Co-based support, with the order as follows: 10%Ni/ZrO_2 > 10%Ni/SiO_2 > 10%Ni/Al_2O_3 ≈ 10%Ni/SiC > 10%Ni/AC > 10%Ni/TiO_2. The zirconia support contributed to the better reducibility and dispersion of Ni species. Besides, the presence of oxygen vacancies on the ZrO_2 structure prevented the formation of carbon deposits during the tests. The same authors [138] studied later the effect of the impregnation solvent for preparing 2 wt% Co catalysts supported over ZrO_2. Among all solvents, citric acid-assisted impregnation led to the best catalytic results. The beneficial effect of citric acid arises from the enhancement of the Co particles dispersion and its interaction with ZrO_2 due to the formation of cobalt citrate complex as precursor. This intensified interaction also provided oxygen vacancies and enhanced nickel reducibility, improving CO_2 adsorption capacity and, consequently, the obtained performances.

Recently, Nagase et al. [139] reported ~3 wt% Ru/ZrO_2 catalysts (using amorphous and crystalline ZrO_2) prepared by selective deposition method and compared them with an equivalent Ru/SiO_2 sample. Ruthenium particles with average sizes below 10 nm were obtained in all cases with amorphous ZrO_2 promoting the activity and selectivity. The effects of the preparation method for Ru/amorphous ZrO_2 was studied, by comparing the use of a NaOH or NH_3 in the selective deposition method with a conventionally impregnated sample. Impregnated and NH_3 samples led to the similar results, but lower than those exhibited by the catalyst prepared using NaOH. The higher activity of the later was related not only to the promoted dispersion, also found when using NH_3, but especially to the presence of residual Na species in the catalyst able to activate the intermediate formate species during the reaction.

5.2. Bimetallic ZrO_2-Supported Catalysts

Takano et al. [140] prepared 50 wt% Ni/Sm–ZrO_2 by mechanical mixture followed by calcination. The best results were obtained for the Zr/Sm ratio of 5 and after calcination at 650 or 800 °C. Sm^{3+} ions were substituted in the ZrO_2 lattice, what promoted the presence of oxygen vacancies, favored the interaction of CO_2 weakening the C–O bonds and, consequently, enhanced the CO_2 activation.

The same authors [141] prepared Ni supported Yttrium–Zirconia catalysts by co-impregnation and with several Y^{3+} concentrations. Ni/Y–ZrO_2 catalysts showed higher catalytic activity than the Ni/ZrO_2 sample, being the performances dependent upon the Y^{3+} concentration, with the best results obtained for the catalyst with a Y/(Zr+Y) molar ratio of 0.333. Kesavan et al. [142] also

studied Ni-based Y-stabilized ZrO_2 (YSZ) catalysts with 10 wt% Ni prepared by different methods: wetness impregnation, wetness impregnation with EDTA, electroless plating, mechanical mixing with commercial NiO nano-powder and mechanical mixing with nano-powder transformed in micro-powder NiO. The most efficient and stable catalyst was the one prepared by wet impregnation with $Ni(EDTA)^{2-}$ complex due to the smaller and highly dispersed Ni^0 particles formed. Additionally, Kosaka et al. [143] studied Ni-based tubular catalysts again supported over Y–stabilized ZrO_2 with different Ni loadings. Even under high gas hourly space velocity (GHSV) conditions, catalysts with higher Ni content showed better catalytic activity, which was also favored by their tubular structure that provided a higher CH_4 yield when compared to the same powder catalysts. Authors studied also the effect of Ni loading on the temperature profiles and realized that the high CO_2 methanation performances arise from the interaction between heat generation and acceleration of the reaction rate in the catalysts. Through a numerical analysis based on reaction kinetics, heat transfer and fluid dynamics, authors deduced that both high CH_4 yield and prevention of hot spots formation can be achieved by properly arranging catalysts with different activities in the reactor.

Ren et al. [144] studied Ni/ZrO_2 catalysts impregnated with a second metal (Fe, Co and Cu). Fe was the metal leading to the best performances, which resulted from the improved dispersion and reducibility of Ni species as well as to the partial reduction of ZrO_2 in the $Ni–Fe/ZrO_2$ sample. Lu et al. [145] also studied the effects of adding Fe, Co, Ce and La to Ni based ZrO_2 modified clays by impregnation. They observed that by adding 1 wt% of promoter to the $15\%Ni/ZrO_2$ catalysts, Ni species dispersion and reducibility and catalysts' thermal stability were enhanced. Even if the performances were quite similar for all the promoted samples, Fe led to the best results attributed to synergistic effects between Fe, ZrO_2 and Ni species. Dumrongbunditkul et al. [146] prepared $Co–Cu–ZrO_2$ catalysts by co-precipitation method and tested them at 30 atm. They also prepared monometallic samples with better results obtained for the $Co–ZrO_2$ than for the $Cu–ZrO_2$ samples. Additionally, the catalyst with Co:Cu:Zr = 20:40:40 molar ratio led to the highest performances due to its high surface area and the more homogeneous dispersion of the mixed metal oxides.

Tan et al. [147] prepared a series of MgO-modified Ni/ZrO_2 catalysts with 6 wt% Ni and Mg/Ni molar ratios ranging from 1/6 to 1/1 using citrate-complexing impregnation method. Among all the synthesized materials, the catalyst with Mg/Ni molar ratio of 1/4 showed the best catalytic performances. In accordance with Li et al. [138], the use of citric acid was considered as responsible for a reduction in the Ni particles size. Furthermore, the addition of MgO stabilizes the highly dispersed Ni nanoparticles and has a confinement effect, limiting the growth of Ni and improving the resistance towards sintering and carbon deposition. Takano et al. [148] also studied tetragonal ZrO_2 doped with Ca^{2+} and Ni^{2+} ions. The incorporation of Ca^{2+} and Ni^{2+} ions to the zirconia led to the formation of oxygen vacancies in the ZrO_2 lattice and favored the performances.

In order to compare the different promoters reported for Ni-based ZrO_2 catalysts prepared by impregnation and calcined under thermal conditions, CH_4 production rates were determined for a Ni/ZrO_2 catalyst [135] and for bimetallic materials containing Y [141], Fe [144], Co [144], Cu [144], Mg [147] and Ca [148] (Figure 10). As seen, the main effect of the promoters is verified at lower reaction temperatures while Mg, Co or Fe are suitable candidates for developing further optimization studies.
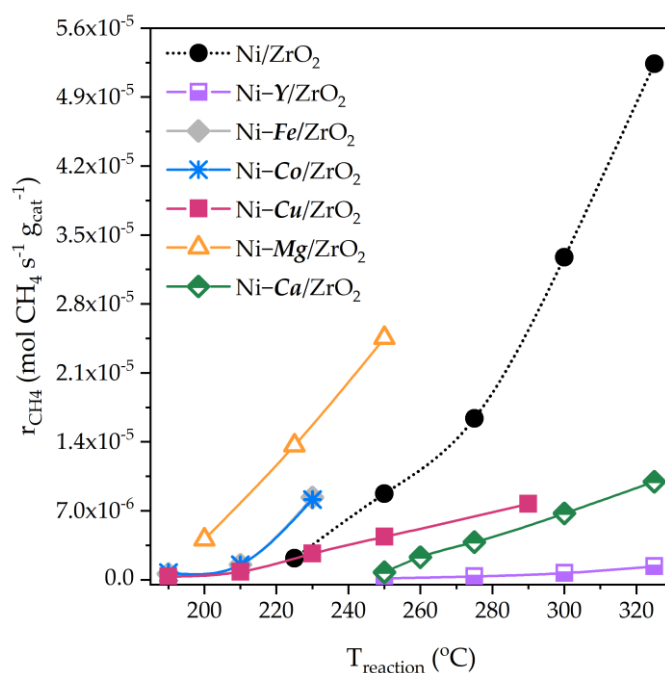
Figure 10. CH$_4$ production rates per gram of catalyst determined, far from thermodynamic equilibrium, for a series of Ni-based ZrO$_2$ materials with without promoters all prepared by impregnation method as a function of the reaction temperatures.

5.3. Mechanistic Aspects

Takano et al. [140,141,148] proposed a mechanism for Ni/ZrO$_2$ catalysts where CO$_2$ is adsorbed as carbonate species on zirconia oxygen vacancy sites rather than CO while hydrogen is activated on Ni particles. Then, H atoms must be supplied from Ni to ZrO$_2$ sites to reduce the adsorbed carbonate species progressively into formates, formaldehydes, methoxy species and, finally, methane.

6. MgO and Hydrotalcite-Based Catalysts

Besides all the catalysts already presented in this work and containing Mg as a promoter, in this chapter catalysts supported on MgO and hydrotalcite(HT)-derived materials will be summarized, with their main results shown in Table 6

Table 6. MgO and HT-derived materials reported in literature for CO$_2$ methanation reaction.

Catalyst	Preparation Method	T_{red} (°C)	H$_2$:CO$_2$	Q_T/W (mL g^{-1} h^{-1})	Best Catalytic Performances			Ref.
					T (°C)	X_{CO2} (%)	S_{CH4} (%)	
27Ni/MgO	Impregnation	n.a.	4:1	3700	325	87	>99	[149]
42.5Ni–HT$_{derived}$	Co-precipitation	900	4:1	n.a.	300	82	99	[150]
59Ni–HT$_{derived}$	Co-precipitation	900	4:1	1100	330	74	95	[151]
80Ni–HT$_{derived}$	Co-precipitation	500	4:1	20,000	300	85	100	[152]
Ni–WO$_x$–MgO	Co-precipitation	500	4:1	60,000	300	85	100	[153]
2Co/NiO–MgO	Impregnation	120	8:1	60,000	325	92	100	[154]
56Ni–La$_2$O$_3$–HT$_{derived}$	Co-precipitation	600	4:1	80,000	275	70	96	[155]
15Ni–La$_2$O$_3$–Ni–HT$_{derived}$	Co-precipitation	900	4:1	n.a.	300	75	98	[156]
21Ni–La$_2$O$_3$–HT$_{derived}$	Ion-exchanged	900	4:1	n.a.	300	82	100	[157]
15Ni–La$_2$O$_3$–HT$_{derived}$	Urea hydrolysis	700	4:1	45000	300	90	95	[158]
Ni–Fe–HT$_{derived}$	Co-precipitation	700	4:1	12000	300	95	100	[159]
12Ni–Fe–HT$_{derived}$	Co-precipitation	500	4:1	n.a.	300	83	97	[160]
78Ni–K$_2$O–Al$_2$O$_3$–HT$_{derived}$	Co-precipitation	500	4:1	75,000	350	85	100	[161]

6.1. Monometallic MgO and Hydrotalcite-Derived Catalysts

Loder et al. [149] prepared a bifunctional Ni/MgO catalyst for CO_2 methanation. They tested the influence of Ni loading (11, 17, 20 and 27 wt% of Ni) and the matrix composition (MgO pure and MgO/CaO). Results confirmed that MgO is an active compound and the CaO did not participate actively in the reaction, since the thermal stability of $CaCO_3$ is much higher than $MgCO_3$. In this way, Ni/MgO catalyst showed better results than those obtained for Ni/MgO–CaO. The catalytic activity increased linearly with the Ni loading since a remarkable number of active sites were found even at high Ni loadings (27 wt%). Based on the reaction kinetics, authors also modelled a Langmuir–Hinshelwood based rate law taking the bifunctional catalytic action of the catalyst into account.

Wierzbicki et al. [150] studied the effect of the Ni loading (10 to 43 wt%) on Ni based hydrotalcite-derived materials with constant M(II)/M(III) (valence II to valence III metals) molar ratio, prepared by pH controlled co-precipitation and the decomposition of the precursor hydrotalcites carried out by thermal treatment. After this treatment, periclase-like structured (homogeneous mixed oxide) materials were formed being Ni present as NiO. Increasing Ni contents weakened the interaction between Ni and the hydrotalcite matrix, improving its reducibility and increasing the number of active sites. This resulted in an enhancement of the performances. Additionally, Bette et al. [151] prepared a ~59 wt% Ni catalyst supported on a $(Mg,Al)O_x$ mixed oxide derived from a (Ni,Mg,Al)–hydrotalcite-like (HT) precursor. The precursor HT structure was synthesized by pH-controlled co-precipitation and the reduction at 900 °C led to metallic Ni particles supported on a $(Mg,Al)O_x$ matrix. Authors reported that the hydrotalcite-like derived material provided anti-sintering and stability properties to the catalysts, what justified the good performances revealed by the supported materials. Finally, Abate et al. [152] prepared Ni–Al–hydrotalcite materials and compared them to a Ni/Al_2O_3 commercial sample with 80 wt% Ni. Ni content was fixed with an Al/(Al + Ni) = 0.25–0.27 corresponding to a theoretical loading of 75–80 wt% NiO. Better results were obtained for the HT derived sample due to the favored catalysts reducibility and the higher metal surface area and metal dispersion.

6.2. Bi- and Trimetallic MgO and Hydrotalcite-Derived Catalysts

Yan et al. [153] prepared Ni–Mg mixed oxides promoted with Co, Mo, Mn, Fe, Cu and W. Authors also prepared MgO, NiO, Ni_aMgO_x (a = 0.5, 0.8, 1.0, 1.2) and $Ni/MgO_{Impregnated}$ samples. NiO and MgO catalysts revealed quite poor activity, Ni–Mg mixed oxides led to considerably higher levels of CO_2 conversion and CH_4 selectivity and the $Ni/MgO_{Impregnated}$ sample presented intermediate results between the NiO and the mixed oxides. Being $Ni_{1.0}MgO_x$ the best mixed oxide, samples containing transition metals were synthesized using this optimized composition. The performances varied as follows: W > Co > No promoter > Mo > Mn > Fe > Cu. Then, as the W-promoted sample presented the best results, authors optimized the W/Ni molar ratio with the best performances obtained for the 1/1 value. They considered that the remarkable results reported by the $NiWMgO_x$ catalyst were related to the great anti-CO-poison ability, strong resistance against coke formation and sintering and the higher amount of CO_2 adsorption sites due to the contribution of W species. Varun et al. [154] studied NiO–MgO and M/NiO–MgO (M = 2 wt% Co, Cu or Fe) catalysts and evaluated the composites preparation method and the promoter nature. They reported three NiO–MgO materials synthesized by solution combustion, sonochemical and co-precipitation methods and obtained the best results when using the second due to the highly dispersed particles formed. Regarding the promoter nature (Co, Cu or Fe; incorporated by impregnation), Co led to the best performances, explained by the lowest activation energy determined for this catalyst due to Co reducing nature.

Ho et al. [155] reported hydrotalcite-derived ~60 wt% Ni catalysts promoted with 9.5 wt% La, 6.3 wt% Y or 9.5 wt% Ce. The best catalytic performances were exhibited by the Ni-La sample (Ni–La > Ni–Ce ≈ Ni–Y > Ni) and were attributed to La_2O_3 species ability to simultaneously promote basicity and Ni^0 dispersion. Authors concluded that an equilibrium between Ni^0 particle size and basicity is fundamental for obtaining the best CO_2 methanation performances. Furthermore, Wierzbicki et al. [156] studied the promoter effect of La on the performances of Ni–HT derived materials,

keeping the M(III)/(M(III)+M(II)) molar ratio equal to 0.25. Authors verified that the addition of lanthanum resulted in the formation of a separate phase, not integrated in the hydrotalcite-derived structure. Indeed, the incorporation of 2 wt% of lanthanum favored the catalytic performances due to the enhanced basicity, reducibility and dispersion of Ni species. Lately, the same authors [157] studied different preparation methods for La introduction (e.g., co-precipitation, impregnation and ion exchange using La–EDTA) in order to investigate its influence on the catalytic performances. La affected catalysts CO_2 adsorption capacity in terms of medium strength basic sites, which were strongly influenced by the used preparation method. Among all, ion exchange was the most efficient method to increase the amount of medium strength basic sites, leading to the best catalytic performances. Zhang et al. [158] also studied La-promoted Ni/Mg–Al catalysts with different La contents (0 to 8 wt%) and prepared by two different methods: urea hydrolysis and co-precipitation. La-promoted catalysts showed an enhanced catalytic activity, with the one containing 5 wt% of La presenting the best Ni dispersion. Besides, La increased significantly the amount of moderate basic sites that enhanced CO_2 adsorption capacity. Furthermore, urea hydrolysis was a more efficient preparation method than co-precipitation, as it promoted Ni dispersion and CO_2 adsorption capacity, leading to better catalytic performances.

Wang et al. [159] studied a Ni–Al–hydrotalcite-derived catalyst modified with Fe or Mg and prepared by co-precipitation. Authors prepared samples with different (Fe or Mg)/Al molar ratios (Fe/Al = 0.05 and 0.25, Mg/Al = 0.1 and 1). The performances of Fe catalysts were the same for both ratios while, in Mg samples, the lower the Mg content, the better the results. They suggested that both Fe and Mg favored Ni dispersion while Mg enhanced also the basicity, helping in CO_2 adsorption and activation, and Fe improved the reducibility and changed the pore distribution. Mebrathu et al. [162] also studied Ni–Fe bimetallic catalysts derived from hydrotalcites and prepared by co-precipitation, using variable Fe/Ni ratios (0.1 to 1.5, corresponding to 12 wt% Ni and 1.2 to 18 wt% Fe). Bimetallic catalysts showed higher activities and stabilities than monometallic ones, with the sample presenting the lowest Fe content (1.2 wt% Fe, Fe/Ni = 0.1) being the most outstanding. The incorporation of Fe led to weaker Ni-support interactions, promoting nickel reducibility. Additionally, an improvement of the metallic dispersion (with lower Fe loadings) and basicity was associated with Fe incorporation. In accordance with other studies already discussed in this work, the basicity of the support and the metal particle size were found as key catalysts properties. Later, the same authors [160] studied the deactivation mechanism for the best catalyst reported in the previous work (Fe/Ni = 0.1) and for the monometallic Ni sample. They observed the formation of nickel hydroxide by the reaction of Ni species with the water from methanation during the long-term tests (30–40 h). The formation of these species decreased the number of available Ni^0 sizes for the reaction, favored sintering processes and facilitated the formation of hardly reducible nickel aluminates. Authors concluded that water partial pressure was the main factor influencing the deactivation rate of the Ni catalyst, while the higher resistance of Ni–Fe material was due to Fe ability to limit the formation of nickel hydroxide.

Finally, He et al. [161] prepared Ni–Al_2O_3–HT catalysts as well as reference samples with Ni incorporated by impregnation. Ni–Al_2O_3–HT catalyst presented highly dispersed Ni particles along with strong basic sites, what led to considerably better results than the impregnated samples. Additionally, one sample containing K (K–Ni–Al_2O_3–HT) was synthesized contributing to results slightly higher than those of the un-promoted catalyst, due to the extra strong basic sites provided by K. Therefore, authors proposed that the combination of small metallic Ni particles with strong basic sites over Al_2O_3 could effectively promote the conversion of CO_2 into CH_4. This study contrasts with other works where medium strength basic sites are considered as the most favorable for CO_2 methanation reaction, as the strongest ones lead to inactive carbonate phases.

7. Carbon-Based Catalysts

Few studies have focused on the use of carbon-based catalysts for this reaction. In summary, their main results (Table 7) and findings can be found in the following sections.

Table 7. Carbon-based materials reported in literature for CO_2 methanation reaction.

Catalyst	Preparation Method	T_{red} (°C)	H_2:CO_2	Q_T/W (mL g^{-1} h^{-1})	Best Catalytic Performances			Ref.
					T (°C)	X_{CO2} (%)	S_{CH4} (%)	
*0.5*Ru/CNFs	Impregnation	300	3.3:1	80,000	500	52	100	[163]
*32.5*Co–PC	Carbonization	400	4:1	72,000	270	53	99	[164]
*30*Ni/NCNTs	Impregnation	420	4:1	50,000	340	51	96	[165]
*5*Ni/ZrO$_2$/CNTs	Impregnation	500	5:1	20,000	400	55	96	[166]
*12*Ni–CeO$_2$/CNTs	Ultrasonic-assisted co-impregnation	350	4:1	30,000	350	84	100	[167]
*7*Ni/Ce$_{0.2}$Zr$_{0.8}$O$_2$/AC	Impregnation	600	4:1	40,000	300	85	100	[168]
*30*Fe–Co/CF	Uniform infiltration	300	27:1	6600	390	65	88	[169]

7.1. Monometallic Carbon-Supported Catalysts

Jiménez et al. [163] prepared Ru impregnated carbon nanofibers (CNFs) with different natures (orientation of graphite planes): platelet, fishbone and ribbon. The catalytic performances were not affected by the nature of the carbon nanofibers used as support. In addition, Li et al. [164] studied Co-based porous carbon (PC) catalysts with controlled crystal morphology and size by using ZIF–67 metal organic framework (MOF) as template and with the aid of surfactants. After carbonization, the obtained samples inherited the original morphology and size of ZIF–67 crystals with a distorted surface. Catalytic tests were carried out at 30 atm and Co nanoparticles inside the carbon matrix ranged between 7 and 20 nm were separated by the graphite-like carbon effectively avoiding metal sintering. Consequently, interesting performances were reported for these samples, especially when compared with similar catalysts supported on commercial activated carbon. Finally, Gödde et al. [165] prepared Ni nanoparticles supported on nitrogen functionalized carbon nanotubes (CNTs) with different Ni loadings (10 to 50 wt%). The optimum loading of 30–40 wt% led to high surface area and small Ni particle sizes, ascribed to the efficient anchoring on the N-doped CNTs. Besides, high stability of the catalysts was demonstrated for 100 h time-on-stream.

7.2. Bi- and Trimetallic Carbon-Supported Catalysts

Romero-Sáez et al. [166] reported Ni–Zr-supported CNTs catalysts by both sequential and co-impregnation methods (metal loadings: 5 wt% Ni and 20 wt% Zr). Authors obtained better results after sequential impregnations, since co-impregnation method resulted in the formation of a core-shell structure where NiO particles were surrounded by ZrO_2, limiting the access of the reactants to Ni active sites during the catalytic tests. On the contrary, sequential impregnation favored Ni reducibility and CO_2 adsorption capacity. Wang et al. [167] prepared Ni-based catalysts supported on multi-walled CNTs and promoted with Ce by ultrasonic-assisted co-impregnation (12 wt% of Ni and Ce contents of 0, 1.5, 3, 4.5 and 6 wt%). Additionally, authors prepared samples supported on γ–Al$_2$O$_3$ for comparison purposes. They verified, in accordance with other studies previously discussed in this work, that Ce enhanced the Ni^0 dispersion, promoted the reduction of metal oxides and favored the CO_2 activation. Meanwhile, the confinement effect of CNTs and the promotion effect of cerium could efficiently prevent active species migration and sintering, as well as restrict carbon deposition. The best results were reported for the 12%Ni–4.5%Ce/CNTs. Le et al. [168] prepared Ni based activated carbons (AC) and verified the effect of adding Ce–Zr oxides as promoters. 7%Ni/AC reference sample was prepared by impregnation while the promoted 7%Ni/Ce$_{0.2}$Zr$_{0.8}$O$_2$/AC sample was prepared by depositing the Ce$_{0.2}$Zr$_{0.8}$O$_2$ mixed oxide prepared by hydrothermal method over the activated carbon and later impregnating 7 wt% Ni over the Ce$_{0.2}$Zr$_{0.8}$O$_2$/AC support. Authors verified that the ceria-zirconia solid solution phase could effectively disperse and stabilize nickel species as well as favor activated carbon CO_2 adsorption capacity. Consequently, 7%Ni/Ce$_{0.2}$Zr$_{0.8}$O$_2$/AC catalyst exhibited higher activity than 7%Ni/AC sample. Finally, Gaidai et al. [169] synthesized carbon fiber (CF) supported Fe–Co catalysts by uniform infiltration of a metal nitrate solution through the carrier (CF) surface, followed by drying. Authors, who performed several treatments in the carbon fibers, found out that oxygenation

increased the amount of oxygen in the surface layer, decreasing active metals reducibility. Carbon fibers pre-reduction increased the amount of oxygen containing groups on the surface through pulling them from the bulk, which was detrimental for the catalytic performances.

7.3. Mechanistic Aspects

Lapidus et al. [170] studied CO_2 methanation mechanism over copper and nickel-based carbon catalysts (Ni/C and Cu/C). They only found CO and water as products on Cu/C, suggesting that CO_2 was so strongly adsorbed on the catalyst's surface that there was not enough adsorbed hydrogen to convert the formed CO into CH_4. In the case of the Ni/C sample, authors observed that CH_4, CO and water were produced, indicating the presence of a sufficient amount of adsorbed hydrogen on the Ni catalyst surface. However, they observed that a longer period of time was needed for detecting CH_4 in the reactor effluent, whereas CO appeared from the beginning of the reaction. Thus, they proposed that CO was an indispensable reaction intermediate. Wang et al. [167] studied Ni–Ce/CNTs and proposed a mechanism where Ce, in conjunction with the CNTs support, donated electrons and facilitated their transfer from the support to the metallic nickel and the absorbed CO_2, accelerating the activation of CO_2 molecules and the formation of atomic hydrogen. Then, the activated CO_2 dissociated on the surface of Ni formed carbonate species further hydrogenated to methane. They also pointed out that CO could be formed as by-product during this process, without playing a role in CH_4 formation.

8. Zeolite-Based Catalysts

Several works have been reported in the last few years dealing with the utilization of zeolite-based materials as catalysts for CO_2 methanation, with a recent review recently published on this topic [24]. Consequently, only the main results found in the literature recently are shown in Table 8 in order to allow a proper comparison with the rest of the catalysts presented in the current work.

Starting by an interesting study recently reported by Hussain et al. [171], fibrous silica-mordenite (without any additional active metal) was synthesized by microemulsion and tested under CO_2 methanation conditions, comparing its properties and performances with those obtained by a commercial MOR zeolite. Both samples presented CH_4 yields below 50% in all the temperature range studied (250–500 °C), but fibrous SiO_2–MOR exhibited better performances (conversion, selectivity and stability for 50 h under reaction conditions), especially at higher temperatures. This behavior was explained by the higher basicity, textural properties and oxygen vacancies found in the sample, able to promote the activity towards CO_2 methanation and suppress coke deposition, boosting stability with time-on-stream.

Table 8. Zeolite-based materials reported in literature for CO_2 methanation reaction.

Catalyst	Preparation Method	T_{red} (°C)	H_2:CO_2	Q_T/W (mL g^{-1} h^{-1})	Best Catalytic Performances			Ref.
					T (°C)	X_{CO2} (%)	S_{CH4} (%)	
SiO_2–MOR [a]	Microemulsion	500	4:1	45,000	500	65	68	[171]
1Fe/13X	Impregnation	400	4:1	n.a.	350	89	76	[172]
6Rh–Y	Ion exchange	450	3:1	6000	150	6	100	[173]
15Ni/USY	Impregnation	470	4:1	86,200	400	73	97	[174]
15Ni/MOR	Impregnation	470	4:1	86,200	440	69	95	[175]
15Ni/ZSM-5	Impregnation	470	4:1	86,200	450	68	94	[175]
5Ni/d-S1	Impregnation	500	4:1	72,000	450	57	91	[176]
10Ni/ZSM-5	Impregnation	500	4:1	n.a.	400	76	99	[177]
10Ni–ZSM-5	Hydrothermal method [b]	400	3:1	n.a.	400	66	100	[178]
10Ni/BEA	Impregnation	500	4:1	30,000	450	73	97	[179]
15Ni/X	Impregnation	470	4:1	12,000	450	53	90	[180]
5Ni/13X	Evaporation impregnation	500	4:1	13,333	320	80	100	[181]
5Ni/5A	Evaporation impregnation	500	4:1	13,333	400	65	95	[181]
5Ni/ITQ-2	Impregnation	450	4:1	9000	400	82	99	[182]

<div align="center">**Table 8.** *Cont.*</div>

Catalyst	Preparation Method	T_{red} (°C)	H_2:CO_2	Q_T/W (mL g^{-1} h^{-1})	Best Catalytic Performances			Ref.
					T (°C)	X_{CO2} (%)	S_{CH4} (%)	
MgO/*13*Ni/USY	Impregnation	700	4:1	86,200	400	63	93	[183]
CeO$_2$/*14*Ni/USY	Impregnation	470	4:1	86,200	400	68	95	[184]
*20*Ni–CeO$_2$/USY	Co-impregnation	470	4:1	86,200	305	78	99	[185]
*0.5*Pt–Co–MOR	Ion exchange	350	4:1	n.a.	350	41	15	[186]
*10*Ni/La$_2$O$_3$/USY	Impregnation	500	4:1	30,000	400	75	100	[179]
*2.5*Ni–*2.5*Ru/13X	Evaporation impregnation	500	4:1	13,333	400	65	92	[187]
*4*Ni–*1*Ru/5A	Evaporation impregnation	500	4:1	13,333	400	60	94	[187]

[a] Fibrous silica–mordenite; [b] Using as Si source a Ni/SiO$_2$ material with Ni incorporated by impregnation.

8.1. Monometallic Zeolite-Supported Catalysts

Franken et al. [172] recently reported Fe/13X (intact and collapsed zeolite structure) catalysts with increasing metal loadings (1, 5 and 10 wt%) and tested under atmospheric and elevated pressures (5–15 bar). Authors verified that the preservation of the zeolite structure allows obtaining higher metallic dispersion and, hence, more favorable performances. In addition, better performances were obtained for the sample presenting the lowest Fe loading, where highly dispersed metallic particles were formed. Generally, authors verified that higher pressures favored the catalytic performances as expected taking into account the characteristics of the Sabatier reaction. However, the 1 wt% Fe/13X catalyst exhibited lower reaction rates at 15 than at 10 bar, which was ascribed to limitations in terms of intermediate species desorption or modifications on Fe species nature at elevated pressure.

Kitamura Bando et al. [173] studied Rh–Y zeolite and Rh/SiO$_2$ catalysts and performed tests at 30 atm. Authors reported better performances for the Rh–Y but it possessed an intense deactivation after 100 min due to the accumulation of H$_2$O (arising from the reaction) inside the cavities of the zeolite. Later, Graça et al. [184] reported Ni/USY catalysts and evaluated the effects of the Ni incorporation method (ion exchange or impregnation) and Ni loading, with 15 wt% found to be the best compromise. The same authors [188,189] reported that the chosen calcination and reduction temperatures as well as the impregnation solvent can be crucial in these materials. Bacariza et al. evaluated the effects of the compensating cation nature [190], Si/Al ratio [174] and zeolite framework type [175] in the performances of Ni-based zeolites. Among all, larger cations (e.g., Cs$^+$), higher Si/Al ratios and USY zeolite led to the best results. In these studies, an additional relevant property of the support was proposed: the hydrophobicity. In fact, several zeolite samples series presenting a systematic and gradual enhancement of hydrophobicity exhibited improved methane yields, which was attributed to a reduced negative effect of the competitive adsorption of produced water over the same sites adsorbing CO$_2$ [118].

Goodarzi et al. [176] prepared 5 wt% Ni catalysts supported over silicalite-1 (S1) and desilicated silicalite–1 (d–S1) zeolites. Authors observed an improvement of the catalytic performances when using as support d–S1 support, mainly due to the confinement effect induced in Ni^0 particles. Chen et al. [178] reported recently a novel Ni–ZSM–5 catalyst synthesized by hydrothermal method and using as Si source a Ni/SiO$_2$ catalyst prepared by impregnation. They compared the properties and performances of this material with conventional Ni/SiO$_2$ and Ni/ZSM–5 catalysts (all with ~10 wt%). Ni–ZSM–5 was strongly stable exhibiting an excellent stability over 40 h time on stream, attributed to an embedment structure able to hinder sintering, while the others reflected severe deactivation after 5 h. Guo et al. [177] compared a Ni/ZSM–5 catalyst with equivalent Ni samples supported over SBA–15, MCM–41, Al$_2$O$_3$ and SiO$_2$. Among them, the Ni/ZSM–5 sample presented the best performances. As already found by Goodarzi et al. [176], desilication provided an encapsulation effect for Ni particles, being CH$_4$ yields significantly improved.

Czuma et al. [180] synthetized an X zeolite from waste fly ashes to be used as support in the preparation of Ni catalysts for CO$_2$ methanation. Despite the partial micropores blockage due to Ni incorporation, the catalyst still presented an adequate surface area, showing a predominant presence of strong basic sites promoting the formation of very stable CO$_2$ species and, consequently, low methane

yields. In spite of the CO_2 conversions obtained (~50%) being slightly lower than those obtained when using commercial zeolites, the use of fly ash zeolites offers the opportunity to use waste from energy sector, which is a positive economic and ecological aspect. Wei et al. [181] prepared 5 wt% Ni supported 5A and 13X zeolites and studied the effects of the Ni precursor salt (nitrate, citrate or acetate) and calcination temperature (300, 350, 400 and 450 °C) on the properties and performances. While no remarkable enhancements were found in the 5A-based samples, the activity, selectivity and stability were highly improved when using nickel citrate as salt and 350–400 °C as calcination temperature for 5Ni/13X (320 °C: 79% of CO_2 conversion, 100% of CH_4 selectivity and stability after 200 h of time-on-stream). They attributed the higher performances of 13X samples to the location of Ni species in the zeolite channels, allowing a confinement effect, while the use of citrate and a mild calcination temperature improved Ni species reducibility and metallic dispersion. Recently, Da Costa-Serra et al. [182] reported a series of ITQ–2 (prepared by delamination using ITQ–1 and MCM–22 as starting materials) and ZSM–5 zeolites impregnated with 5 wt% Ni. They evaluated the effect of the zeolite framework type and the Si/Al ratio and elaborated an enhancement of the performances when decreasing the Al content for both structures due to the improvement of the materials' hydrophobic properties. The best results were revealed by the sample supported over the ITQ–2 with Si/Al = ∞, a purely silica zeolite that led the formation of highly dispersed Ni^0 nanoparticles (<3 nm).

As shown, many works have dealt with the preparation of Ni-supported zeolites. Based on a comparison of the zeolite type (USY [174], MOR [175], ZSM–5 [175], BEA [179], 13X [181], 5A [181] or ITQ–2 [182]—Figure 11), one can observe that USY, MOR, ZSM–5 and ITQ–2 present generally better performances, while 5A is the zeolite leading to the lowest performances.

Monometallic zeolites have been also applied in sorption-enhanced methanation. Indeed, Delmelle et al. [191] prepared 5Ni/13X and 5Ni/5A catalysts by impregnation obtaining similar CH_4 yields. Borgschulte et al. [192] studied a Ni–5A catalyst prepared by ion exchange with <6 wt% Ni, obtaining a CH_4 yield of ~100% when using a H_2:CO_2 ratio of 8:1. Walspurger et al. [193] mixed a Ni-based commercial catalyst with a hydrophilic 4A zeolite and, as suggested by the previous studies from Delmelle et al. [191] and Borgschulte et al. [192], attributed the beneficial effects of using an hydrophilic zeolite to the displacement of the reaction equilibrium to the formation of CH_4. In this context, Isah et al. [178] reported recently a beneficial effect when adding a small fraction (2 wt%) of zeolite over a 10 wt% Ni/Al_2O_3 catalyst, that improved the textural properties without affecting the metallic surface area available.
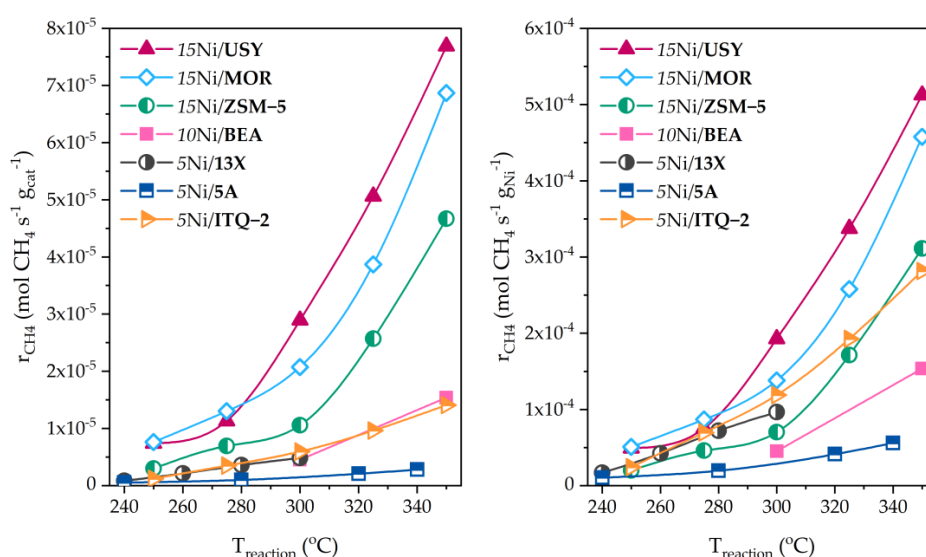

Figure 11. CH_4 production rates per mass of catalyst (left) or Ni (right) determined, far from thermodynamic equilibrium, for a series of Ni/zeolites prepared by impregnation method as a function of the reaction temperatures. Italic numbers correspond to the wt% of Ni in the catalysts.

8.2. Bimetallic Zeolite-Supported Catalysts

Regarding bimetallic catalysts, several studies reported the beneficial effects of adding promoters such as Mg (Bacariza et al. [183]), Ce (Graça et al. [184], Bacariza et al. [185]) or La (Quindimil et al. [179]) over Ni/Zeolite catalysts due to the general enhancement of the CO_2 adsorption capacity and Ni^0 dispersion. In addition, Boix et al. [186] reported interesting results when using Pt-Co/MOR catalysts due to the formation of $PtCo_xO_y$ active species. Recently, Wei et al. [187] reported bimetallic Ni–Ru catalysts supported over 13X and 5A zeolites. Authors kept constant the total metal content (5 wt%) and varied Ru and Ni loadings. They also prepared two monometallic reference samples containing 5 and 2.5 wt% Ni and Ru, respectively. Despite the effects of Ru on the selectivity to CH_4, no remarkable enhancement of the catalytic performances was generally achieved when preparing bimetallic Ni–Ru/Zeolite catalysts, being 5Ni/13X and 5Ni/5A the catalysts exhibiting the highest CO_2 conversions. In terms of mechanism, Westermann et al. proposed some mechanism insights for Ni/USY [194] and Ce/Ni/USY [195] zeolites prepared by impregnation. In both cases formate species were reported as key intermediates.

9. Other Types of Supported Catalysts

Finally, some catalysts not included in the previous chapters, found in the literature, are presented in Table 9 and discussed below.

In this way, Lu et al. [196] studied the promotion effect of VO_x (3, 5 and 8 wt% of V_2O_5) on 20 wt% Ni catalysts supported on raw (RB) and modified bentonite (B) and prepared by impregnation method. The presence of more dispersed Ni^0 particles in the modified bentonite explained the better results obtained for this sample. After adding VO_x, the catalytic activity was further improved due to the higher H_2 uptakes, the increased Ni^0 dispersion and the superior anti-coking and anti-sintering properties of the promoted samples.

Table 9. Different supported materials reported in literature for CO_2 methanation.

Catalyst	Preparation Method	T_{red} (°C)	$H_2:CO_2$	Q_T/W (mL g^{-1} h^{-1})	Best Catalytic Performances			Ref.
					T (°C)	X_{CO2} (%)	S_{CH4} (%)	
20Ni/Bentonite	Impregnation	550	4:1	30,000	400	74	90	[196]
20Ni–VO$_x$/Bentonite	Impregnation	550	4:1	30,000	380	89	87	[196]
20Ni/SiC	Deposition-precipitation	600	50:1	60,000	325	100	100	[197]
15Ni/SiC	Impregnation	400	4:1	n.a.	400	80	99	[198]
15Ni–La$_2$O$_3$/SiC	Co-impregnation	400	4:1	n.a.	350	85	99	[198]
γ–Fe$_2$O$_3$	Commercial	450	200:1	150,000	400	50	70	[199]
Mg/α–Fe$_2$O$_3$	Impregnation	350	4:1	150,000	400	49	65	[200]
12Ni/Co$_3$O$_4$	Impregnation	450	4:1	48,000	250	100	100	[201]
3Pd–LaCoO3	One pot	n.a.	3:1	18,000	300	62	>99	[202]
10Ni/MOF-5	Impregnation	n.a.	4:1	7500	320	75	100	[203]
6.2Ni/TiO$_2$	Impregnation [a]	700	4:1	n.a.	350	73	100	[204]
15Ni/TiO$_2$	Deposition-precipitation	450	4:1	2400	260	96	99	[205]
5Ru/TiO$_2$	Impregnation	300	4:1	90,000	300	80	100	[206]
20Co/Y$_2$O$_3$–TiO$_2$	Deposition-precipitation	400	4:1	3600	350	86	100	[207]
5Ni–Sepiolite	Precipitation	450	4:1	9000	400	88	100	[208]
15Ni–Todorokite	Sequential method	450	4:1	9000	300	90	100	[208]
25Ni/Attapulgite	Impregnation	600	4:1	11,400	400	85	99	[209]

[a] Calcination under DBD plasma.

Additionally, Le et al. [197] reported Ni-based catalysts using SiC and SiO_2 as supports prepared by wet impregnation and deposition-precipitation (DP) methods. Authors observed an enhancement of the metal-support interactions and metallic dispersion when using DP method, which induced a significant effect in the improvement of the CO/CO_2 methanation performances over the SiC supported catalyst. SiC turned out to be the most behaving support due to its superior thermal conductivity.

Additionally, authors reported the beneficial effect of including Mn in the formulation, due to the favored metallic dispersion and CO_2 activation capacity. In addition, Zhi et al. [198] studied Ni and 15%Ni–5%La catalysts supported on SiC and prepared by impregnation. La_2O_3 promoted the dispersion of Ni species on the SiC support simultaneously increasing the number of active sites on the catalyst surface and leading to better performances than the one reported for the Ni/SiC catalyst.

Kirchner et al. [199] studied different Fe_2O_3 catalysts and reported the best activity for nanosized γ–Fe_2O_3. Authors associated the efficiency of this catalyst with reactive surface carbon species. Baysal and Kureti [200] also reported the use of commercial α–Fe_2O_3 promoted with alkali (Li, Na, K, Rb and Cs), alkali earth (Mg, Ca and Ba), transition (Al, Mn, Cu and Mo) or rare earth (La, Ce and Sm) metals for CO_2 methanation at variable pressures. Among all, Mg (2 wt%) was identified as the most promising promoter. Indeed, MgO species, highly dispersed over iron oxide, were responsible for favorable changes in the iron phase composition and in the intermediate carbon species (e.g., Fe carbides).

Wang et al. [201] prepared hierarchically porous network-like Ni/3D draped Co_3O_4 catalysts, where Ni clusters and nanodeposits were uniformly dispersed across the high surface area of the Co_3O_4 support. The pre-reduction treatment was found to induce oxygen vacancies formation, improving Ni-Co interaction, enhancing the catalytic performances and lowering the activation energy. Wang et al. [202] studied two perovskite $LaCoO_3$ based catalysts: PdO–$LaCoO_3$ with an encapsulated structure and $PdO/LaCoO_3$ with a surface dispersing structure. The best catalytic performances were achieved by the encapsulated structure, which was attributed to the strong interaction of PdO NPs and $LaCoO_3$ and also to the H_2 spillover effect of Pd. Thus, the decomposition of perovskite structure was significantly promoted, benefiting the extraction of metallic Co NPs from $LaCoO_3$ to prepare a well-dispersed catalyst. Besides, the spent catalysts revealed that well-dispersed catalytically active Co_2C was in situ formed accompanied with perovskite structure decomposition during the catalytic reaction. $LaCoO_3$ and $PdO/LaCoO_3$ catalysts showed a weak interaction and the perovskite structure remained with few Co_2C, explaining the significant difference of catalytic performance.

Branco and Ferreira [210–213] reported a series of Co and Ni-based bimetallic materials containing f block elements such as Th, U, La, Ce, Sm, Dy or Yb. Starting by Ni–Th and Ni–U catalysts [210], authors studied two preparation methods: controlled oxidation under dry air, using intermetallic binary compounds as precursors, and a modified sol-gel. The intermetallic route induced more favorable interactions between Ni and f block elements, resulting in better performances. Additionally, Th led to better results than U. Furthermore, authors used electrospinning followed by a controlled oxidation treatment for synthesizing Ni–La, Ni–Ce, Ni–Sm, Ni–Dy and Ni–Yb catalysts in the form of nanofibers and nanoparticles [211]. While the morphology of the catalysts did not affect the performances, results were found to increase along the lanthanide series, with Dy and Ce leading to the best performances. Authors also compared Ni–La, Fe–Dy and Co–Sm catalytic systems prepared by electrospinning followed by oxidation [212], being the first catalyst the most significantly active towards CO_2 methanation (Fe–Dy and Co–Sm presented >95% selectivity towards CO). Finally, Branco et al. [213] evaluated the effect of the calcination temperature on Co–Lanthanide (La, Ce, Sm, Gd, Dy and Yb) aerogels prepared by epoxide addition method. They observed that higher temperatures promote the formation of perovskite structures (except for Ce and Yb), enhancing catalysts basicity and activity, but presenting lower selectivity towards methane. Among all, the use of Ce as promoter and a calcination temperature of 900 °C led to the best results.

Zhen et al. [203] prepared a series of Ni/MOF–5 with increasing Ni loadings and obtained the highest catalytic activity with 10Ni/MOF–5 catalyst. This material presented high specific surface area and large pore volume that provided highly uniform dispersed Ni particles in the framework. Besides, this catalyst showed high stability and almost no deactivation during a long-term stability test (100 h).

Zhou et al. [204] studied Ni/TiO_2 catalysts prepared by impregnation followed by DBD plasma decomposition. Authors found out the structure-sensitivity of the reaction over Ni/TiO_2 catalysts and reported the beneficial effect of Ni(111) in the activity achieved. They suggested that, while the existence of multiple Ni facets induces a reaction mechanism passing through formate species as intermediates

and with Ni only participating in H_2 dissociation, Ni(111) promotes also CO_2 dissociation into CO, leading to a mechanism where carbon monoxide acts as an intermediate for the final production of CH_4. Kim et al. [214] studied Ru/TiO_2 catalysts and the effect of mixing anatase and rutile TiO_2 phases. Mixtures were done by using several ratios and at different stages: before RuO_2 deposition and before or after annealing. A synergetic effect was verified when the mixing was done before the annealing, leading to a higher catalytic activity. In this case, RuO_2 nanoparticles migrated towards the TiO_2 phase to be stabilized and lately reduced. Petala et al. [206] studied the effects of alkali (Li, Na, K, Cs) incorporation on Ru/TiO_2 based catalysts (0.5 and 5 wt% of Ru). The effect of the alkali promoters in the observed performances was stronger over the low Ru content catalyst ($0.5\%Ru/TiO_2$) while, in the $5\%Ru/TiO_2$ sample no significant effects were verified. Catalytic activity was strongly improved with the addition of small alkali contents (0.2 wt%), following the order: TiO_2 (unpromoted) < Li ~ K < Cs < Na, with Na-promoted sample being 3 times more active that the unpromoted catalyst. Zuzeng et al. [207] evaluated the effects of doping TiO_2 with Y (0, 1.0, 2.0 and 3.0 wt%) to obtain $Co/Y-TiO_2$ catalysts (20 wt% Co). The best catalytic activity was exhibited by the $20\%Co/2\%Y-TiO_2$ and the incorporation of Y increased the specific surface area, enhanced the reducibility, generated oxygen vacancies and improved CO_2 adsorption capacity through the creation of medium basic sites. Finally, Marwood et al. [215] used $2\%Ru/TiO_2$ to perform CO_2 methanation mechanism studies and observed the formation of CO as a reaction intermediate. However, they suggested that CO was not formed as a result of the dissociative adsorption of CO_2 but as a product of formate species.

Cerdá-Moreno et al. [208] reported Ni–Sepiolite catalysts, prepared by precipitation and impregnation, and a Ni–Todorokite synthesized by sequential method and with 5 wt% Ni. Authors studied not only the properties and performances but also proposed the mechanism over these two materials based on Operando DRIFTS studies. Overall, todorokite led to higher performances, even at lower reaction temperatures, mainly due to its ability to activate CO_2 forming intermediate species (carbonates) further hydrogenated to formates and, later, CH_4 (associative mechanism). Oppositely, sepiolite did not adsorb CO_2, being CO the main reaction intermediate (dissociative mechanism). Regarding the preparation method followed for Ni/Sepiolite catalysts, precipitation improved the reducibility of the Ni species formed and the metallic dispersion.

Liang et al. [209] reported Ni/Attapulgite catalysts prepared by impregnation with varied Ni loading (5, 15 and 25 wt%). Higher Ni content reduced the textural properties of the material, the metallic-support interactions and the number of basic sites, while the average Ni^0 size increased. However, and in line with several works already discussed, increasing the metal loading improved the activity and, mainly, the selectivity to CH_4 as a result of the CO formation suppression.

In order to compare among the different types of new or not widely explored supports and as previously done, CH_4 production rates were determined far from the equilibrium for Ni-based bentonite [196], SiC [197], Co_3O_4 [201], MOF–5 [203], sepiolite [208], todorokite [208] and attapulgite [209] (Figure 12). Based on the plotted data, the use and optimization of Co_2O_3, todorokite and sepiolite-based catalysts in CO_2 methanation reaction constitute an interesting topic for further research in this area.
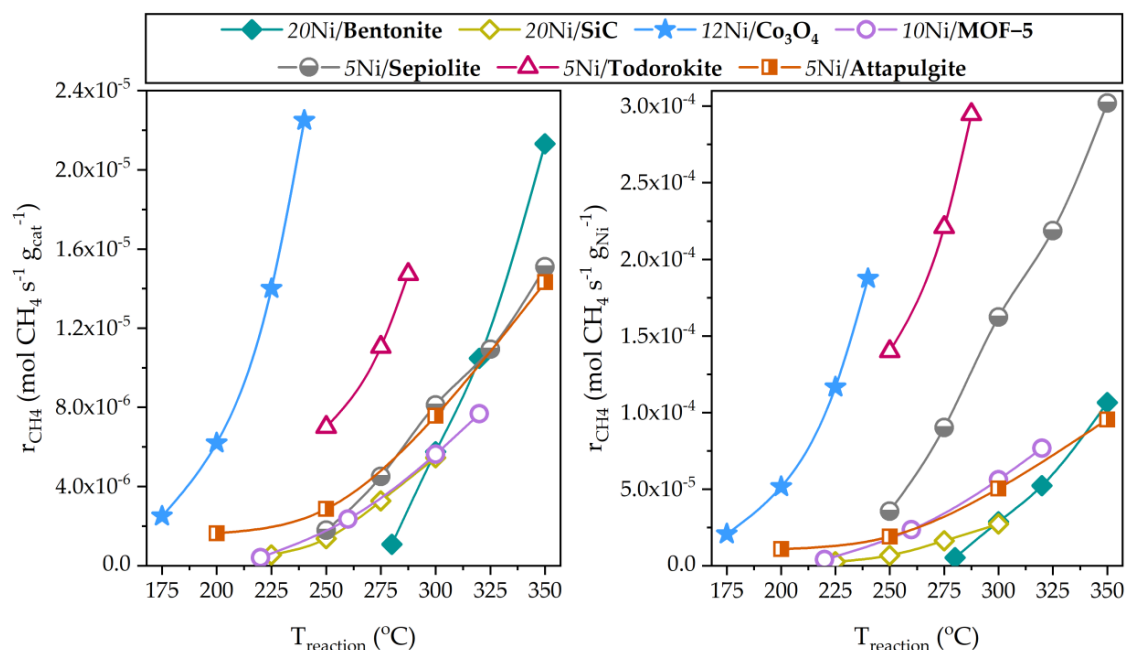
Figure 12. CH_4 production rates per mass of catalyst (left) or Ni (right) determined, far from thermodynamic equilibrium, for a series of Ni-supported catalysts prepared using non-conventional supports a function of the reaction temperatures. Italic numbers correspond to the wt% of Ni in the catalysts.

10. Final Remarks and Conclusions

As concluded from the results presented in previous chapters, supported nickel catalysts are the most studied for CO_2 methanation reaction. However, their main drawback arises from their sintering processes and the deactivation at low temperatures, which is due to the interaction of nickel metal particles with CO and the formation of mobile nickel sub-carbonyls. Consequently, nickel catalysts are typically modified by adding promoters and stabilizers (e.g., Ce, Zr, La, Ti, Mg) in order to avoid deactivation processes [216]. Additionally, ruthenium could be considered as the alternative metal used on CO_2 methanation catalysts since, although more expensive, is highly active and stable for this reaction. Even if several studies have also reported interesting results when using alternative metals (e.g., iron, cobalt), they typically required pressures above the atmospheric, as their activity is generally lower than that exhibited by Ni catalysts.

Regarding the supports, it can be concluded that their nature is crucial for the achievement of significant catalytic performances. Indeed, the dispersion and reducibility of the active metals, the activation of CO_2 and H_2, and the reaction mechanisms are deeply influenced by the choice of the support. As seen, SiO_2 and Al_2O_3 have been widely and extensively studied due to their good initial activities and relatively cheap prices. However, SiO_2 and Al_2O_3 based catalysts often suffer from sintering and serious carbon deposition at high temperatures. Additionally, CeO_2 and ZrO_2 have been revealed responsible for CO_2 activation due to the presence of oxygen vacancies in their structure as well as promoting the reducibility and dispersion of other metals. Mesoporous SiO_2 materials allow the favorable dispersion of Ni particles due to their porous structure, as occurs also in some carbon and zeolite-based supports, with the last being easily tunable in terms of hydrophobicity and basicity. MgO and hydrotalcite-derived materials present beneficial effects in terms of interaction with CO_2 due to the enhanced basicity of these materials even if the reducibility of the metal species is sometimes compromised due to the strong metal-support interactions. Finally, some other materials were found promising for CO_2 methanation, such as Fe and Co oxides, SiC, MOFs, sepiolite, todorokite or TiO_2.

To conclude, this work aims to become a starting point or a roadmap for researchers intending to enhance heterogeneous catalysts properties and performances towards CO_2 methanation. Indeed,

a remarkable number of publications regarding supported catalysts for thermal Sabatier reaction were summarized not only in terms of main conclusions but also in terms of achieved catalytic performances and preparation conditions used so that researchers could have an idea about the main properties to guarantee and the main drawbacks of the chosen supports.

Based on the previous findings, we claim that the main properties to be considered for CO_2 methanation catalysts must be the ones summarized in Figure 13 and described below.

- Metallic dispersion. Based on the analyzed studies, catalysts presenting higher metallic dispersion and smaller particles present typically better performances due to the favored H_2 dissociation capacity. These properties can be enhanced by tuning the preparation conditions (e.g., method, solvent, calcination and reduction temperatures), adding promoters (e.g., CeO_2, MgO, ZrO_2, La_2O_3) or, among all, through encapsulation strategies;

- Basicity. CO_2 can be, based on the previously summarized works, adsorbed and activated on basic sites. Generally, authors have identified medium strength basic sites as the most promising for CO_2 methanation, since stronger sites lead to the formation of inactive carbonate species. These types of sites can be obtained by adding a basic promoter, such as MgO, or using a support able to interact with CO_2 (e.g., CeO_2, zeolites, Al_2O_3);

- Oxygen vacancies. Several authors referred to the presence of oxygen vacancies and its responsibility in the enhancement of CO_2 activation. This can be achieved by using pure or modified CeO_2, ZrO_2 or TiO_2 oxides or even KCC–1 mesoporous material;

- Metal-support interactions. Typically, this property is related to the metal dispersion and average particle sizes. Indeed, strong metal-support interactions (SMSI) can promote the formation of smaller and well-dispersed metallic particles, typically resisting sintering and carbon formation. However, the use of higher reduction temperatures could be required. SMSI can be obtained by tuning the preparation conditions. Indeed, while impregnation typically leads to weaker interactions, the insertion of the active metals into the support framework (e.g., ZrO_2, CeO_2, Al_2O_3, TiO_2) represents a promising alternative;

- Reducibility. Even if few works suggested a possible role of metal oxides in the reaction (e.g., NiO), metallic states of transition or noble metals are typically considered as the active phases for the CO_2 methanation reaction. This property, hardly dependent on the metal-support interactions, could be responsible for a reduction in the number of available active sites. It is important to deem in mind that increasing the reduction temperature to maximize the amount of reduced species can lead to severe sintering processes, which can negatively influence the observed performances. Authors found improvements in reducibility by adding promoters (e.g., CeO_2, MgO, ZrO_2, La_2O_3);

- Hydrophobicity. Water inhibitory effect in the CO_2 methanation reaction was proved by several research studies. From the literature about zeolite supports, it was pointed out that the lower the affinity of the support for water adsorption (higher hydrophobicity), the higher the methane yields produced. The adsorption of water on the same sites for CO_2 adsorption may comprehensively induce a negative kinetic effect on the methanation process. Consequently, it is important to use supports and/or promoters presenting low and weak affinity with water;

- Textural properties. Mesoporous materials have gained attention in the last years for this reaction as they can be responsible for encapsulation effects able to reduce metallic particle sizes and strengthen metal-support interactions, resulting in higher catalytic performances. Apart from the use of conventional mesoporous materials, carbons or zeolites as supports, strategies for obtaining ordered mesoporous structures such as Al_2O_3 represent promising strategies.
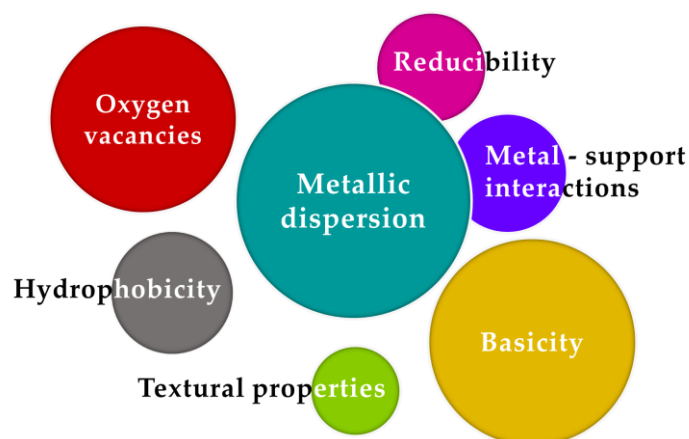
Figure 13. Favorable properties for obtaining active, selective and stable CO_2 methanation catalysts.

Finally, further research on the topics presented below could be useful towards a better understanding of CO_2 methanation reaction and its application at industrial scale:

- Supports. The optimization and further development of new catalysts based on promising but not deeply explored materials such as MOFs or mesoporous silicas would be a promising pathway [217–219]. In addition, the utilization of waste materials (e.g., fly ash, rice husk) as support precursors constitutes an interesting route towards higher cost-efficient catalysts [220];
- Active metals. The systematic analysis of alternative transition (e.g., Co, Fe) or noble (e.g., Ru, Rh) active metals for CO_2 methanation is a topic of high interest. Complementary, further efforts towards the identification and optimization of synergistic effects in bimetallic systems (e.g., Ni-Co, Ni–Fe) through advanced characterization techniques would be highly valuable;
- Mechanistic approaches. Modelling and in situ/Operando spectroscopy studies carried out using density-functional theory (DFT), DRIFTS or Operando FTIR under conventional and more realistic methanation conditions (e.g., incorporation of pollutants/minor compounds present in flue gases, biogas or hydrogen streams in the feed) will be advantageous. In addition, further studies dealing with the elucidation of the deactivation mechanisms over different types of catalysts, using as basis long-term and aging experiments, will be helpful;
- Catalytic testing. Although few works dealt with the effects of incorporating CO, CH_4 or even steam in the reactor feed, evaluating CO_2 methanation performances under realistic conditions will be key for identifying strategies to obtain catalysts with high resistance to, among all, oxygen, steam or H_2S. In addition, further research on the preparation of scale-up catalysts (e.g., monoliths) will be important.

References

1. Denholm, P.; Ela, E.; Kirby, B.; Milligan, M. *The Role of Energy Storage with Renewable Electricity Generation*; Technical Report; National Renewable Energy Laboratory: Golden, CO, USA, 2010; pp. 1–61.
2. Weitzel, T.; Glock, C.H. Energy management for stationary electric energy storage systems: A systematic literature review. *Eur. J. Oper. Res.* **2018**, *264*, 582–606. [CrossRef]

3. Chen, H.; Cong, T.N.; Yang, W.; Tan, C.; Li, Y.; Ding, Y. Progress in electrical energy storage system: A critical review. *Prog. Nat. Sci.* **2009**, *19*, 291–312. [CrossRef]

4. Blanco, H.; Faaij, A. A review at the role of storage in energy systems with a focus on Power to Gas and long-term storage. *Renew. Sustain. Energy Rev.* **2018**, *81*, 1049–1086. [CrossRef]

5. Schaaf, T.; Grünig, J.; Schuster, M.R.; Rothenfluh, T.; Orth, A. Methanation of CO_2 - storage of renewable energy in a gas distribution system. *Energy Sustain. Soc.* **2014**, *4*, 2. [CrossRef]

6. Ghaib, K.; Ben-Fares, F.-Z. Power-to-Methane: A state-of-the-art review. *Renew. Sustain. Energy Rev.* **2018**, *81*, 433–446. [CrossRef]

7. Sterner, M. *Bioenergy and Renewable Power Methane in Integrated 100% Renewable Energy Systems: Limiting Global Warming By Transforming Energy Systems*; Kassel University Press GmbH: Kassel, Germany, 2009; ISBN 978-3-89958-799-9.

8. International Renewable Energy Agency (IRENA). *Global Energy Transformation: A Roadmap to 2050 (2019 edition)*; International Renewable Energy Agency: Abu Dhabi, UAE, 2019.

9. U.S. Energy Information Administration (EIA). *International Energy Outlook 2019*; U.S. Energy Information Administration (EIA): Washington, DC, USA, 2019.

10. Pachauri, R.K.; Meyer, L.A. *Climate Change 2014: Synthesis Report. Contribution of Working Groups I, II and III to the Fifth Assessment Report of the Intergovernmental Panel on Climate Change*; Intergovernmental Panel on Climate Change (IPCC): Geneva, Switzerland, 2014.

11. Andrew, R.M. Global CO_2 emissions from cement production, 1928–2018. *Earth Syst. Sci. Data* **2019**, *11*, 1675–1710. [CrossRef]

12. IEA. Technology Roadmap-Low-Carbon Transition in the Cement Industry–Analysis, IEA, Paris. 2018. Available online: https://www.iea.org/reports/technology-roadmap-low-carbon-transition-in-the-cement-industry (accessed on 30 June 2020).

13. Aresta, M.; Dibenedetto, A.; Quaranta, E. State of the art and perspectives in catalytic processes for CO_2 conversion into chemicals and fuels: The distinctive contribution of chemical catalysis and biotechnology. *J. Catal.* **2016**, *343*, 2–45. [CrossRef]

14. Aresta, M.; Dibenedetto, A. Utilisation of CO_2 as a chemical feedstock: opportunities and challenges. *Dalton Trans.* **2007**, 2975. [CrossRef]

15. Aresta, M.; Dibenedetto, A.; Angelini, A. The changing paradigm in CO_2 utilization. *J. CO2 Util.* **2013**, *3–4*, 65–73. [CrossRef]

16. Wang, W.; Wang, S.; Ma, X.; Gong, J. Recent advances in catalytic hydrogenation of carbon dioxide. *Chem. Soc. Rev.* **2011**, *40*, 3703–3727. [CrossRef]

17. Frontera, P.; Macario, A.; Ferraro, M.; Antonucci, P. Supported Catalysts for CO_2 Methanation: A Review. *Catalysts* **2017**, *7*, 59. [CrossRef]

18. Ghaib, K.; Nitz, K.; Ben-Fares, F.-Z. Chemical Methanation of CO_2: A Review. *ChemBioEng Rev.* **2016**, *3*, 266–275. [CrossRef]

19. Jin Lee, W.; Li, C.; Prajitno, H.; Yoo, J.; Patel, J.; Yang, Y.; Lim, S. Recent trend in thermal catalytic low temperature CO_2 methanation: A Critical Review. *Catal. Today* **2020**. [CrossRef]

20. Rönsch, S.; Schneider, J.; Matthischke, S.; Schlüter, M.; Götz, M.; Lefebvre, J.; Prabhakaran, P.; Bajohr, S. Review on methanation – From fundamentals to current projects. *Fuel* **2016**, *166*, 276–296. [CrossRef]

21. Malara, A.; Frontera, P.; Antonucci, P.; Macario, A. Smart recycling of carbon oxides: Current status of methanation reaction. *Curr. Opin. Green Sustain. Chem.* **2020**, *26*, 100376. [CrossRef]

22. Ashok, J.; Pati, S.; Hongmanorom, P.; Tianxi, Z.; Junmei, C.; Kawi, S. A review of recent catalyst advances in CO_2 methanation processes. *Catal. Today* **2020**. [CrossRef]

23. Huynh, H.L.; Yu, Z. CO_2 Methanation on Hydrotalcite-Derived Catalysts and Structured Reactors: A Review. *Energy Technol.* **2020**, *8*, 1901475. [CrossRef]

24. Bacariza, M.C.; Graça, I.; Lopes, J.M.; Henriques, C. Tuning Zeolite Properties towards CO_2 Methanation: An Overview. *Chem. Cat. Chem.* **2019**, *11*, 2388–2400. [CrossRef]

25. Tsiotsias, A.I.; Charisiou, N.D.; Yentekakis, I.V.; Goula, M.A. The Role of Alkali and Alkaline Earth Metals in the CO_2 Methanation Reaction and the Combined Capture and Methanation of CO2. *Catalysts* **2020**, *10*, 812. [CrossRef]

26. Lv, C.; Xu, L.; Chen, M.; Cui, Y.; Wen, X.; Li, Y.; Wu, C.; Yang, B.; Miao, Z.; Hu, X.; et al. Recent Progresses in Constructing the Highly Efficient Ni Based Catalysts With Advanced Low-Temperature Activity Toward CO_2 Methanation. *Front. Chem.* **2020**, *8*. [CrossRef]

27. Solis-Garcia, A.; Fierro-Gonzalez, J.C. Mechanistic Insights into the CO2 Methanation Catalyzed by Supported Metals: A Review. Available online: https://www.ingentaconnect.com/content/asp/jnn/2019/00000019/00000006/art00005 (accessed on 28 April 2020).

28. Kuznecova, I.; Gusca, J. Property based ranking of CO and CO_2 methanation catalysts. *Energy Procedia* **2017**, *128*, 255–260. [CrossRef]

29. Erdőhelyi, A. Hydrogenation of Carbon Dioxide on Supported Rh Catalysts. *Catalysts* **2020**, *10*, 155. [CrossRef]

30. Choe, S.-J.; Kang, H.-J.; Kim, S.-J.; Park, S.-B.; Park, D.-H.; Huh, D.-S. Adsorbed Carbon Formation and Carbon Hydrogenation for CO_2 Methanation on the Ni(111) Surface: ASED-MO Study. *Bull. Korean Chem. Soc.* **2005**, *26*, 1682–1688. [CrossRef]

31. Ren, J.; Guo, H.; Yang, J.; Qin, Z.; Lin, J.; Li, Z. Insights into the mechanisms of CO_2 methanation on Ni(111) surfaces by density functional theory. *Appl. Surf. Sci.* **2015**, *351*, 504–516. [CrossRef]

32. Zhao, K.; Calizzi, M.; Moioli, E.; Li, M.; Borsay, A.; Lombardo, L.; Mutschler, R.; Luo, W.; Züttel, A. Unraveling and optimizing the metal-metal oxide synergistic effect in a highly active $Co_x(CoO)_{1-x}$ catalyst for CO_2 hydrogenation. *J. Energy Chem.* **2021**, *53*, 241–250. [CrossRef]

33. Wu, H.C.; Chang, Y.C.; Wu, J.H.; Lin, J.H.; Lin, I.K.; Chen, C.S. Methanation of CO_2 and reverse water gas shift reactions on Ni/SiO_2 catalysts: The influence of particle size on selectivity and reaction pathway. *Catal. Sci. Technol.* **2015**, *5*, 4154–4163. [CrossRef]

34. Ye, R.-P.; Gong, W.; Sun, Z.; Sheng, Q.; Shi, X.; Wang, T.; Yao, Y.; Razink, J.J.; Lin, L.; Zhou, Z.; et al. Enhanced stability of Ni/SiO_2 catalyst for CO_2 methanation: Derived from nickel phyllosilicate with strong metal-support interactions. *Energy* **2019**, *188*, 116059. [CrossRef]

35. Guo, M.; Lu, G. The effect of impregnation strategy on structural characters and CO_2 methanation properties over MgO modified Ni/SiO_2 catalysts. *Catal. Commun.* **2014**, *54*, 55–60. [CrossRef]

36. Kim, H.Y.; Lee, H.M.; Park, J.-N. Bifunctional Mechanism of CO_2 Methanation on $Pd-MgO/SiO_2$ Catalyst: Independent Roles of MgO and Pd on CO_2 Methanation. *J. Phys. Chem. C* **2010**, *114*, 7128–7131. [CrossRef]

37. Park, J.-N.; McFarland, E.W. A highly dispersed $Pd–Mg/SiO_2$ catalyst active for methanation of CO_2. *J. Catal.* **2009**, *266*, 92–97. [CrossRef]

38. Ali, S.A.M.; Hamid, K.H.K.; Ismail, K.N. Effect of Calcination Temperature on The Structure and Catalytic Performance Of $80Ni20CO/SiO_2$ Catalyst for CO_2 Methanation. In *3rd Electronic and Green Materials International Conference 2017 (egm 2017)*; Abdullah, M.M.A., Ramli, M.M., AbdRahim, S.Z., Isa, S.S.M., Saad, M.N.M., Ismail, R.C., Ghazli, M.F., Eds.; Amer Inst Physics: Melville, NY, USA, 2017; Volume 1885, p. UNSP 020272-1. ISBN 978-0-7354-1565-2.

39. Trovarelli, A.; Deleitenburg, C.; Dolcetti, G.; Lorca, J.L. CO_2 Methanation Under Transient and Steady-State Conditions over Rh/CeO_2 and CeO_2-Promoted Rh/SiO_2: The Role of Surface and Bulk Ceria. *J. Catal.* **1995**, *151*, 111–124. [CrossRef]

40. Li, S.; Guo, S.; Gong, D.; Kang, N.; Fang, K.-G.; Liu, Y. Nano composite composed of MoO_x-La_2O_3Ni on SiO_2 for storing hydrogen into CH_4 via CO_2 methanation. *Int. J. Hydrogen Energy* **2019**, *44*, 1597–1609. [CrossRef]

41. Branco, J.B.; Brito, P.E.; Ferreira, A.C. Methanation of CO_2 over nickel-lanthanide bimetallic oxides supported on silica. *Chem. Eng. J.* **2020**, *380*, 122465. [CrossRef]

42. Vogt, C.; Wijten, J.; Madeira, C.L.; Kerkenaar, O.; Xu, K.; Holzinger, R.; Monai, M.; Weckhuysen, B.M. Alkali Promotion in the Formation of CH_4 from CO_2 and Renewably Produced H_2 over Supported Ni Catalysts. *Chem. Cat. Chem.* **2020**, *12*, 2792–2800. [CrossRef]

43. Aziz, M.A.A.; Jalil, A.A.; Triwahyono, S.; Sidik, S.M. Methanation of carbon dioxide on metal-promoted mesostructured silica nanoparticles. *Appl. Catal. A* **2014**, *486*, 115–122. [CrossRef]

44. Aziz, M.A.A.; Jalil, A.A.; Triwahyono, S.; Saad, M.W.A. CO_2 methanation over Ni-promoted mesostructured silica nanoparticles: Influence of Ni loading and water vapor on activity and response surface methodology studies. *Chem. Eng. J.* **2015**, *260*, 757–764. [CrossRef]

45. Nguyen, P.-A.; Luu, C.-L.; Nguyen, T.-T.-V.; Nguyen, T.; Hoang, T.-C. Improving the performance of nickel catalyst supported on mesostructured silica nanoparticles in methanation of CO_2-rich gas by urea–nitrate combustion. *Chem. Pap.* **2020**. [CrossRef]

46. Zhou, G.; Wu, T.; Xie, H.; Zheng, X. Effects of structure on the carbon dioxide methanation performance of Co-based catalysts. *Int. J. Hydrogen Energy* **2013**, *38*, 10012–10018. [CrossRef]

47. Zhou, G.; Wu, T.; Zhang, H.; Xie, H.; Feng, Y. Carbon Dioxide Methanation on Ordered Mesoporous Co/KIT-6 Catalyst. *Chem. Eng. Commun.* **2014**, *201*, 233–240. [CrossRef]

48. Liu, H.; Xu, S.; Zhou, G.; Xiong, K.; Jiao, Z.; Wang, S. CO_2 hydrogenation to methane over Co/KIT-6 catalysts: Effect of Co content. *Fuel* **2018**, *217*, 570–576. [CrossRef]

49. Liu, H.; Xu, S.; Zhou, G.; Huang, G.; Huang, S.; Xiong, K. CO_2 hydrogenation to methane over Co/KIT-6 catalyst: Effect of reduction temperature. *Chem. Eng. J.* **2018**, *351*, 65–73. [CrossRef]

50. Merkache, R.; Fechete, I.; Maamache, M.; Bernard, M.; Turek, P.; Al-Dalama, K.; Garin, F. 3D ordered mesoporous Fe-KIT-6 catalysts for methylcyclopentane (MCP) conversion and carbon dioxide (CO_2) hydrogenation for energy and environmental applications. *Appl. Catal. A-Gen.* **2015**, *504*, 672–681. [CrossRef]

51. Cao, H.; Wang, W.; Cui, T.; Wang, H.; Zhu, G.; Ren, X. Enhancing CO_2 Hydrogenation to Methane by Ni-Based Catalyst with V Species Using 3D-mesoporous KIT-6 as Support. *Energies* **2020**, *13*, 2235. [CrossRef]

52. Liu, Q.; Tian, Y. One-pot synthesis of NiO/SBA-15 monolith catalyst with a three-dimensional framework for CO_2 methanation. *Int. J. Hydrogen Energy* **2017**, *42*, 12295–12300. [CrossRef]

53. Lu, B.; Ju, Y.; Abe, T.; Kawamoto, K. Grafting Ni particles onto SBA-15, and their enhanced performance for CO_2 methanation. *RSC Adv.* **2015**, *5*, 56444–56454. [CrossRef]

54. Bacariza, M.C.; Graça, I.; Bebiano, S.S.; Lopes, J.M.; Henriques, C. Micro- and mesoporous supports for CO_2 methanation catalysts: A comparison between SBA-15, MCM-41 and USY zeolite. *Chem. Eng. Sci.* **2018**, *175*, 72–83. [CrossRef]

55. Li, Y.; Zhang, H.; Zhang, L.; Zhang, H. Bimetallic NiPd/SBA-15 alloy as an effective catalyst for selective hydrogenation of CO_2 to methane. *Int. J. Hydrogen Energy* **2019**, *44*, 13354–13363. [CrossRef]

56. Du, G.; Lim, S.; Yang, Y.; Wang, C.; Pfefferle, L.; Haller, G.L. Methanation of carbon dioxide on Ni-incorporated MCM-41 catalysts: The influence of catalyst pretreatment and study of steady-state reaction. *J. Catal.* **2007**, *249*, 370–379. [CrossRef]

57. Wang, X.; Zhu, L.; Liu, Y.; Wang, S. CO_2 methanation on the catalyst of Ni/MCM-41 promoted with CeO_2. *Sci. Total Environ.* **2018**, *625*, 686–695. [CrossRef]

58. Taherian, Z.; Khataee, A.; Orooji, Y. Promoted nickel-based catalysts on modified mesoporous silica support: The role of yttria and magnesia on CO_2 methanation. *Microporous Mesoporous Mater.* **2020**, *306*, 110455. [CrossRef]

59. Hamid, M.Y.S.; Firmansyah, M.L.; Triwahyono, S.; Jalil, A.A.; Mukti, R.R.; Febriyanti, E.; Suendo, V.; Setiabudi, H.D.; Mohamed, M.; Nabgan, W. Oxygen vacancy-rich mesoporous silica KCC-1 for CO_2 methanation. *Appl. Catal. A* **2017**, *532*, 86–94. [CrossRef]

60. Shahul Hamid, M.Y.; Triwahyono, S.; Jalil, A.A.; Che Jusoh, N.W.; Izan, S.M.; Tuan Abdullah, T.A. Tailoring the Properties of Metal Oxide Loaded/KCC-1 toward a Different Mechanism of CO_2 Methanation by in Situ IR and ESR. *Inorg. Chem.* **2018**, *57*, 5859–5869. [CrossRef] [PubMed]

61. Lv, C.; Xu, L.; Chen, M.; Cui, Y.; Wen, X.; Wu, C.; Yang, B.; Wang, F.; Miao, Z.; Hu, X.; et al. Constructing highly dispersed Ni based catalysts supported on fibrous silica nanosphere for low-temperature CO_2 methanation. *Fuel* **2020**, *278*, 118333. [CrossRef]

62. Liu, Q.; Dong, H. In Situ Immobilizing Ni Nanoparticles to FDU-12 via Trehalose with Fine Size and Location Control for CO_2 Methanation. *ACS Sustainable Chem. Eng.* **2020**, *8*, 2093–2105. [CrossRef]

63. Aziz, M.A.A.; Jalil, A.A.; Triwahyono, S.; Mukti, R.R.; Taufiq-Yap, Y.H.; Sazegar, M.R. Highly active Ni-promoted mesostructured silica nanoparticles for CO_2 methanation. *Appl. Catal. B* **2014**, *147*, 359–368. [CrossRef]

64. Wang, W.; Qi, R.; Shan, W.; Wang, X.; Jia, Q.; Zhao, J.; Zhang, C.; Ru, H. Synthesis of KIT-6 type mesoporous silicas with tunable pore sizes, wall thickness and particle sizes via the partitioned cooperative self-assembly process. *Microporous Mesoporous Mater.* **2014**, *194*, 167–173. [CrossRef]

65. Soni, K.; Rana, B.S.; Sinha, A.K.; Bhaumik, A.; Nandi, M.; Kumar, M.; Dhar, G.M. 3-D ordered mesoporous KIT-6 support for effective hydrodesulfurization catalysts. *Appl. Catal. B* **2009**, *90*, 55–63. [CrossRef]

66. Singh, S.; Kumar, R.; Setiabudi, H.D.; Nanda, S.; Vo, D.-V.N. Advanced synthesis strategies of mesoporous SBA-15 supported catalysts for catalytic reforming applications: A state-of-the-art review. *Appl. Catal. A* **2018**, *559*, 57–74. [CrossRef]

67. Vallet-Regi, M.; Rámila, A.; Del Real, R.P.; Pérez-Pariente, J. A New Property of MCM-41: Drug Delivery System. *Chem. Mater.* **2001**, *13*, 308–311. [CrossRef]

68. Corma, A.; Fornes, V.; Navarro, M.T.; Perezpariente, J. Acidity and Stability of MCM-41 Crystalline Aluminosilicates. *J. Catal.* **1994**, *148*, 569–574. [CrossRef]

69. Gao, J.; Wang, Y.; Ping, Y.; Hu, D.; Xu, G.; Gu, F.; Su, F. A thermodynamic analysis of methanation reactions of carbon oxides for the production of synthetic natural gas. *RSC Adv.* **2012**, *2*, 2358. [CrossRef]

70. Ocampo, F. *Développement de catalyseurs pour la réaction de méthanation du dioxyde de carbone*; University of Strasbourg: Strasbourg, France, 2011.

71. Polshettiwar, V.; Cha, D.; Zhang, X.; Basset, J.M. High-Surface-Area Silica Nanospheres (KCC-1) with a Fibrous Morphology. *Angew. Chem. Int. Ed.* **2010**, *49*, 9652–9656. [CrossRef] [PubMed]

72. Riani, P.; Garbarino, G.; Lucchini, M.A.; Canepa, F.; Busca, G. Unsupported versus alumina-supported Ni nanoparticles as catalysts for steam/ethanol conversion and CO_2 methanation. *J. Mol. Catal. A* **2014**, *383–384*, 10–16. [CrossRef]

73. Garbarino, G.; Riani, P.; Magistri, L.; Busca, G. A study of the methanation of carbon dioxide on Ni/Al_2O_3 catalysts at atmospheric pressure. *Int. J. Hydrogen Energy* **2014**, *39*, 11557–11565. [CrossRef]

74. Quindimil, A.; De-La-Torre, U.; Pereda-Ayo, B.; Davó-Quiñonero, A.; Bailón-García, E.; Lozano-Castelló, D.; González-Marcos, J.A.; Bueno-López, A.; González-Velasco, J.R. Effect of metal loading on the CO_2 methanation: A comparison between alumina supported Ni and Ru catalysts. *Catal. Today* **2019**. [CrossRef]

75. Garbarino, G.; Bellotti, D.; Riani, P.; Magistri, L.; Busca, G. Methanation of carbon dioxide on Ru/Al_2O_3 and Ni/Al_2O_3 catalysts at atmospheric pressure: Catalysts activation, behaviour and stability. *Int. J. Hydrogen Energy* **2015**, *40*, 9171–9182. [CrossRef]

76. Hwang, S.; Hong, U.G.; Lee, J.; Seo, J.G.; Baik, J.H.; Koh, D.J.; Lim, H.; Song, I.K. Methanation of carbon dioxide over mesoporous $Ni–Fe–Al_2O_3$ catalysts prepared by a coprecipitation method: Effect of precipitation agent. *J. Ind. Eng. Chem.* **2013**, *19*, 2016–2021. [CrossRef]

77. Serrer, M.-A.; Gaur, A.; Jelic, J.; Weber, S.; Fritsch, C.; Clark, A.H.; Saraçi, E.; Studt, F.; Grunwaldt, J.-D. Structural dynamics in Ni–Fe catalysts during CO_2 methanation – role of iron oxide clusters. *Catal. Sci. Technol.* **2020**, *10*, 7542–7554. [CrossRef]

78. Burger, T.; Augenstein, H.M.S.; Hnyk, F.; Döblinger, M.; Köhler, K.; Hinrichsen, O. Targeted Fe-Doping of Ni–Al Catalysts via the Surface Redox Reaction Technique for Unravelling its Promoter Effect in the CO_2 Methanation Reaction. *ChemCatChem* **2020**, *12*, 649–662. [CrossRef]

79. Burger, T.; Koschany, F.; Thomys, O.; Köhler, K.; Hinrichsen, O. CO_2 methanation over Fe- and Mn-promoted co-precipitated Ni-Al catalysts: Synthesis, characterization and catalysis study. *Appl. Catal. A: General* **2018**, *558*, 44–54. [CrossRef]

80. Xu, L.; Lian, X.; Chen, M.; Cui, Y.; Wang, F.; Li, W.; Huang, B. CO_2 methanation over CoNi bimetal-doped ordered mesoporous Al_2O_3 catalysts with enhanced low-temperature activities. *Int. J. Hydrogen Energy* **2018**, *43*, 17172–17184. [CrossRef]

81. Alrafei, B.; Polaert, I.; Ledoux, A.; Azzolina-Jury, F. Remarkably stable and efficient Ni and Ni-Co catalysts for CO_2 methanation. *Catal. Today* **2020**, *346*, 23–33. [CrossRef]

82. Rahmani, S.; Rezaei, M.; Meshkani, F. Preparation of promoted nickel catalysts supported on mesoporous nanocrystalline gamma alumina for carbon dioxide methanation reaction. *J. Ind. Eng. Chem.* **2014**, *20*, 4176–4182. [CrossRef]

83. Liu, H.; Zou, X.; Wang, X.; Lu, X.; Ding, W. Effect of CeO_2 addition on Ni/Al_2O_3 catalysts for methanation of carbon dioxide with hydrogen. *J. Nat. Gas Chem.* **2012**, *21*, 703–707. [CrossRef]

84. Guo, X.; He, H.; Traitangwong, A.; Gong, M.; Meeyoo, V.; Li, P.; Li, C.; Peng, Z.; Zhang, S. Ceria imparts superior low temperature activity to nickel catalysts for CO_2 methanation. *Catal. Sci. Technol.* **2019**, *9*, 5636–5650. [CrossRef]

85. Tada, S.; Ochieng, O.J.; Kikuchi, R.; Haneda, T.; Kameyama, H. Promotion of CO_2 methanation activity and CH_4 selectivity at low temperatures over $Ru/CeO_2/Al_2O_3$ catalysts. *Int. J. Hydrogen Energy* **2014**, *39*, 10090–10100. [CrossRef]

86. Ahmad, W.; Younis, M.N.; Shawabkeh, R.; Ahmed, S. Synthesis of lanthanide series (La, Ce, Pr, Eu & Gd) promoted $Ni/gamma-Al_2O_3$ catalysts for methanation of CO_2 at low temperature under atmospheric pressure. *Catal. Commun.* **2017**, *100*, 121–126. [CrossRef]

87. Karam, L.; Bacariza, M.C.; Lopes, J.M.; Henriques, C.; Massiani, P.; El Hassan, N. Assessing the potential of xNi-yMg-Al$_2$O$_3$ catalysts prepared by EISA-one-pot synthesis towards CO$_2$ methanation: An overall study. *Int. J. Hydrogen Energy* **2020**. [CrossRef]

88. Nie, W.-X.; Zou, X.-J.; Wang, X.-G.; Ding, W.-Z.; Lu, X.-G. Preparation of Highly Dispersed Ni-Ce-Zr Oxides over Mesoporous Y-Alumina and Their Catalytic Properties for CO$_2$ Methanation. *Acta Phys.-Chim. Sin.* **2016**, *32*, 2803–2810. [CrossRef]

89. Toemen, S.; Bakar, W.A.W.A.; Ali, R. Investigation of Ru/Mn/Ce/Al$_2$O$_3$ catalyst for carbon dioxide methanation: Catalytic optimization, physicochemical studies and RSM. *J. Taiwan Inst. Chem. Eng.* **2014**, *45*, 2370–2378. [CrossRef]

90. Wan Abu Bakar, W.A.; Ali, R.; Mohammad, N.S. The effect of noble metals on catalytic methanation reaction over supported Mn/Ni oxide based catalysts. *Arab. J. Chem.* **2015**, *8*, 632–643. [CrossRef]

91. Do, J.Y.; Park, N.-K.; Seo, M.W.; Lee, D.; Ryu, H.-J.; Kang, M. Effective thermocatalytic carbon dioxide methanation on Ca-inserted NiTiO$_3$ perovskite. *Fuel* **2020**, *271*, 117624. [CrossRef]

92. Cai, M.; Wen, J.; Chu, W.; Cheng, X.; Li, Z. Methanation of carbon dioxide on Ni/ZrO$_2$-Al$_2$O$_3$ catalysts: Effects of ZrO$_2$ promoter and preparation method of novel ZrO$_2$-Al$_2$O$_3$ carrier. *J. Nat. Gas Chem.* **2011**, *20*, 318–324. [CrossRef]

93. Lin, J.; Ma, C.; Wang, Q.; Xu, Y.; Ma, G.; Wang, J.; Wang, H.; Dong, C.; Zhang, C.; Ding, M. Enhanced low-temperature performance of CO$_2$ methanation over mesoporous Ni/Al$_2$O$_3$-ZrO$_2$ catalysts. *Appl. Catal. B* **2019**, *243*, 262–272. [CrossRef]

94. Xu, J.; Lin, Q.; Su, X.; Duan, H.; Geng, H.; Huang, Y. CO$_2$ methanation over TiO$_2$-Al$_2$O$_3$ binary oxides supported Ru catalysts. *Chin. J. Chem. Eng.* **2016**, *24*, 140–145. [CrossRef]

95. Yang, W.; Feng, Y.; Chu, W. Promotion Effect of CaO Modification on Mesoporous Al$_2$O$_3$-Supported Ni Catalysts for CO$_2$ Methanation. *Int. J. Chem. Eng.* **2016**, 2041821. [CrossRef]

96. Liu, Q.; Wang, S.; Zhao, G.; Yang, H.; Yuan, M.; An, X.; Zhou, H.; Qiao, Y.; Tian, Y. CO$_2$ methanation over ordered mesoporous NiRu-doped CaO-Al$_2$O$_3$ nanocomposites with enhanced catalytic performance. *Int. J. Hydrog. Energy* **2018**, *43*, 239–250. [CrossRef]

97. Abate, S.; Mebrahtu, C.; Giglio, E.; Deorsola, F.; Bensaid, S.; Perathoner, S.; Pirone, R.; Centi, G. Catalytic Performance of gamma-Al$_2$O$_3$-ZrO$_2$-TiO$_2$-CeO$_2$ Composite Oxide Supported Ni-Based Catalysts for CO$_2$ Methanation. *Ind. Eng. Chem. Res.* **2016**, *55*, 4451–4460. [CrossRef]

98. Mebrahtu, C.; Abate, S.; Perathoner, S.; Chen, S.; Centi, G. CO$_2$ methanation over Ni catalysts based on ternary and quaternary mixed oxide: A comparison and analysis of the structure-activity relationships. *Catal. Today* **2018**, *304*, 181–189. [CrossRef]

99. Djinović, P.; Galletti, C.; Specchia, S.; Specchia, V. CO Methanation Over Ru–Al$_2$O$_3$ Catalysts: Effects of Chloride Doping on Reaction Activity and Selectivity. *Top Catal.* **2011**, *54*, 1042. [CrossRef]

100. Konishcheva, M.V.; Potemkin, D.I.; Snytnikov, P.V.; Stonkus, O.A.; Belyaev, V.D.; Sobyanin, V.A. The insights into chlorine doping effect on performance of ceria supported nickel catalysts for selective CO methanation. *Appl. Catal. B* **2018**, *221*, 413–421. [CrossRef]

101. Gao, Z.; Wang, L.; Ma, H.; Li, Z. Durability of catalytic performance of the chlorine-doped catalyst Ni(Cl$_x$)/ZrO$_2$ for selective methanation of CO in H$_2$-rich gas. *Appl. Catal. A* **2017**, *534*, 78–84. [CrossRef]

102. Serrer, M.-A.; Kalz, K.F.; Saraçi, E.; Lichtenberg, H.; Grunwaldt, J.-D. Role of Iron on the Structure and Stability of Ni$_{3.2}$Fe/Al$_2$O$_3$ during Dynamic CO$_2$ Methanation for P2X Applications. *ChemCatChem* **2019**, *11*, 5018–5021. [CrossRef]

103. Mutz, B.; Belimov, M.; Wang, W.; Sprenger, P.; Serrer, M.-A.; Wang, D.; Pfeifer, P.; Kleist, W.; Grunwaldt, J.-D. Potential of an Alumina-Supported Ni$_3$Fe Catalyst in the Methanation of CO$_2$: Impact of Alloy Formation on Activity and Stability. *ACS Catal.* **2017**, *7*, 6802–6814. [CrossRef]

104. Burger, T.; Ewald, S.; Niederdränk, A.; Wagner, F.E.; Köhler, K.; Hinrichsen, O. Enhanced activity of co-precipitated NiFeAlOx in CO$_2$ methanation by segregation and oxidation of Fe. *Appl. Catal. A* **2020**, *604*, 117778. [CrossRef]

105. Rosid, S.J.M.; Toemen, S.; Iqbal, M.M.A.; Bakar, W.A.W.A.; Mokhtar, W.N.A.W.; Aziz, M.M.A. Overview performance of lanthanide oxide catalysts in methanation reaction for natural gas production. *Environ. Sci. Pollut. Res.* **2019**, *26*, 36124–36140. [CrossRef]

106. Bernardon, C.; Ben Osman, M.; Laugel, G.; Louis, B.; Pale, P. Acidity versus metal-induced Lewis acidity in zeolites for Friedel–Crafts acylation. *Comptes Rendus Chim.* **2017**, *20*, 20–29. [CrossRef]

107. Zamani, A.H.; Ali, R.; Abu Bakar, W.A.W. Optimization of CO_2 methanation reaction over M*/Mn/Cu–Al_2O_3 (M*: Pd, Rh and Ru) catalysts. *J. Ind. Eng. Chem.* **2015**, *29*, 238–248. [CrossRef]

108. Franken, T.; Terreni, J.; Borgschulte, A.; Heel, A. Solid solutions in reductive environment – A case study on improved CO_2 hydrogenation to methane on cobalt based catalysts derived from ternary mixed metal oxides by modified reducibility. *J. Catal.* **2020**, *382*, 385–394. [CrossRef]

109. Daroughegi, R.; Meshkani, F.; Rezaei, M. Enhanced activity of CO_2 methanation over mesoporous nanocrystalline Ni-Al_2O_3 catalysts prepared by ultrasound-assisted co-precipitation method. *Int. J. Hydrogen Energy* **2017**, *42*, 15115–15125. [CrossRef]

110. Xu, Y.; Chen, Y.; Li, J.; Zhou, J.; Song, M.; Zhang, X.; Yin, Y. Improved low-temperature activity of Ni-Ce/gamma-Al_2O_3 catalyst with layer structural precursor prepared by cold plasma for CO_2 methanation. *Int. J. Hydrogen Energy* **2017**, *42*, 13085–13091. [CrossRef]

111. Song, F.; Zhong, Q.; Yu, Y.; Shi, M.; Wu, Y.; Hu, J.; Song, Y. Obtaining well-dispersed Ni/Al_2O_3 catalyst for CO_2 methanation with a microwave-assisted method. *Int. J. Hydrogen Energy* **2017**, *42*, 4174–4183. [CrossRef]

112. Schubert, M.; Pokhrel, S.; Thome, A.; Zielasek, V.; Gesing, T.M.; Roessner, F.; Maedler, L.; Baeumer, M. Highly active Co-Al_2O_3-based catalysts for CO_2 methanation with very low platinum promotion prepared by double flame spray pyrolysis. *Catal. Sci. Technol.* **2016**, *6*, 7449–7460. [CrossRef]

113. Aljishi, A.; Veilleux, G.; Lalinde, J.A.H.; Kopyscinski, J. The effect of synthesis parameters on ordered mesoporous nickel alumina catalyst for CO_2 methanation. *Appl. Catal. A* **2018**, *549*, 263–272. [CrossRef]

114. Xu, L.; Wang, F.; Chen, M.; Zhang, J.; Yuan, K.; Wang, L.; Wu, K.; Xu, G.; Chen, W. CO_2 methanation over a Ni based ordered mesoporous catalyst for the production of synthetic natural gas. *RSC Adv.* **2016**, *6*, 28489–28499. [CrossRef]

115. Shang, X.; Deng, D.; Wang, X.; Zou, X.; Ding, W.; Lu, X. Low Temperature Synthesis of Mesoporous gamma-Alumina supported Nickel Oxides and their Catalytic Application for CO2 Methanation. In Proceedings of the 2015 International Symposium on Energy Science and Chemical Engineering (isesce 2015); He, Y., Ed.; Atlantis Press: Paris, France, 2016; Volume 45, pp. 117–123, ISBN 978-94-6252-140-7.

116. Le, T.A.; Kim, T.W.; Lee, S.H.; Park, E.D. CO and CO_2 methanation over Ni catalysts supported on alumina with different crystalline phases. *Korean J. Chem. Eng.* **2017**, *34*, 3085–3091. [CrossRef]

117. Beuls, A.; Swalus, C.; Jacquemin, M.; Heyen, G.; Karelovic, A.; Ruiz, P. Methanation of CO_2: Further insight into the mechanism over Rh/γ-Al_2O_3 catalyst. *Appl. Catal. B* **2012**, *113–114*, 2–10. [CrossRef]

118. Zhang, Z.; Tian, Y.; Zhang, L.; Hu, S.; Xiang, J.; Wang, Y.; Xu, L.; Liu, Q.; Zhang, S.; Hu, X. Impacts of nickel loading on properties, catalytic behaviors of Ni/γ–Al_2O_3 catalysts and the reaction intermediates formed in methanation of CO_2. *Int. J. Hydrogen Energy* **2019**, *44*, 9291–9306. [CrossRef]

119. Cárdenas-Arenas, A.; Quindimil, A.; Davó-Quiñonero, A.; Bailón-García, E.; Lozano-Castelló, D.; De-La-Torre, U.; Pereda-Ayo, B.; González-Marcos, J.A.; González-Velasco, J.R.; Bueno-López, A. Isotopic and in situ DRIFTS study of the CO_2 methanation mechanism using Ni/CeO_2 and Ni/Al_2O_3 catalysts. *Appl. Catal. B* **2020**, *265*, 118538. [CrossRef]

120. Tada, S.; Shimizu, T.; Kameyama, H.; Haneda, T.; Kikuchi, R. Ni/CeO_2 catalysts with high CO_2 methanation activity and high CH_4 selectivity at low temperatures. *Int. J. Hydrogen Energy* **2012**, *37*, 5527–5531. [CrossRef]

121. Atzori, L.; Cutrufello, M.G.; Meloni, D.; Cannas, C.; Gazzoli, D.; Monaci, R.; Sini, M.F.; Rombi, E. Highly active NiO-CeO_2 catalysts for synthetic natural gas production by CO_2 methanation. *Catal. Today* **2018**, *299*, 183–192. [CrossRef]

122. Ratchahat, S.; Sudoh, M.; Suzuki, Y.; Kawasaki, W.; Watanabe, R.; Fukuhara, C. Development of a powerful CO_2 methanation process using a structured Ni/CeO_2 catalyst. *J. CO2 Util.* **2018**, *24*, 210–219. [CrossRef]

123. Cárdenas-Arenas, A.; Quindimil, A.; Davó-Quiñonero, A.; Bailón-García, E.; Lozano-Castelló, D.; De-La-Torre, U.; Pereda-Ayo, B.; González-Marcos, J.A.; González-Velasco, J.R.; Bueno-López, A. Design of active sites in Ni/CeO_2 catalysts for the methanation of CO_2: Tailoring the Ni-CeO2 contact. *Appl. Mater. Today* **2020**, *19*, 100591. [CrossRef]

124. Sharma, S.; Hu, Z.; Zhang, P.; McFarland, E.W.; Metiu, H. CO_2 methanation on Ru-doped ceria. *J. Catal.* **2011**, *278*, 297–309. [CrossRef]

125. Vita, A.; Italiano, C.; Pino, L.; Frontera, P.; Ferraro, M.; Antonucci, V. Activity and stability of powder and monolith-coated Ni/GDC catalysts for CO_2 methanation. *Appl. Catal. B* **2018**, *226*, 384–395. [CrossRef]

126. Aldana, P.A.U.; Ocampo, F.; Kobl, K.; Louis, B.; Thibault-Starzyk, F.; Daturi, M.; Bazin, P.; Thomas, S.; Roger, A.C. Catalytic CO_2 valorization into CH_4 on Ni-based ceria-zirconia. Reaction mechanism by operando IR spectroscopy. *Catal. Today* **2013**, *215*, 201–207. [CrossRef]

127. Ocampo, F.; Louis, B.; Roger, A.-C. Methanation of carbon dioxide over nickel-based $Ce_{0.72}Zr_{0.28}O_2$ mixed oxide catalysts prepared by sol–gel method. *Appl. Catal. A* **2009**, *369*, 90–96. [CrossRef]

128. Ashok, J.; Ang, M.L.; Kawi, S. Enhanced activity of CO_2 methanation over Ni/CeO_2-ZrO_2 catalysts: Influence of preparation methods. *Catal. Today* **2017**, *281*, 304–311. [CrossRef]

129. Le, T.A.; Kim, T.W.; Lee, S.H.; Park, E.D. Effects of Na content in Na/Ni/SiO_2 and Na/Ni/CeO_2 catalysts for CO and CO_2 methanation. *Catal. Today* **2018**, *303*, 159–167. [CrossRef]

130. Pastor-Pérez, L.; Patel, V.; Le Saché, E.; Reina, T.R. CO_2 methanation in the presence of methane: Catalysts design and effect of methane concentration in the reaction mixture. *J. Energy Inst.* **2020**, *93*, 415–424. [CrossRef]

131. Sun, H.; Zhang, Y.; Guan, S.; Huang, J.; Wu, C. Direct and highly selective conversion of captured CO_2 into methane through integrated carbon capture and utilization over dual functional materials. *J. CO2 Util.* **2020**, *38*, 262–272. [CrossRef]

132. Konishcheva, M.V.; Potemkin, D.I.; Badmaev, S.D.; Snytnikov, P.V.; Paukshtis, E.A.; Sobyanin, V.A.; Parmon, V.N. On the Mechanism of CO and CO_2 Methanation Over Ni/CeO_2 Catalysts. *Top. Catal.* **2016**, *59*, 1424–1430. [CrossRef]

133. da Silva, D.C.D.; Letichevsky, S.; Borges, L.E.P.; Appel, L.G. The Ni/ZrO_2 catalyst and the methanation of CO and CO_2. *Int. J. Hydrogen Energy* **2012**, *37*, 8923–8928. [CrossRef]

134. Lu, H.; Yang, X.; Gao, G.; Wang, K.; Shi, Q.; Wang, J.; Han, C.; Liu, J.; Tong, M.; Liang, X.; et al. Mesoporous zirconia-modified clays supported nickel catalysts for CO and CO_2 methanation. *Int. J. Hydrogen Energy* **2014**, *39*, 18894–18907. [CrossRef]

135. Jia, X.; Zhang, X.; Rui, N.; Hu, X.; Liu, C. Structural effect of Ni/ZrO_2 catalyst on CO_2 methanation with enhanced activity. *Appl. Catal. B* **2019**, *244*, 159–169. [CrossRef]

136. Zhao, K.; Wang, W.; Li, Z. Highly efficient Ni/ZrO_2 catalysts prepared via combustion method for CO_2 methanation. *J. CO2 Util.* **2016**, *16*, 236–244. [CrossRef]

137. Li, W.; Nie, X.; Jiang, X.; Zhang, A.; Ding, F.; Liu, M.; Liu, Z.; Guo, X.; Song, C. ZrO_2 support imparts superior activity and stability of Co catalysts for CO_2 methanation. *Appl. Catal. B* **2018**, *220*, 397–408. [CrossRef]

138. Li, W.; Liu, Y.; Mu, M.; Ding, F.; Liu, Z.; Guo, X.; Song, C. Organic acid-assisted preparation of highly dispersed Co/ZrO_2 catalysts with superior activity for CO_2 methanation. *Appl. Catal. B* **2019**, *254*, 531–540. [CrossRef]

139. Nagase, H.; Naito, R.; Tada, S.; Kikuchi, R.; Fujiwara, K.; Nishijima, M.; Honma, T. Ru nanoparticles supported on amorphous ZrO_2 for CO_2 methanation. *Catal. Sci. Technol.* **2020**, *10*, 4522–4531. [CrossRef]

140. Takano, H.; Izumiya, K.; Kumagai, N.; Hashimoto, K. The effect of heat treatment on the performance of the Ni/(Zr-Sm oxide) catalysts for carbon dioxide methanation. *Appl. Surf. Sci.* **2011**, *257*, 8171–8176. [CrossRef]

141. Takano, H.; Kirihata, Y.; Izumiya, K.; Kumagai, N.; Habazaki, H.; Hashimoto, K. Highly active Ni/Y-doped ZrO_2 catalysts for CO_2 methanation. *Appl. Surf. Sci.* **2016**, *388*, 653–663. [CrossRef]

142. Kesavan, J.K.; Luisetto, I.; Tuti, S.; Meneghini, C.; Iucci, G.; Battocchio, C.; Mobilio, S.; Casciardi, S.; Sisto, R. Nickel supported on YSZ: The effect of Ni particle size on the catalytic activity for CO2 methanation. *J. CO_2 Util.* **2018**, *23*, 200–211. [CrossRef]

143. Kosaka, F.; Yamaguchi, T.; Ando, Y.; Mochizuki, T.; Takagi, H.; Matsuoka, K.; Fujishiro, Y.; Kuramoto, K. Effect of Ni content on CO_2 methanation performance with tubular-structured Ni-YSZ catalysts and optimization of catalytic activity for temperature management in the reactor. *Int. J. Hydrogen Energy* **2020**, *45*, 12911–12920. [CrossRef]

144. Ren, J.; Qin, X.; Yang, J.-Z.; Qin, Z.-F.; Guo, H.-L.; Lin, J.-Y.; Li, Z. Methanation of carbon dioxide over Ni–M/ZrO_2 (M = Fe, Co, Cu) catalysts: Effect of addition of a second metal. *Fuel Process. Technol.* **2015**, *137*, 204–211. [CrossRef]

145. Lu, H.; Yang, X.; Gao, G.; Wang, J.; Han, C.; Liang, X.; Li, C.; Li, Y.; Zhang, W.; Chen, X. Metal (Fe, Co, Ce or La) doped nickel catalyst supported on ZrO_2 modified mesoporous clays for CO and CO_2 methanation. *Fuel* **2016**, *183*, 335–344. [CrossRef]

146. Dumrongbunditkul, P.; Witoon, T.; Chareonpanich, M.; Mungcharoen, T. Preparation and characterization of Co-Cu-ZrO_2 nanomaterials and their catalytic activity in CO_2 methanation. *Ceram. Int.* **2016**, *42*, 10444–10451. [CrossRef]

147. Tan, J.; Wang, J.; Zhang, Z.; Ma, Z.; Wang, L.; Liu, Y. Highly dispersed and stable Ni nanoparticles confined by MgO on ZrO_2 for CO_2 methanation. *Appl. Surf. Sci.* **2019**, *481*, 1538–1548. [CrossRef]

148. Takano, H.; Shinomiya, H.; Izumiya, K.; Kumagai, N.; Habazaki, H.; Hashimoto, K. CO_2 methanation of Ni catalysts supported on tetragonal ZrO_2 doped with Ca^{2+} and Ni^{2+} ions. *Int. J. Hydrogen Energy* **2015**, *40*, 8347–8355. [CrossRef]

149. Loder, A.; Siebenhofer, M.; Lux, S. The reaction kinetics of CO_2 methanation on a bifunctional Ni/MgO catalyst. *J. Ind. Eng. Chem.* **2020**, *85*, 196–207. [CrossRef]

150. Wierzbicki, D.; Baran, R.; Debek, R.; Motak, M.; Grzybek, T.; Galvez, M.E.; Da Costa, P. The influence of nickel content on the performance of hydrotalcite-derived catalysts in CO_2 methanation reaction. *Int. J. Hydrogen Energy* **2017**, *42*, 23548–23555. [CrossRef]

151. Bette, N.; Thielemann, J.; Schreiner, M.; Mertens, F. Methanation of CO_2 over a (Mg,Al)O-x Supported Nickel Catalyst Derived from a (Ni,Mg,Al)-Hydrotalcite-like Precursor. *ChemCatChem* **2016**, *8*, 2903–2906. [CrossRef]

152. Abate, S.; Barbera, K.; Giglio, E.; Deorsola, F.; Bensaid, S.; Perathoner, S.; Pirone, R.; Centi, G. Synthesis, Characterization, and Activity Pattern of Ni-Al Hydrotalcite Catalysts in CO_2 Methanation. *Ind. Eng. Chem. Res.* **2016**, *55*, 8299–8308. [CrossRef]

153. Yan, Y.; Dai, Y.; He, H.; Yu, Y.; Yang, Y. A novel W-doped Ni-Mg mixed oxide catalyst for CO_2 methanation. *Appl. Catal. B* **2016**, *196*, 108–116. [CrossRef]

154. Varun, Y.; Sreedhar, I.; Singh, S.A. Highly stable M/NiO–MgO (M = Co, Cu and Fe) catalysts towards CO_2 methanation. *Int. J. Hydrogen Energy* **2020**. [CrossRef]

155. Ho, P.H.; de Luna, G.S.; Angelucci, S.; Canciani, A.; Jones, W.; Decarolis, D.; Ospitali, F.; Aguado, E.R.; Rodríguez-Castellón, E.; Fornasari, G.; et al. Understanding structure-activity relationships in highly active La promoted Ni catalysts for CO_2 methanation. *Appl. Catal. B* **2020**, *278*, 119256. [CrossRef]

156. Wierzbicki, D.; Debek, R.; Motak, M.; Grzybek, T.; Galvez, M.E.; Da Costa, P. Novel Ni-La-hydrotalcite derived catalysts for CO_2 methanation. *Catal. Commun.* **2016**, *83*, 5–8. [CrossRef]

157. Wierzbicki, D.; Motak, M.; Grzybek, T.; Gálvez, M.E.; Da Costa, P. The influence of lanthanum incorporation method on the performance of nickel-containing hydrotalcite-derived catalysts in CO_2 methanation reaction. *Catal. Today* **2018**, *307*, 205–211. [CrossRef]

158. Zhang, L.; Bian, L.; Zhu, Z.; Li, Z. La-promoted Ni/Mg-Al catalysts with highly enhanced low-temperature CO_2 methanation performance. *Int. J. Hydrogen Energy* **2018**, *43*, 2197–2206. [CrossRef]

159. Wang, X.; Zhen, T.; Yu, C. Application of Ni-Al-hydrotalcite-derived catalyst modified with Fe or Mg in CO_2 methanation. *Appl. Petrochem. Res.* **2016**, *6*, 217–223. [CrossRef]

160. Mebrahtu, C.; Perathoner, S.; Giorgianni, G.; Chen, S.; Centi, G.; Krebs, F.; Palkovits, R.; Abate, S. Deactivation mechanism of hydrotalcite-derived Ni–AlO_x catalysts during low-temperature CO_2 methanation via Ni-hydroxide formation and the role of Fe in limiting this effect. *Catal. Sci. Technol.* **2019**, *9*, 4023–4035. [CrossRef]

161. He, L.; Lin, Q.; Liu, Y.; Huang, Y. Unique catalysis of Ni-Al hydrotalcite derived catalyst in CO_2 methanation: Cooperative effect between Ni nanoparticles and a basic support. *J. Energy Chem.* **2014**, *23*, 587–592. [CrossRef]

162. Mebrahtu, C.; Krebs, F.; Perathoner, S.; Abate, S.; Centi, G.; Palkovits, R. Hydrotalcite based Ni–Fe/(Mg, Al)O_x catalysts for CO_2 methanation – tailoring Fe content for improved CO dissociation, basicity, and particle size. *Catal. Sci. Technol.* **2018**, *8*, 1016–1027. [CrossRef]

163. Jiménez, V.; Sánchez, P.; Panagiotopoulou, P.; Valverde, J.L.; Romero, A. Methanation of CO, CO_2 and selective methanation of CO, in mixtures of CO and CO_2, over ruthenium carbon nanofibers catalysts. *Appl. Catal. A* **2010**, *390*, 35–44. [CrossRef]

164. Li, W.; Zhang, A.; Jiang, X.; Chen, C.; Liu, Z.; Song, C.; Guo, X. Low Temperature CO_2 Methanation: ZIF-67-Derived Co-Based Porous Carbon Catalysts with Controlled Crystal Morphology and Size. *ACS Sustain. Chem. Eng.* **2017**, *5*, 7824–7831. [CrossRef]

165. Gödde, J.; Merko, M.; Xia, W.; Muhler, M. Nickel nanoparticles supported on nitrogen–doped carbon nanotubes are a highly active, selective and stable CO_2 methanation catalyst. *J. Energy Chem.* **2021**, *54*, 323–331. [CrossRef]

166. Romero-Sáez, M.; Dongil, A.B.; Benito, N.; Espinoza-González, R.; Escalona, N.; Gracia, F. CO_2 methanation over nickel-ZrO_2 catalyst supported on carbon nanotubes: A comparison between two impregnation strategies. *Appl. Catal. B* **2018**, *237*, 817–825. [CrossRef]

167. Wang, W.; Chu, W.; Wang, N.; Yang, W.; Jiang, C. Mesoporous nickel catalyst supported on multi-walled carbon nanotubes for carbon dioxide methanation. *Int. J. Hydrogen Energy* **2016**, *41*, 967–975. [CrossRef]

168. Le, M.C.; Le Van, K.; Nguyen, T.H.T.; Nguyen, N.H. The Impact of Ce-Zr Addition on Nickel Dispersion and Catalytic Behavior for CO_2 Methanation of Ni/AC Catalyst at Low Temperature. *J. Chem.* **2017**, 4361056. [CrossRef]

169. Gaidai, S.V.; Gryn'ko, V.S.; Zhludenko, M.G.; Dyachenko, A.G.; Tkach, V.M.; Ishchenko, O.V. Activity of Carbon-Fiber-Supported Fe-Co Catalysts in the CO_2 Methanation Reaction. *J. Superhard Mater.* **2017**, *39*, 122–128. [CrossRef]

170. Lapidus, A.L.; Gaidai, N.A.; Nekrasov, N.V.; Tishkova, L.A.; Agafonov, Y.A.; Myshenkova, T.N. The mechanism of carbon dioxide hydrogenation on copper and nickel catalysts. *Pet. Chem.* **2007**, *47*, 75–82. [CrossRef]

171. Hussain, I.; Jalil, A.A.; Hassan, N.S.; Hambali, H.U.; Jusoh, N.W.C. Fabrication and characterization of highly active fibrous silica-mordenite (FS@SiO$_2$-MOR) cockscomb shaped catalyst for enhanced CO_2 methanation. *Chem. Eng. Sci.* **2020**, *228*, 115978. [CrossRef]

172. Franken, T.; Heel, A. Are Fe based catalysts an upcoming alternative to Ni in CO_2 methanation at elevated pressure? *J. CO2 Util.* **2020**, *39*, 101175. [CrossRef]

173. Kitamura Bando, K.; Soga, K.; Kunimori, K.; Ichikuni, N.; Okabe, K.; Kusama, H.; Sayama, K.; Arakawa, H. CO_2 hydrogenation activity and surface structure of zeolite-supported Rh catalysts. *Appl. Catal. A* **1998**, *173*, 47–60. [CrossRef]

174. Bacariza, M.C.; Graça, I.; Lopes, J.M.; Henriques, C. Enhanced activity of CO_2 hydrogenation to CH_4 over Ni based zeolites through the optimization of the Si/Al ratio. *Microporous Mesoporous Mater.* **2018**, *267*, 9–19. [CrossRef]

175. Bacariza, M.C.; Maleval, M.; Graça, I.; Lopes, J.M.; Henriques, C. Power-to-methane over Ni/zeolites: Influence of the framework type. *Microporous Mesoporous Mater.* **2019**, *274*, 102–112. [CrossRef]

176. Goodarzi, F.; Kang, L.; Wang, F.R.; Joensen, F.; Kegnæs, S.; Mielby, J. Methanation of Carbon Dioxide over Zeolite-Encapsulated Nickel Nanoparticles. *ChemCatChem* **2018**, *10*, 1566–1570. [CrossRef]

177. Guo, X.; Traitangwong, A.; Hu, M.; Zuo, C.; Meeyoo, V.; Peng, Z.; Li, C. Carbon Dioxide Methanation over Nickel-Based Catalysts Supported on Various Mesoporous Material. *Energy Fuels* **2018**, *32*, 3681–3689. [CrossRef]

178. Isah, A.; Akanyeti, İ.; Oladipo, A.A. Methanation of CO_2 over zeolite–promoted Ni/Al$_2$O$_3$ nanocatalyst under atmospheric pressure. *Reac. Kinet. Mech. Cat.* **2020**, *130*, 217–228. [CrossRef]

179. Quindimil, A.; De-La-Torre, U.; Pereda, B.; González-Marcos, J.A.; González-Velasco, J.R. Ni catalysts with La as promoter supported over Y- and Beta- zeolites for CO_2 methanation. *Appl. Catal. B* **2018**, *238*, 393–403. [CrossRef]

180. Czuma, N.; Zarębska, K.; Motak, M.; Gálvez, M.E.; Da Costa, P. Ni/zeolite X derived from fly ash as catalysts for CO_2 methanation. *Fuel* **2020**, *267*, 117139. [CrossRef]

181. Wei, L.; Haije, W.; Kumar, N.; Peltonen, J.; Peurla, M.; Grenman, H.; de Jong, W. Influence of nickel precursors on the properties and performance of Ni impregnated zeolite 5A and 13X catalysts in CO_2 methanation. *Catal. Today* **2020**. [CrossRef]

182. da Costa-Serra, J.F.; Cerdá-Moreno, C.; Chica, A. Zeolite-Supported Ni Catalysts for CO_2 Methanation: Effect of Zeolite Structure and Si/Al Ratio. *Appl. Sci.* **2020**, *10*, 5131. [CrossRef]

183. Bacariza, M.C.; Graça, I.; Bebiano, S.S.; Lopes, J.M.; Henriques, C. Magnesium as Promoter of CO_2 Methanation on Ni-Based USY Zeolites. *Energy Fuels* **2017**, *31*, 9776–9789. [CrossRef]

184. Graça, I.; González, L.V.; Bacariza, M.C.; Fernandes, A.; Henriques, C.; Lopes, J.M.; Ribeiro, M.F. CO_2 hydrogenation into CH_4 on NiHNaUSY zeolites. *Appl. Catal. B* **2014**, *147*, 101–110. [CrossRef]

185. Bacariza, M.C.; Graça, I.; Lopes, J.M.; Henriques, C. Ni-Ce/Zeolites for CO_2 Hydrogenation to CH_4: Effect of the Metal Incorporation Order. *ChemCatChem* **2018**, *10*, 2773–2781. [CrossRef]

186. Boix, A.V.; Ulla, M.A.; Petunchi, J.O. Promoting effect of Pt on Co mordenite upon the reducibility and catalytic behavior of CO_2 hydrogenation. *J. Catal.* **1996**, *162*, 239–249. [CrossRef]

187. Wei, L.; Kumar, N.; Haije, W.; Peltonen, J.; Peurla, M.; Grénman, H.; de Jong, W. Can bi-functional nickel modified 13X and 5A zeolite catalysts for CO_2 methanation be improved by introducing ruthenium? *Mol. Catal.* **2020**, *494*, 111115. [CrossRef]

188. Bacariza, M.C.; Graça, I.; Westermann, A.; Ribeiro, M.F.; Lopes, J.M.; Henriques, C. CO_2 Hydrogenation Over Ni-Based Zeolites: Effect of Catalysts Preparation and Pre-reduction Conditions on Methanation Performance. *Top Catal.* **2015**, *59*, 314–325. [CrossRef]

189. Bacariza, M.C.; Amjad, S.; Teixeira, P.; Lopes, J.M.; Henriques, C. Boosting Ni Dispersion on Zeolite-Supported Catalysts for CO_2 Methanation: The Influence of the Impregnation Solvent. *Energy Fuels* **2020**, *34*, 14656–14666. [CrossRef]

190. Bacariza, M.C.; Bértolo, R.; Graça, I.; Lopes, J.M.; Henriques, C. The effect of the compensating cation on the catalytic performances of Ni/USY zeolites towards CO_2 methanation. *J. CO2 Util.* **2017**, *21*, 280–291. [CrossRef]

191. Delmelle, R.; Duarte, R.B.; Franken, T.; Burnat, D.; Holzer, L.; Borgschulte, A.; Heel, A. Development of improved nickel catalysts for sorption enhanced CO_2 methanation. *Int. J. Hydrogen Energy* **2016**, *41*, 20185–20191. [CrossRef]

192. Borgschulte, A.; Gallandat, N.; Probst, B.; Suter, R.; Callini, E.; Ferri, D.; Arroyo, Y.; Erni, R.; Geerlings, H.; Züttel, A. Sorption enhanced CO_2 methanation. *Phys. Chem. Chem. Phys.* **2013**, *15*, 9620–9625. [CrossRef] [PubMed]

193. Walspurger, S.; Elzinga, G.D.; Dijkstra, J.W.; Sarić, M.; Haije, W.G. Sorption enhanced methanation for substitute natural gas production: Experimental results and thermodynamic considerations. *Chem. Eng. J.* **2014**, *242*, 379–386. [CrossRef]

194. Westermann, A.; Azambre, B.; Bacariza, M.C.; Graça, I.; Ribeiro, M.F.; Lopes, J.M.; Henriques, C. Insight into CO_2 methanation mechanism over NiUSY zeolites: An operando IR study. *Appl. Catal. B* **2015**, *174–175*, 120–125. [CrossRef]

195. Westermann, A.; Azambre, B.; Bacariza, M.C.; Graça, I.; Ribeiro, M.F.; Lopes, J.M.; Henriques, C. The promoting effect of Ce in the CO_2 methanation performances on NiUSY zeolite: A FTIR In Situ/Operando study. *Catal. Today* **2017**, *283*, 74–81. [CrossRef]

196. Lu, X.; Gu, F.; Liu, Q.; Gao, J.; Liu, Y.; Li, H.; Jia, L.; Xu, G.; Zhong, Z.; Su, F. VO_x promoted Ni catalysts supported on the modified bentonite for CO and CO_2 methanation. *Fuel Process. Technol.* **2015**, *135*, 34–46. [CrossRef]

197. Le, T.A.; Kang, J.K.; Park, E.D. CO and CO_2 Methanation Over Ni/SiC and Ni/SiO_2 Catalysts. *Top Catal.* **2018**, *61*, 1537–1544. [CrossRef]

198. Zhi, G.; Guo, X.; Wang, Y.; Jin, G.; Guo, X. Effect of La_2O_3 modification on the catalytic performance of Ni/SiC for methanation of carbon dioxide. *Catal. Commun.* **2011**, *16*, 56–59. [CrossRef]

199. Kirchner, J.; Anolleck, J.K.; Loesch, H.; Kureti, S. Methanation of CO_2 on iron based catalysts. *Appl. Catal. B-Environ.* **2018**, *223*, 47–59. [CrossRef]

200. Baysal, Z.; Kureti, S. CO_2 methanation on Mg-promoted Fe catalysts. *Appl. Catal. B* **2020**, *262*, 118300. [CrossRef]

201. Wang, Y.; Arandiyan, H.; Scott, J.; Dai, H.; Amal, R. Hierarchically Porous Network-Like Ni/Co_3O_4: Noble Metal-Free Catalysts for Carbon Dioxide Methanation. *Adv. Sustain. Syst.* **2018**, *2*. [CrossRef]

202. Wang, K.; Li, W.; Huang, J.; Huang, J.; Zhan, G.; Li, Q. Enhanced active site extraction from perovskite $LaCoO_3$ using encapsulated PdO for efficient CO_2 methanation. *J. Energy Chem.* **2021**, *53*, 9–19. [CrossRef]

203. Zhen, W.; Li, B.; Lu, G.; Ma, J. Enhancing catalytic activity and stability for CO_2 methanation on Ni@MOF-5 via control of active species dispersion. *Chem. Commun.* **2015**, *51*, 1728–1731. [CrossRef] [PubMed]

204. Zhou, R.; Rui, N.; Fan, Z.; Liu, C. Effect of the structure of Ni/TiO_2 catalyst on CO_2 methanation. *Int. J. Hydrogen Energy* **2016**, *41*, 22017–22025. [CrossRef]

205. Liu, J.; Li, C.; Wang, F.; He, S.; Chen, H.; Zhao, Y.; Wei, M.; Evans, D.G.; Duan, X. Enhanced low-temperature activity of CO_2 methanation over highly-dispersed Ni/TiO_2 catalyst. *Catal. Sci. Technol.* **2013**, *3*, 2627–2633. [CrossRef]

206. Petala, A.; Panagiotopoulou, P. Methanation of CO_2 over alkali-promoted Ru/TiO_2 catalysts: I. Effect of alkali additives on catalytic activity and selectivity. *Appl. Catal. B* **2018**, *224*, 919–927. [CrossRef]

207. Qin, Z.; Wang, X.; Dong, L.; Su, T.; Li, B.; Zhou, Y.; Jiang, Y.; Luo, X.; Ji, H. CO_2 methanation on Co/TiO_2 catalyst: Effects of Y on the support. *Chem. Eng. Sci.* **2019**, *210*, 115245. [CrossRef]

208. Cerdá-Moreno, C.; Chica, A.; Keller, S.; Rautenberg, C.; Bentrup, U. Ni-sepiolite and Ni-todorokite as efficient CO_2 methanation catalysts: Mechanistic insight by operando DRIFTS. *Appl. Catal. B* **2020**, *264*, 118546. [CrossRef]

209. Liang, C.; Gao, Z.; Lian, H.; Li, X.; Zhang, S.; Liu, Q.; Dong, D.; Hu, X. Impacts of metal loading in Ni/attapulgite on distribution of the alkalinity sites and reaction intermediates in CO_2 methanation reaction. *Int. J. Hydrogen Energy* **2020**, *45*, 16153–16160. [CrossRef]

210. Branco, J.B.; Ferreira, A.C. Methanation of CO_2 Over Bimetallic Ni–5f Block Element (Th, U) Oxides. *Eur. J. Inorg. Chem.* **2019**, *2019*, 1039–1045. [CrossRef]

211. Ferreira, A.C.; Branco, J.B. Methanation of CO_2 over nanostructured nickel-4f block element bimetallic oxides. *Int. J. Hydrogen Energy* **2019**, *44*, 6505–6513. [CrossRef]

212. Ferreira, A.C.; Branco, J.B. New approach for the synthesis of nanostructured binary f-block intermetallic compounds: CO_2 methanation studies. *Intermetallics* **2019**, *108*, 32–38. [CrossRef]

213. Branco, J.B.; da Silva, R.P.; Ferreira, A.C. Methanation of CO_2 over Cobalt-Lanthanide Aerogels: Effect of Calcination Temperature. *Catalysts* **2020**, *10*, 704. [CrossRef]

214. Kim, A.; Debecker, D.P.; Devred, F.; Dubois, V.; Sanchez, C.; Sassoye, C. CO_2 methanation on Ru/TiO_2 catalysts: On the effect of mixing anatase and rutile TiO_2 supports. *Appl. Catal. B* **2018**, *220*, 615–625. [CrossRef]

215. Marwood, M.; Doepper, R.; Renken, A. In-situ surface and gas phase analysis for kinetic studies under transient conditions The catalytic hydrogenation of CO_2. *Appl. Catal. A* **1997**, *151*, 223–246. [CrossRef]

216. Wei, W.; Jinlong, G. Methanation of carbon dioxide: An overview. *Front. Chem. Sci. Eng.* **2010**, *5*, 2–10. [CrossRef]

217. Remya, V.R.; Kurian, M. Synthesis and catalytic applications of metal–organic frameworks: A review on recent literature. *Int. Nano. Lett.* **2019**, *9*, 17–29. [CrossRef]

218. Safaei, M.; Foroughi, M.M.; Ebrahimpoor, N.; Jahani, S.; Omidi, A.; Khatami, M. A review on metal-organic frameworks: Synthesis and applications. *TrAC Trends Anal. Chem.* **2019**, *118*, 401–425. [CrossRef]

219. Liang, J.; Liang, Z.; Zou, R.; Zhao, Y. Heterogeneous Catalysis in Zeolites, Mesoporous Silica, and Metal–Organic Frameworks. *Adv. Mater.* **2017**, *29*, 1701139. [CrossRef]

220. Balakrishnan, M.S.; Batra, V.J.; Hargreaves, J.S.; Pulford, D.I. Waste materials – catalytic opportunities: An overview of the application of large scale waste materials as resources for catalytic applications. *Green Chem.* **2011**, *13*, 16–24. [CrossRef]